



JIMMA UNIVERSITY

JIMMA INSTITUTE OF TECHNOLOGY

SCHOOL OF GRADUATE STUDIES

FACULTY OF CIVIL AND ENVIRONMENTAL ENGINEERING

STRUCTURAL ENGINEERING STREAM

**NUMERICAL INVESTIGATION ON STRUCTURAL BEHAVIOR OF ARCHED
CELLULAR STEEL BEAM.**

**A Thesis Submitted to School of Graduate Studies of Jimma University in Partial
Fulfillment Of the requirements for the Degree of Masters of Science in Structural
Engineering.**

By BESUKAL BEFEKADU ZEWUDIE

January, 2020

JIMMA, ETHIOPIA

JIMMA UNIVERSITY
JIMMA INSTITUTE OF TECHNOLOGY
SCHOOL OF GRADUATE STUDIES
FACULTY OF CIVIL AND ENVIRONMENTAL ENGINEERING
STRUCTURAL ENGINEERING STREAM

**NUMERICAL INVESTIGATION ON STRUCTURAL BEHAVIOR OF ARCHED
CELLULAR STEEL BEAM.**

A Thesis Submitted to School of Graduate Studies of Jimma University in Partial Fulfillment of the Requirements for the Degree of Masters of Science in Structural Engineering.

By BESUKAL BEFEKADU ZEWUDIE

Main advisor: Eng. Elmer C.Agon (Asso.Prof)

Co-advisor:Eng.Kefiyalew Zerfu (M.Eng.)

January, 2020

JIMMA, ETHIOPIA

JIMMA UNIVERSITY
SCHOOL OF GRADUATE STUDIES
JIMMA INSTITUTE OF TECHNOLOGY
FACULTY OF CIVIL AND ENVIRONMENTAL ENGINEERING
STRUCTURAL ENGINEERING CHAIR

**NUMERICAL INVESTIGATION ON STRUCTURAL BEHAVIOR OF ARCHED
CELLULAR STEEL BEAM**

BESUKAL BEFEKADU

APPROVED BY BOARD OF EXAMINERS



1. Engr. Elmer C. Agon		04 / 02 / 2020
Main advisor	Signature	Date
2. Engr. Kefiyalew Zerfu		04 / 02 / 2020
Co-advisor	Signature	Date
3. Dr. S. Moses Aranganathan		04 / 02 / 2020
External Examiner	Signature	Date
4. Engr. Diosdado John Corpuz		04 / 02 / 2020
Internal Examiner	Signature	Date
5. Engr. Solomon Biratu		04 / 02 / 2020
Chairperson	Signature	Date

DECLARATION

I, undersigned declare that this thesis work is my original work and has not been presented for a degree in any other university and all reference materials used while compiling these paper were fully cited.

Name	Signature	Date
Besukal Befekadu	_____	_____

This Thesis has been submitted for evaluation whith my approval as a university advisor.

Main Advisor

Eng. Elmer C.Agon	_____	_____
-------------------	-------	-------

Co-advisor

Eng.Kefiyalew Zerfu	_____	_____
---------------------	-------	-------

ACKNOWLEDGEMENT

My first and foremost gratitude goes to Almighty God through my Lord and savior JESUS CHRIST who is there for me always through the times of trouble and good times.

I would like to express my gratitude to my families and friends for their insistent and rigorous moral support not only on my educational careers but throughout my life.

Heart fully, I would like to thanks my advisors Eng. Elmer C. Agon and Eng. Kafeyalew Zerfu for their remarkable comments while compiling this thesis paper.

Finally, my special thanks goes to Jimma institute of Technology for facilitating this program which helps me for upgrading my profession.

ABSTRACT

In recent year due to its design and construction advantages, engineers are increasingly utilizing open web steel sections (cellular) in their designs. Design advantages include a reduced weight per unit length of beam and an improved flexural stiffness due larger section modulus resulting from the increased depth, thus allowing longer spans, which provide for a more open floor plan. Construction advantages include the ability to run electrical, mechanical and plumbing utilities through the openings, which can save several inches of floor-to-floor height. The open webs also provide aesthetic advantages when used in structures with exposed beams. These added benefits make cellular beams an efficient and cost effective material for modern building constructions. The evolution of the fabrication technology and the aesthetical and mechanical performances implied the extension of the fields of application of these beams. Nowadays, the cellular beams can be designed using a variation of heights (tapered beams) or a curvature (arched beams).

However, in spite of numerous advantage of curved cellular steel beam previous studies mainly focused on the structural behavior arched steel beam with solid webs and little research has been reported for structural in plane stability and performance of cellular arched steel .to narrow this gap This paper presents a study on in plane structural strength of cellular steel arches using validated ABAQUS/CAE standard version 6.14 finite element program for the nonlinear elastic-plastic analysis of cellular steel arches.

In these paper to investigate the in-plane elastic-plastic buckling and strength of pinned circular and parabolic cellular arches of total 32 samples were randomly selected considering degree of curvature(shallow and deep) ,geometry of arch(parabolic and circular) and applicability.

The finite element program considers the effects of large deformations, material nonlinearities and initial geometric imperfection in predicting the elastic-plastic behavior of cellular steel arches under mid span concentrated and uniform radially distributed vertical loads ,which induce combined bending and compression in the arch .the complex effect of rise-to-span ratio, arch geometry and radius of curvature on the in plane elastic-plastic stability and strength of cellular steel arches are included and elucidated in these study.

Finally numerical result buckling load to in plane deflection, buckling load to out of plane deflection and mode of failure from finite element analysis extracted, further analyzed and interpreted to draw conclusion. In conclusion, the stiffness of arched cellular beam is directly proportional to rise-to-span ratio regardless of arch geometry and degree of curvature under mid span concentrated load ,but this is valid up to rise-to- span ratio($H_s/L=0.35$) and ($H_s/L=0.419$) for circular and parabolic arch respectively under uniform vertical load. Under the same rise-to-span ratio deep parabolic arches are structurally stiffer and can carry larger load than deep circular cellular arches. Increasing radius curvature without altering rise-to-span ratio reduces the stiffness of arched cellular steel under mid-point load.

Key words: *cellular arched, ultimate buckling load, rise-to-span ratio, arch geometry, radius of curvature*

TABLE OF CONTENTS

ACKNOWLEDGEMENT i

ABSTRACT ii

LIST OF TABLES x

ACRONYMS xi

SYMBOLS xii

CHAPTRE ONE 1

INTRODUCTION 1

 1.1 Background of the study 1

 1.2. Statement of problem 3

 1.3 Research question..... 3

 1.4 Objective of the study 4

 1.4.1. General objective 4

 1.4.2. Specific objective. 4

 1.5 Significance of study..... 4

 1.6. Scope of the study 5

CHAPTER TWO 6

REVIEW OF RELATED LITERATURE 6

 2.1. General overview 6

 2.2 .Fabrication arts of cellular beam 7

 2.2.1. Straight cellular beam..... 7

 2.2.2. Arched cellular beam..... 7

 2.3. Application and advantage of cellular beam 9

 2.3.1. Long spans and service integration 9

 2.4. Classification of vertically curved steel structure 10

2.4.1. Geometry of vertical curve	10
2.5. Structural behavior of arched steel beam	13
2.5.1. In-plane stability of arched steel structure.....	13
2.5.2. Out-of-plane stability of arches	20
2.6.1. Out of plane elastic buckling of circular arches in uniform compression	21
2.6. Behavior of cellular beam	24
2.6.1. Vierendeel yielding of cellular beam.....	24
2.6.2. Web post buckling yielding of cellular beam	26
2.6.3. Rupture of the welded joint	27
2.7. Analysis and design of cellular beam.....	28
2.7.1. Guidelines for web perforations	28
2.7.2. Overall beam flexural capacity.....	29
2.7.3. Beam shear capacity	29
2.7.4. Flexural and buckling strength of web-post	30
2.7.5. Vierendeel bending of upper and lower tees	32
2.7.6. Lateral torsional buckling.....	32
2.8. Factors determine structural performance of cellular beam.....	33
CHAPTER THREE	34
METHEDODOLOGY	34
3.1. Population.....	35
3.2. Sampling size and sampling procedure.....	35
3.2.1 Section geometry selection.....	35
3.2.2. Sampling.....	36
3.3. Study variable.....	37
3.3.1. Independent variables	37

3.3.2. Dependent variables	37
3.4. Finite element modelling.....	37
3.5. Modelling and analyzing of arched cellular beam	38
3.5.1 Modelling geometry of arched cellular beam.....	39
3.5.2 Mechanical material properties	40
3.5.3. Part assembly	42
3.5.4. Model meshing	43
3.5.5. Boundary condition and loading.....	46
3.5.6. Analysis step.....	47
CHAPTER FOUR.....	54
RESULT AND DISCUSSION	54
4.1. Bench mark experiment	54
4.1.1. General description on the genesis of data used in the experiment.....	54
4.1.2. Geometrical property.....	54
4.1.3. Material property	55
4.1.4. Test setup and loading	55
4.1.5. Experimental result.....	56
4.2. Finite element simulation result of experimentally tested models.....	57
4.3. Comparison of finite element and experimental result	60
4.4. The result of FE analysis and simulation	61
4.5. Structural behavior of arched cellular beam under mid span vertical load.....	61
4.5.1. Effect of rise to span ratio on shallow circular arched cellular steel.....	61
4.5.2. Effect of rise to span ratio on shallow parabolic arch	63
4.5.3. Effect of rise to span ratio on deep circular cellular arch.....	64
4.5.4. Effect of rise to span ratio on deep parabolic arch	65

4.6. Effect of arch geometry under mid span point load	67
4.7. Structural behavior of arched cellular beam under uniform distributed vertical load.	68
4.7.1. Effect of rise to span ratio on shallow circular cellular arch	68
4.7.2. Effect of rise to span ratio on shallow parabolic cellular arch	69
4.7.3. Effect of rise to span ratio on deep parabolic arched cellular steel beam	70
4.7.4. Effect of rise to span ratio on deep circular arched cellular steel beam	71
4.8. Effect arch geometry under uniform radially distributed vertical load	73
4.9. Effect of radius of curvature.....	76
4.9.1. Effect of radius of curvature under mid-span point load.....	76
4.9.2. Effect of radius curvature under uniform radially distributed vertical load	77
CHAPTER FIVE	79
CONCLUSION AND RECOMMENDATION.....	79
5.1. CONCLUSION	79
5.2. RECOMMENDATION	81
REFERENCES	82
APPENDIX-A 3-D simulation of circular arched cellular model	85
APPENDIX-B 3D simulation of parabolic arched cellular model	92
APPENDIX –C Buckling load to displacement contour	99
APPENDIX –D Buckling load to displacement contour	106
APPENDIX –E Class clasification of model.....	113

LIST OF FIGURES

Figure 2. 1: Manufacturing of straight symmetric cellular beam (Sameer S.Fares, et.al 2016). 7

Figure 2. 2: Manufacturing of vertically curved symmetric cellular beam. 8

Figure 2. 3: Circular arch geometry(Dowswell, 2018)..... 12

Figure 2. 4: Parabolic arch geometry(Dowswell, 2018)..... 12

Figure 2. 5: Geometry and loading. 13

Figure 2. 6: In plane buckling shapes (Dowswell, 2018) 15

Figure 2. 7: Geometry of arch (Ziemain, 2010)..... 22

Figure 2. 8: Vierendeel yielding mechanism(Durif, Bouchaïr and Vassart, 2013) 25

Figure 2. 9: Vierendeel mechanism of a steel beam with circular opening 26

Figure 2. 10: web post buckling failure mode 27

Figure 2. 11: Geometrical parameters of cellular beam..... 28

Figure 2. 12 :Horizontal shear in the web post of cellular beam (Erdal and Polat, 2013)..... 30

Figure 2. 13: Location of critical buckling section of cellular beam..... 31

Figure 3. 2: Parameters of cellular beam 35

Table 3. 1: Selected sample parameters..... 36

Figure 3. 4: Modelled parts of cellular arched steel..... 40

Figure 3. 5: Idealized stress-strain relationship for structural steel. (N.S.Trahair et al, 2008)..... 41

Figure 3. 6: Stress-strain relation test from a)web and b)flange (Dou et al., 2015) 42

Figure 3. 7:Commonly used element families (ABAQUS, 2014)..... 43

Figure 3. 8: Element shape (ABAQUS, 2013) 44

Figure 3. 9: Linear brick, quadratic brick and modified tetrahedral elements..... 44

Figure 3. 10: Meshing of model B-3..... 45

Figure 3. 11: Boundery and loading of model 46

Figure 3. 12: Analysis step procedure..... 47

Figure 3. 13: Non linear load displacement curve(ABAQUS, 2013)..... 48

Figure 3. 14: Internal and External loads on a body. (ABAQUS, 2013)..... 49

Figure 3. 15: Frist iteration (ABAQUS, 2013) 49

Figure 3. 16: Second iteration. (ABAQUS, 2013)..... 51

Figure 3. 17: Proportional loading with unstable response. (ABAQUS, 2013) 52

Figure 4. 1:Deimension of tested specimen(Zaher,et al 2018) 55

Figure 4. 2: Complete test set up (Zaher et al., 2018)..... 56

Figure 4. 4:Abaqus result of buckling load to Dispacement contour for specimen B-3..... 58

Figure 4. 3:Abaqus result of buckling load to displacement contour of B-2 57

Figure 4. 5: Abaqus buckling load to displacement contour result for B-4..... 58

Figure 4. 6: Load to in plane vertical deflection of FE and EXP of B-3 59

Figure 4. 7: Buckling load to in plane vertical deflection of B-2 59

Figure 4. 8: Buckling load to vertical deflection of FE and EXP for B-4 60

Figure 4. 9: Buckling load to in plane vertical deflection of shallow circular arched 62

Figure 4. 10:Buckling load to out of plane deflection 62

Table 4. 5: Shallow parabolic arch ultimate buckling load variation to rise –to-span ratio 63

Figure 4. 11 :Buckling load versus in plane vertical deflection shallow arched parabola..... 63

Figure 4. 12: Buckling load versus out of plane deflection of parabolic shallow arch..... 64

Table 4. 6: Ultimate buckling load and maximum vertical deflection of deep circular curve 64

Figure 4. 13: Buckling load to in plane vertical deflection of deep circular arched..... 65

Figure 4. 14: Buckling load to out of plane deflection curve of deep circular arch. 65

Figure 4. 15: Buckling load to vertical deflection of parabolic deep arch..... 66

Figure 4. 16: Buckling load versus out of plane deflection parabolic deep arch..... 66

Figure 4. 17 : Buckling load to deflection curve comparison of shallow arch geometry 67

Figure 4. 18: Buckling load to deflection curve comparison of deep arch geometry..... 68

Table 4. 10: Ultimate load and maximum vertical deflection of SCC under URDVL..... 69

Figure 4. 19: Buckling load to deflection of shallow circular under URDVL 69

Figure 4. 20: Buckling load to deflection of PSC..... 70

Figure 4. 21: Buckling load to deflection PDC..... 71

Figure 4. 22: Buckling load to inplane vertical deflection of DCC under URDVL 72

Figure 4. 23: Buckling load to out of plane deflection DCC under URDVL 73

Figure 4. 24: Deep arched cellular beam geometric comparison under URDVL..... 74

Figure 4. 25: Shallow arched cellular geometric comparison under URDVL..... 75

Figure 4. 26: Buckling load to deflection curve of SCC-3000, SCC-2500, PSC-3000, and PSC-2500 under MSPL 76

Figure 4. 27: Buckling load to deflection curve of DCC-3000, DCC-2500, PDC-3000 and PDC-2500 under MSPL 77

Figure 4. 28: Buckling load to deflection SCC-3000, SCC-2500, PSC-3000, PSC-2500 under URDVL..... 78

Figure 4. 29: Buckling load to deflection DCC-3000, DCC-2500, PDC-3000, and PDC-2500 under URDVL..... 78

LIST OF TABLES

Table 2. 1: Minimum span slenderness (CEN, 2009; Pi et al., 2002; Schreyer). 14

Table 2. 2: Modification factors for in-plane strength of pin-ended arches 19

Table 2. 3: Modification factor for in-plane strength of fixed arches..... 20

Table 2. 4: Factors for the out -of plane design of circular arches 24

Table 3. 1: Selected sample parameters 36

Table 3. 2: Mechanical properties of steel used for parametric investigation 41

Table 3. 3: Steel material properties used for validation 42

Table 3. 4: Mesh detail for B-3 cellular steel arch..... 45

Table 3. 5: Boundary condition. 46

Table 4. 1: Dimensions of expermintally tested speceimens 55

Table 4. 2: Steel properties of tested specimens 55

Table 4. 3: Experimental result..... 56

Table 4. 4: Ultimate buckling load and maximum deflection of shallow circular cellular 61

Table 4. 5: Shallow parabolic arch ultimate buckling load variation to rise –to-span ratio 63

Table 4. 6: Ultimate buckling load and maximum vertical deflection of deep circular curve 64

Table 4. 7: Ultimate buckling load and maximum vertical deflection of deep parabolic arch..... 66

Table 4. 8: Shallow arch geometry buckling load comparison under MSPL 67

Table 4. 9: Ultimate buckling load comparison of deep arch geometry under MSPL 67

Table 4. 10: Ultimate load and maximum vertical deflection of SCC under URDVL..... 69

Table 4. 11: Ultimate buckling load and maximum vertical deflection PSC under URDVL 70

Table 4. 12: Ultimate buckling load variation to rise-to span ratio of deep parabola under URDVL..... 71

Table 4. 13: Buckling load variation with span to rise ratio under URDVL 72

Table 4. 14 : Ultimate load comparison of deep arch geometry under URDVL 74

Table 4. 15: Ultimate buckling load comparison of shallow curve geometry under URDVL 75

ACRONYMS

ACI	American Concrete institute
AISC	American institute of steel construction
CAE	Complete ABAQUS environment
CCB	Curved cellular beam
DCC	Deep circular curve
EBCS	Ethiopian building code standard
EQ	Equation
ES	Europe standard
EXP	Experiment
FE	Finite element
HSS	Hot rolled steel section
LTB	Lateral torsional buckling
LVDT	Linear variable differential transformer
MSPL	Mid-span point load
PDC	Parabolic deep arch
PSC	Parabolic shallow curve
SCC	Shallow circular curve
URDVL	Uniform radially distributed vertical load
WPB	Web post buckling

SYMBOLS

A	Cross-sectional area
A_{LT}	Cross-sectional area of lower tees
D_O	Diameter of web opening
E	Elastic modulus of material
EI	Flexural rigidity of section
f_u	Ultimate tensile stress
f_y	Yield stress
H	Arch rise
H_u	Distance between centers of upper and lower tees
I_x	Moment of inertia along strong axis
L_s	span length
M^*	Amplified moment
M_E	Elastic moment
M_m	First order moment
M_p	plastic section capacity at major axis
M_{yz}	Torsional buckling moment
N^*	Applied (acting) load
N_{acr}	Buckling load of arch
N_{cr}	Buckling load corresponding to column
N_T	Torsional buckling load
P_{vy}	Vertical shear resistance
P_y	Design strength of steel
R	Radius of curvature
r_x	Radius of gyration
S	Center to center spacing of opening
S_x	Section modulus
α_{am}	axial compression modification factor

α_{an}	moment modification factor
δ_b	moment amplification factor
ε_u	engineering strain hardening
Θ	subtended angle
λ	slenderness ratio of arch
λ^*	load proportional factor
ρ	density of steel
Φ	reduction factor
P_{VH}	horizontal shear resistance
t_w	thickness of web
t_f	thickness of flange

CHAPTRE ONE

INTRODUCTION

1.1 Background of the study

Construction industry has been one of the leading fields among many others in the world. Structural engineering has a major role in the construction field which every day becoming more widespread and sophisticated. One of the main materials used by structural engineers is structural steel. The history of structural steel industry is over one hundred years old. As the technology of steel structures progress, more types of steel sections were produced to improve the structural steel's mechanical properties and also to obtain sections that allow usage for more aesthetic applications by satisfying the architectural needs. Beams with expanded web sections with repeating web openings, such as, castellated, cellular and sinusoidal beams are good example.

The history of using structural steel beams with expanded web sections with repeating web openings were first used in 1910 by the Chicago Bridge and Iron Works (Das and Srimani, 1984). This idea was also developed independently by G.M. Boyd in Argentina in 1935 and was later patented in the United Kingdom (Knowles, 1991).

Cellular beams are steel beams with repeating circular web openings. They are generally made of hot rolled profiles by flame cutting of the parent profile, by cutting two semicircular sections through the web of a common steel I-beam section. Once the two cuts are completed, the Halves are then separated, shifted and welded together with one another to form a new, deeper, stiffer, stronger section known as open-web expanded steel beam. The resulting beam is deeper than the Original I-beam section, resulting in a larger section modulus.

In comparison to their root beams, cellular beams offer many design and construction advantages. As a result of expanding the web and introducing web openings, these members have a decreased weight per unit length of beam , an increased section modulus and increased strong-axis moment of inertia, These increases not only make longer spans possible, but their increased efficiency also provides the potential for significant cost savings when used in long spans. These advantages come at the expense of a more complex analysis

In recent years due to its design and construction advantages, engineers are increasingly utilizing cellular steel beams sections in their designs. Design advantages include a reduced weight per unit length of beam and an improved flexural stiffness (larger section modulus) resulting from the increased depth, thus allowing longer spans, which provide for a more open floor plan. Construction advantages include the ability to run utilities through the openings, which can save several inches of floor-to-floor height. The open webs also provide aesthetic advantages when used in structures with exposed beams. Open web sections are considered to be particularly economical in structures that have medium to high design loads over medium to long spans. Recent applications of open web beams range from commercial and industrial buildings to parking garages. (Hennessey, et. al., 2004).

These added benefits make arched cellular beams an efficient and cost-effective material for modern building construction. It is evident that cellular beams offer tremendous advantages for longer spans.

The evolution of the fabrication technology and the aesthetical and mechanical performances implied the extension of the fields of application of these beams. Nowadays, the cellular beams can be designed using a variation of heights (tapered beams) or a curvature (curved beams). For tapered cellular beam, the fabrication uses an inclined oxy-cutting line in comparison with the straight beam.

In the case of curved cellular beam, the two members of the cellular beam are curved separately before re-welding. Thus, it is necessary to well estimate the curvature to be realized, in order to obtain circular openings in the final curved cellular beam. Because of curved cellular steel beams combine aesthetics, versatility and economy in steel design engineers currently incorporate cellular arched steel in to a variety of modern building and bridges.

However, in spite of numerous advantage of curved cellular steel beam previous studies mainly focused on the structural behavior curved steel beam with solid webs .to narrow this gap these research extend understanding on the structural behavior of long span curved cellular beam under different parameter like geometry of arch, rise-span ratio and radius of curvature subjected to static loading.

1.2. Statement of problem

In recent years, the use of arched cellular steel beams has become increasingly popular in building design primarily to achieve longer spans and to reduce overall building height and steel weight costs. Due to the design and construction advantages of cellular beam engineers incorporate cellular beams into a variety of modern buildings. Because of their elegant shape, curved cellular beams offer architects opportunities to express their ideas. These advantages come at the expense of extensive experimental, analytical and numerical research and analysis.

However, in spite of numerous advantages of curved cellular steel beams and complex structural behavior due to opening introduction on the web previous studies mainly focused on the structural behavior of arched steel beams with solid webs. Numerous studies have reported on the structural stability behavior of solid web steel arches (vertically curved) and design rules have been proposed for both in-plane buckling and out-of-plane buckling of solid web steel beams but, very few studies reported on the structural stability of arched cellular steel beams. To narrow this gap this study aimed to numerically investigate the in-plane structural stability and performance of cellular arched steel under mid-point concentrated load and uniform radially distributed vertical static loading.

In addition, with respect to versatility and various design and construction advantages of cellular arched steel beams, its practicability in the Ethiopian construction industry is very limited. Nearly null this study planned to remind construction industry stakeholders to consider arched cellular beams as an alternative and extending these structural advantages to the domestic construction sector by serving as a reference material.

1.3. Research question

This study investigated numerically the structural performance, associated failure modes and structural response of arched cellular steel beams, and answered the following research question.

- How geometry of arch (circular and parabolic) related to structural performance of arched cellular steel beams?
- What is the relation between structural responses, performances of arched cellular steel and rise-to-span ratio?
- How radius of curvature affects the in-plane structural performance of curved cellular beams?

1.4. Objective of the study

1.4.1. General objective

The main objective of this research was to investigate the effect of different parameter on the structural performance of arched cellular steel beam under static loading numerically using finite element software.

1.4.2. Specific objective.

- To validate nonlinear finite element packages result to physical experimental work.
- To investigate the effect of arch geometry(circular and parabolic) on the structural performance and structural stability of arched cellular steel.
- To examine the effect of rise-to-span ratio on the ultimate performance and associated structural failure mode on arched cellular steel beam.
- To examine impact of radius of curvature on the structural performance of arched cellular beam.

1.5 Significance of study

The main goal of this research was to enhance the understanding of the structural performance, stability and associated failure mode of arched cellular steel under static loading based on different parameters. These enables architects and structural designer as a basis for preliminary decision on. Besides, these research aimed to remind the advantages of cellular beam to the stakeholders of Ethiopian construction industry by serving as a corner stone references to initiate application of steel cellular beam in the country building construction sector as an alternative of structural member form. Furthermore this paper enables domestic researchers as a basic references on investigating the structural behavior of arched cellular steel beam.

1.6. Scope of the study

These research was limited to numerically investigating the in plane structural stability and performances of arched cellular steel beam under symmetric static load in terms of load deformation relationship of arched cellular I-section steel beam manufactured from hot rolled parent profile of solid web I-sections of nominal steel grade F_e-430 which, lateral torsional buckling were prevented using sufficient lateral support. The arched cellular steel beam was assumed to be used in pure steel frame construction and considering as independent element (bi-supported) simply supported vertically curved cellular steel beam using finite element software Abaqus/CAE 6.14.

CHAPTER TWO

REVIEW OF RELATED LITERATURE

2.1. General overview

Cellular beams are steel beams with repeated circular web openings. They are generally made of hot rolled profiles by flame cutting of the parent profile by cutting two semicircular sections through the web of a common steel I-beam section. Once the two cuts are completed, the Halves are then separated, shifted and welded together with one other to form a new, deeper, stiffer, stronger section known as open-web expanded steel beam. The resulting beam is deeper than the Original I-beam section, resulting in a larger section modulus.(Durif and Bouchair, 2016)

In recent year due to their design and construction advantages, engineers are increasingly utilizing open web steel sections (castellated and cellular) in their designs. Design advantages include a reduced weight per unit length of beam and an improved flexural stiffness (larger section modulus) resulting from the increased depth, thus allowing longer spans, which provide for a more open floor plan. Construction advantages include the ability to run utilities (mechanical, electrical plumbing etc.) through the openings, which can save several inches of floor-to-floor height. The open webs also provide aesthetic advantages when used in structures with exposed beams. These added benefits make cellular beams an efficient and cost effective material for modern building construction while it's evident that cellular beams offer tremendous advantage to achieve longer spans that have medium to high design loads. (Hennessey,2004)

The evolution of the fabrication technology with the aesthetical and mechanical performances of cellular beam implied the extension of the fields of application of these beams. Nowadays, the cellular beams can be designed and manufactured using a variation of heights (tapered beams) or a curvature (curved beams). For tapered cellular beam, the fabrication uses an inclined oxy-cutting line in comparison with the straight beam. In the case of curved cellular beam, the two members of the cellular beam are curved separately before re-welding. Thus, it is necessary to well estimate the curvature to be realized, in order to obtain circular openings in the final curved cellular beam.(Durif and Bouchair, 2016)

These advantages come at the expense of several years, extensive theoretical, numerical and experimental research has been carried out on the structural behavior of steel beams with web openings of various shapes. An overview of previous studies related to structural behavior of cellular and curved steel beam are presented in these chapter.

2.2 .Fabrication arts of cellular beam

2.2.1. Straight cellular beam

The patented method used for the fabrication of cellular beams is based on the exclusive use of hot rolled sections, a double cut-out is made in the web by flame cutting. The two obtained T-sections are shifted and re-welded. Leading to an increase in height as illustrated in step of Figure 2.1. (Sameer S.Fares, et.al 2016)

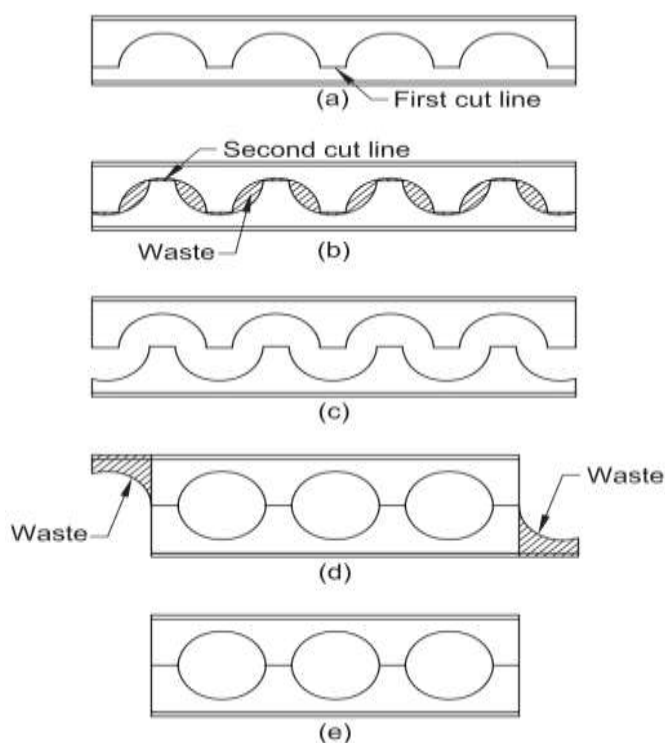


Figure 2. 1: Manufacturing of straight symmetric cellular beam (Sameer S.Fares, et.al 2016).

2.2.2. Arched cellular beam

Curved members can be formed by bending, heat curving, Segmenting, or cutting to curve. Bending, which is the most used and generally the most economical curving process

Several methods are available for bending steel members: pyramid roll bending, incremental step bending, induction bending, rotary draw bending, and other processes. Some methods are more common in the steel construction industry, Cold bending, where the member is bent at room temperature, is usually more economical than hot bending or induction bending; however, there are cases where the required geometry cannot be formed by cold bending. The primary

advantage of hot bending is that the material yield strength is lower compared to the room temperature value, requiring smaller forces to be exerted by the bending machine. Each bending method has advantages and disadvantages, and each bender/roller company has developed unique bending methods and often use one-of-a-kind, patented machines. Developing proper bending techniques that ensure accurate and consistent dimensions requires significant judgment and experience. (Sameer S.Fares and John Coulson, 2016)

When a member is bent to form a permanent curvature, it must be strained beyond its yield point, inevitably causing some level of cross-sectional distortion. The tendency for cross-sectional distortion during the bending process can be controlled using various techniques. HSS wall distortion is often limited by using an internal support mechanism, such as a mandrel, a smaller HSS member, or filling the member with supporting material such as sand. Many bending machines control the distortion of open shapes with specialized rolls and various forms of mechanical restraint. Bender roller companies may have hundreds of specialized rolls, mandrels, die sets and other tooling to bend various HSS and open shapes with minimal distortion. (Dowswell, 2018)

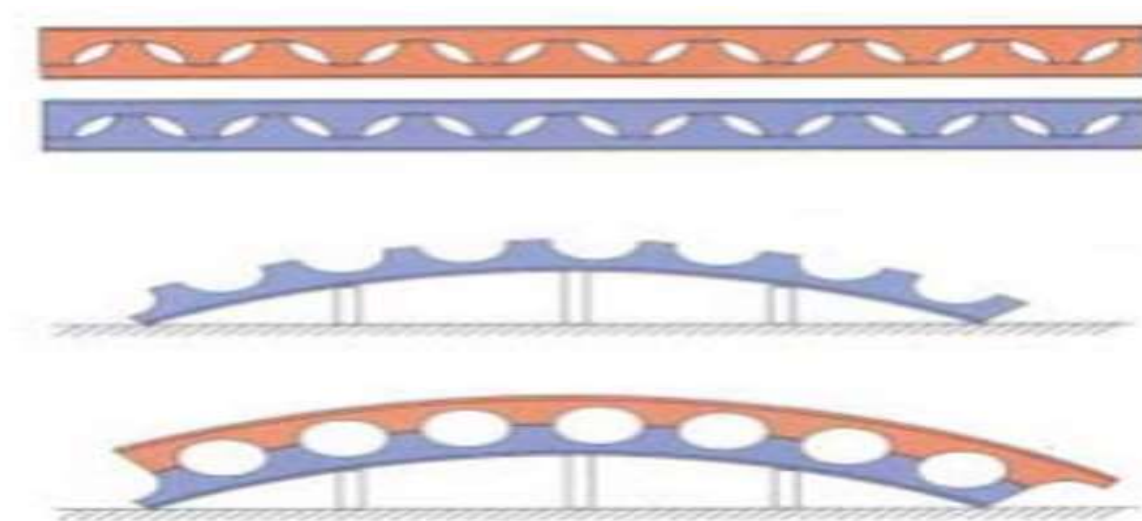


Figure 2. 2: Manufacturing of vertically curved symmetric cellular beam. (Macsteel trading, 2003)

2.3. Application and advantage of cellular beam

A cellular beam is the modern version of the traditional ‘castellated’ beam a cellular beam is up to 2.5 times vertically stiffer than its parent solid web I-section. Cellular beams invariably produce a more efficient and economical solution than castellated beams, due to their greater flexibility. The three flexible dimensions are: Finished Depth, Cell Diameter and Cell Spacing. The circular openings possess on average 30 % more usable area than the openings of a castellated beam.(Pachpor P.D, Gupta L.M, 2011)

In comparison castellated beam of the same parent profile the maximum von-mises stress concentration is less in circular opening as compared to hexagonal opening of same area. The deflections and maximum von-mises stresses increases as the no. of opening increases. This is possible due to more openness in web of beam and development of vierendeel mechanism. (Pachpor P.D, Gupta L.M, 2011).

(Shivatare, 2017) investigate economical comparative study on conventional roof truss system and cellular beam and found that cellular beam as roof structure is efficient economically over conventional roof truss system and tapered cellular beam.

The major use of cellular beams is as secondary floor beams to achieve one or both of the following:-

2.3.1. Long spans and service integration

2.3.1.2. As Roofing beam

The use of cellular beam as roofing elements enables large spans, in the region of 40 meters, to be covered. Whether used as independent elements (simply supported beams) or continuity elements (frame rafter).

Cellular beams offer architects attractive and practical solutions in terms of use of space without screening effect. The diameter of the openings can reach 80 % of the total height of the beam and it is possible to leave only a small distance – required for fabrication – between the openings. This configuration of cellular beams enables their transparency and blending into the space enclosed to be accentuated, which has great appeal for architects.(ArcelorMittal,2016)

2.3.1.2. Decking

Modern constructions increasingly demand the accommodation of technical installations (heating, ventilation, air conditioning, etc.) within the available space enclosed.

The use of cellular beams now provides effective answers to the demands of project owners. This solution allows large uninterrupted spaces over a distance of up to 18 meters and allows various pipes and ducts to be passed through the openings.

The total deck thickness is 25 to 40 cm less than that of conventional solutions. with an imposed height of the order of 35 to 40 meters, a gain of only 20 cm in deck thickness enables an additional floor to be installed.(ArcelorMittal ,2016)

2.3.1.3. In car parks building.

There are four reasons for recommending the use of cellular beams for building car parks where no special fire resistance is required:(ArcelorMittal,2016)

- The traditional spans (15 to 16 m) are within the typical range
- Drainage is facilitated by slightly cambered beams,
- The openings improve the interior appearance of these structures
- The openings facilitate smoke evacuation and permit better air circulation between sections.

2.4. Classification of vertically curved steel structure

Vertically curved steel structure can be classified into circular and parabolic curves depending on the geometry of curvature also can be grouped as shallow and deep curves on the basis of included angle of curve.

2.4.1. Geometry of vertical curve

Accurate information on the geometry of curved members such as rise to span-to- ratio, radius, span and subtended angle must be conveyed to the bender/roller. Arch geometry is often described using the rise-to-span ratio, H/L_s , where H is the arch rise and L_s is the arch span. Rise-to-span ratios between $1/6$ and $1/5$ are the most efficient structurally (Gambhir, 2004). For arched roof structures supported at the floor level, rise-to-span ratios between $1/4$ and $1/3$ provide the most economical compromise between structural efficiency and usable enclosed area (AISC, 1963).

2.4.1.1. Circular Geometry

It is common practice to designate circular member curvature in terms of the radius. Design drawings typically indicate the radius to either the member centroid or to another convenient location on the cross section, such as the inner or outer surface of the member. For detailing, the reference location for the radius dimension is a point on the cross section that is dependent on the member cross-sectional shape and the bending axis, as shown in. Figure 2.3 shows the circular geometry and dimensions commonly used in circular curves. The relationship between the x and y coordinates is provided by Equation 2.1.

$$y = H - R + \sqrt{R^2 - (\frac{L_s}{2} - x)^2} \dots\dots\dots (2.1)$$

The arch length (developed length) is

$$L_d = R\theta \dots\dots\dots (2.2)$$

The chord (span length) is

$$L_s = 2R \sin(\frac{\theta}{2}) \dots\dots\dots (2.3)$$

The rise (H) is

$$H = R \left[1 - \cos(\frac{\theta}{2}) \right] \dots\dots\dots (2.4)$$

The circular arch geometry is commonly described using the rise to span ratio (H/Ls)

$$\frac{H}{L_s} = \frac{1 - \cos(\theta/2)}{2 \sin(\frac{\theta}{2})} \dots\dots\dots (2.5)$$

Where

H=arch rise (m, in)

Ld=arch length (developed length (main)

Ls=cord (span length (m,in)

R=radius (m,in)

θ=subtended angle (rad)

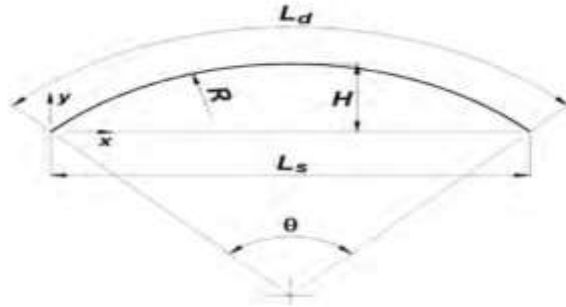


Figure 2. 3: Circular arch geometry(Dowswell, 2018)

2.4.1.2 Parabolic geometry

Because parabolic curves are efficient arch forms, they are often used for long-span structures resisting gravity loads. Design drawings typically indicate the rise and the span dimensions.

Figure 2.4 shows a parabolic curve, with the relationship between the x and y coordinates provided by Equation 2.7.

$$y = 4H \frac{x}{L_s} \left(1 - \frac{x}{L_s}\right) \dots\dots\dots (2.7)$$

The arch length is:

$$L_d = \frac{L_s}{2} \left[\sqrt{1 + \left(\frac{4H}{L_s}\right)^2} + \frac{L_s}{4H} \sin^{-1} \frac{4H}{L_s} \right] \dots\dots\dots (2.8)$$

When $0 < H/L_s \leq 1$, the parabolic arc length can be estimated to simplified.

$$L_d = L_s \left[1 + \frac{8}{3} \left(\frac{H}{L_s}\right)^2 + \frac{32}{5} \left(\frac{H}{L_s}\right)^4 \right] \dots\dots\dots (2.9)$$

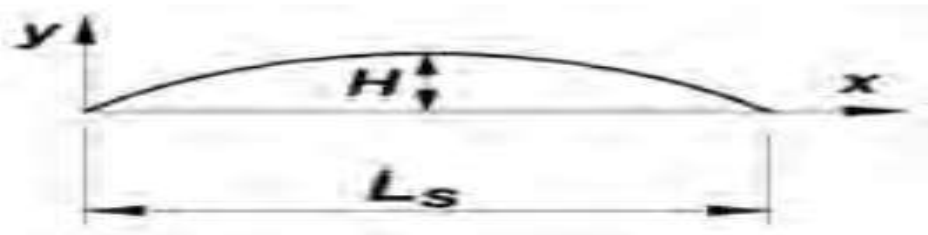


Figure 2. 4: Parabolic arch geometry(Dowswell, 2018)

On the basis of included angle the vertically curved steel structure can be grouped as shallow and deep arches, the expressions for the elastic buckling loads of shallow and deep arches are different. When an arch has an included angle such that $\theta \leq 90^\circ$, it is deemed to be a shallow arch. When an arch has an included angle $\theta > 90^\circ$, it is deemed to be a deep arch. (Pi, Bradford and Tin-loi, 2008)

2.5. Structural behavior of arched steel beam

Arches resist general loading by a combination of predominant axial compression and bending actions. Under these actions, an arch which is adequately braced by lateral restraints so that its out-of-plane failure is fully prevented, may suddenly buckle and fail in the plane of its loading. Figure below shows the most possible loading condition of fixed arched structure.

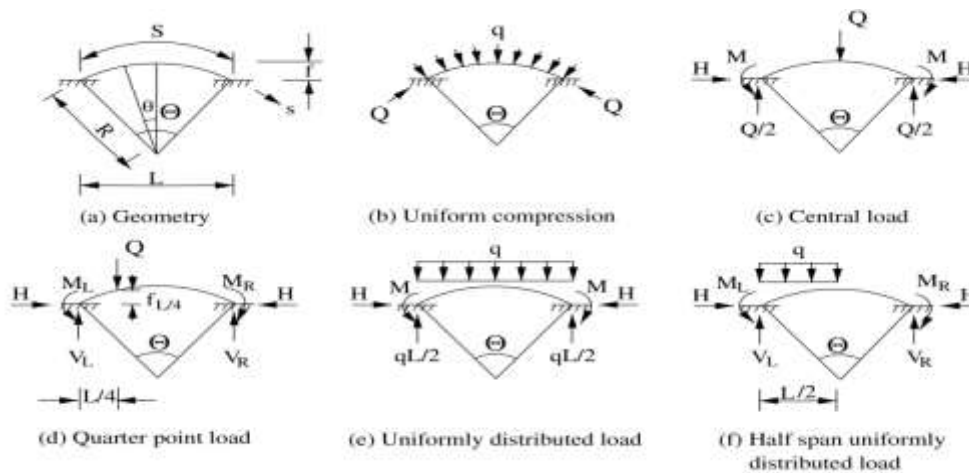


Figure 2. 5: Geometry and loading. (a) Geometry; (b) uniform compression; (c) central load; (d) quarter point load; (e) uniformly distributed load; (f) half span uniformly distributed (Pi, Bradford and Tin-loi, 2008)

2.5.1. In-plane stability of arched steel structure

An arch which is adequately braced by lateral restraints so that its out-of-plane failure is fully prevented, may suddenly buckle and fail in the plane of its loading. Because arch loads are carried primarily by compression, the in-plane strength is dependent on the support stiffness (Pi et al., 2007). Support spreading significantly reduces the strength. Flexible supports and a low rise-to-span ratio can lead to high in-plane arch deflections. Where deflections are significant, a second-order analysis with geometric nonlinearities is required to determine the second-order

arch loads. In this case, the analysis must properly account for in-plane deformations, including the effect of member axial shortening and the horizontal support.

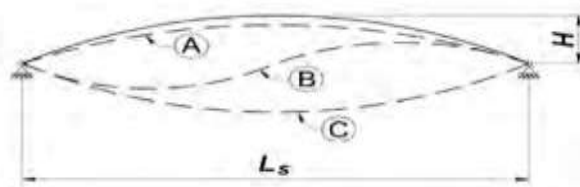
Fully laterally restrained Structural steel arches may fail either through snap-through buckling or by asymmetric buckling mode. Arches must be designed to prevent snap-through buckling, which is a type of in-plane instability that is sensitive to second-order effects and support spreading. Snap-through buckling can occur in a symmetric mode or an asymmetric mode, shown by deformed shapes C and B in Figure 2.6-4(a), respectively. Shape an in Figure 6-4(a) shows the deflected shape at imminent buckling. Because this limit state is difficult to predict, arches are preferably proportioned so that any in-plane instability will be limited by the asymmetric buckling modes shown in Figures 2.6(b) and 2.6(c).

Snap-through buckling mode can be prevented by ensuring the span slenderness, L_s/r_i , exceeds a minimum critical value, where L_s is the span distance and r_i is the in-plane radius of gyration (CEN, 2009; Pi et al., 2002; Schreyer and Masur, 1966). sets minimum span slenderness values, $(L_s/ r_i)_{crit}$, for pinned and fixed-end conditions and rise-to-span ratios, H /L_s , between 0.1 and 0.2 are listed in Table 2.1. Generally, snap-through buckling is not critical for arches with rigid supports and rise-to-span ratios greater than 0.2. (Dowswell, 2018)

Table 2 1: Minimum span slenderness (CEN, 2009; Pi et al., 2002; Schreyer and Masur, 1966).

End conditions	H/L _s		
	0.10	0.15	0.20
Pinned	59	36	35
Fixed	150	71	68

When snap-through buckling is prevented, arches buckle in the asymmetric modes shown in Figures 2.6(b) and 2.6(c) for pinned and fixed arches, respectively. These buckling modes are less sensitive to second-order effects and support spreading



a) Snap-through buckling

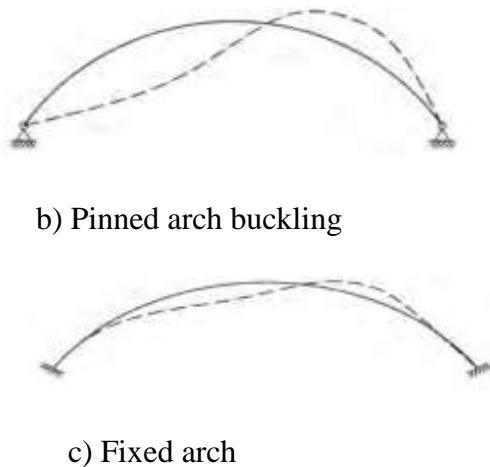


Figure 2. 6: In plane buckling shapes (Dowswell, 2018)

2.5.1.1. Pure compression

In order to prevent an arch form in plane failure, it's important to be able to predict accurately it's in plane elastic buckling load that's is needed for design.

The elastic buckling load of arches under uniform compression can be used as a reference load in the formulation for their in-plane strength design. (Pi, Bradford and Tin-loi, 2008). Studied the elastic buckling of arches under uniform compression. It was found that for in-plane buckling, arches usually buckle in an ant symmetric bifurcation mode and only very shallow arches buckle in a symmetric instability mode.

(Pi, Bradford and Uy, 2002) investigate analytically the elastic in-plane stability of both pin-ended and fixed circular arches with an arbitrary cross-section and subjected to a radial uniformly distributed load around arch axis by using energy method to verify on their research the so called classical buckling theory does not account for the often significant effects of pre-buckling deformation and nonlinearity on buckling, it cannot be used to predict accurately the in-plane buckling of shallow arches . And propose analytical approximation solution to the symmetric buckling of the shallow arches and formulas for the in-plane buckling load of both shallow and non-shallow arches. Buckling load for arches was obtained by as described in the following.

When an arch has an included angle such that $\theta \leq 90^0$, it is deemed to be a shallow arch and Dimensionless parameter λ defined by

$$\lambda = \frac{S\theta}{4r_x} \dots \dots \dots (2.10)$$

Where S is the length of the arch and r_x is the radius of gyration of the cross-section about its major principal axis given by $r_x = \sqrt{I/A}$, with A =being the area of the cross-section and I being the second moment of area of the cross-section about its major principal axis.

For a pin-ended shallow arch, its buckling load is given by

$$N_{acr} = \begin{cases} (0.15 + 0.006\lambda^2)N_{cr} & \text{for } 3.88 \leq \lambda \leq 9.38 \\ \left(0.26 + 0.74\sqrt{1 - \frac{0.63\pi^4}{\lambda^2}}\right) N_{cr} & \text{for } \lambda > 9.38 \end{cases} \dots \dots \dots (2.11)$$

Where N_{cr} is the second mode elastic flexural buckling load of a corresponding pin-ended column with the same length.

For a fixed shallow arch, its buckling load is given

$$N_{acr} = \begin{cases} (0.36 + 0.001\lambda^2)N_{cr} & \text{for } 9.87 \leq \lambda \leq 18.6 \\ \left(0.6 + 0.4\sqrt{1 - \frac{3.109\pi^4}{\lambda^2}}\right) N_{cr} & \text{for } \lambda > 18.6 \end{cases} \dots (2.12)$$

When an arch has an included angle $\Theta > 90^\circ$, it is deemed to be a deep arch, and its elastic buckling load is given by

$$\begin{aligned} N_{acr} &= [1 - (\theta/\pi)^2]N_{cr} && \text{For pin-ended arches} \\ N_{acr} &= [1 - (\theta/1.43\pi)^2]N_{cr} && \text{For fixed-ended arches} \dots \dots \dots (2.13) \end{aligned}$$

Where N_{cr} is the second mode elastic flexural buckling load of a corresponding pin-ended or fixed column with the same length.

The second buckling load N_{cr} of the corresponding column in these equations is given by

$$N_{cr} = \pi^2 EI / (kS)^2, \text{ which } k = \begin{cases} 0.5 & \text{for pin - ended arches} \\ 0.35 & \text{for fixed - ended arches} \end{cases} \dots \dots \dots (2.14)$$

Where E is the young's modulus.

2.5.1.2. Pure flexure

Vertically curved members in building structures are designed for combined axial compression and in-plane flexural loads. Therefore, vertically curved members in building structures are designed for combined axial compression and in-plane flexural loads.

When a beam-column is subjected to moment along its unbraced length it will be displaced laterally in the plane of bending .the result will be an increased or secondary moment equal to the axial compression load times the lateral displacement or eccentricity. This moment will cause additional deflection, which will in cause a larger lateral deflection, and so on until equilibrium is reached. The required total flexural strength of a member must equal at least the sum of the first –order and second moment’s several methods are available for determining this required strength, ranging from very simple approximation to very rigorous procedures.(McCormac, 1995)

Second order effect

Modern stability design provisions are based on the premise that the member forces are calculated by second-order elastic analysis, where equilibrium is satisfied on the deformed geometry of the structure.(ANSI/AISC-360-10, 2010)

Under compression, the arch member shortens, causing a vertical deflection at the apex. For in-plane deflection, arch behavior is similar to that of a beam-column. Second-order moments can be calculated either by using a second-order analysis or by amplifying the moments from a first-order analysis. The amplification factors in AISC Specification Appendix 8 for straight members are also accurate for curved members (Pi and Bradford, 2004; Pi and Trahair, 1999). The required in-plane flexural strength based on the amplified first-order moment is as Equation 2.15.(Dowswell, 2018)

$$M^* = \delta_b M_m \quad \text{With} \quad \delta_b = \frac{1}{1 - \alpha \frac{N^*}{N_{acr}}} \quad \dots\dots\dots (2.15)$$

Where M_m =first-order moment about the axis of curvature causing In-plane flexure

N_{acr} =elastic in-plane critical buckling load

N^* =required (acting) axial load

2.5.1.3. Circular Arches Loaded in Bending and Compression

Beam-columns are structural members which combine the beam function of transmitting transverse forces or moments with the compression (rarely tension) member function of transmitting axial forces.

Many design codes do not give methods for designing steel arches against in-plane failure under combined bending and compression. The few that do provide methods that are essentially based on a linear interaction equation for the in-plane strengths of an equivalent beam-column, which uses the maximum elastic bending moment and axial compression in the arch. However, the linear interaction equation for a beam-column may not be suitable for an arch because it does not consider the strength characteristics of steel arches. It is found that the design equation for steel columns cannot be used directly for steel arches in uniform compression, nor can the design interaction equations for steel beam-columns be used directly for steel arches under non-uniform compression and bending. (Yong -lin pi, 1999).

The in-plane strength of a steel arch subjected to combined bending and axial compressive actions is complex, and is related to a number of factors, such as the buckling behavior, yielding, the initial curvature, the included angle, the slenderness, the shallowness, residual stresses, initial in-plane geometric imperfections, and loading conditions. It is therefore difficult to develop simple and accurate equations for the design of arches that are subjected to the combined bending and axial compressive actions against in-plane failure. Instead, a lower bound interaction equation for the in-plane strength of arches has been sought based on the accurate numerical results. (Pi, Bradford and Tin-loi, 2008).

Pi and Trahair (1999) and Pi and Bradford (2004) studied the in-plane inelastic stability of hinged and fixed circular arches with I-shape cross sections. These studies included initial imperfections, residual stresses, including subtended angle ranging from 10-180 under different loading cases and proposed the following lower bound interaction equation with The modification factor α_{am} accounts for the combined effects of the initial curvature, the included angle and the slenderness of the arch, and the non-uniform distribution of bending moment over the arch length, while the modification factor α_{an} accounts for the non-uniform distribution of axial compressive force over the arch length. The effects of the included angle and the

slenderness of the arch have already been accounted in the in-plane axial compression capacity N_{acr} . The values of α_{an} and α_{am} are given in Table 2.2 for pin-ended arches and in table 2.3 for fixed arches.

$$\frac{N^*}{\Phi\alpha_{an}N_{acx}} + \frac{M^*}{\Phi\alpha_{am}M_P} \leq 1 \text{ -----2.16}$$

Where N^* – maximum axial compression based on first order analysis

M^* -maximum moment

Φ – capacity reduction factor = 0.9

N_{acx} – the axial compression capacity for uniform compression

α_{an} – the axial compression modification factor

α_{am} – the moment modification factor

M_P – plastic section capacity about major axis

λ – slenderness of the arch

Table 2. 2: Modification factors for in-plane strength of pin-ended arches

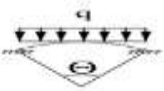
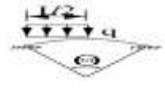
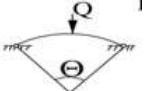

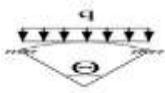


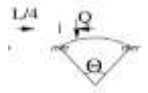
Arch with loading condition					
α_{an}		1.000	1.00	1.10	1.10
α_{am}	$\lambda < 9.38$	1.13 + 0.146 λ	$1 + 0.021\lambda$	$1.35 + 0.069\lambda$	$1.1 + 0.053\lambda$
	$\lambda > 9.38$	2.50	1.20	2.00	1.60

Table 2. 3: Modification factor for in-plane strength of fixed arches

Arch with loading condition					
α_{an}		1.00	1.00	1.10	1.10
α_{am}	$\lambda < 18.6$	2.0 + 0.1(18.6 - λ) θ/π	1.2 + 0.5(18.6 - λ) θ/π	1.5 + 0.05(18.6 - λ) θ/π	1.8 + 0.05(18.6 - λ) θ/π
	$\lambda > 18.6$	2.0	1.20	1.50	1.80

It is noted that for a pin-ended arch with $\lambda < 3.88$ or a fixed arch with $\lambda < 9.87$ that is subjected to a radial load uniformly distributed around it, the arch becomes very shallow and can be treated as a beam with initial in-plane geometric imperfection. Hence, the proposed Eq. 2.16 is not suitable in this case.(Pi, Bradford and Tin-loi, 2008) .

2.5.2. Out-of-plane stability of arches

When applied forces acting in the plane of a curved member such as an arch reach a certain critical level, a combination of twisting and lateral bending will cause the member to deflect laterally and twist out of the plane of loading and fail in a flexural –torsional buckling mode. The critical load is influenced by the nature and distribution of the loads, the shape of the axis of the arch, the variation of the flexural and torsional stiffness of the cross sections along the length axis, and restraint available at the supports and other brace points.

For a steel arch, residual stresses either resulting from non-uniform cooling of the material during fabrication or caused by welding or cold working (roller bending) the material into an arch are also important factors. The multiplicity of impacting parameters prevents the development of simple and widely applicable rules for the determination of buckling loads.(Ziemain, 2010)

(Pi, Yong-lin, Trahair, 1998) and (Pi and Bradford, 2005) studied the out-of-plane stability of pin-ended and fixed –ended freestanding circular arches of I-sections using a finite –element

Where, for hinged arches

$$k_a = \frac{1}{2} \left[- \left(1 + \frac{a^2}{b^2} \right) \frac{N_T}{N_{EY}} - \left(1 - a^2 \right)^2 + \sqrt{\left(1 + \frac{a^2}{b^2} \right)^2 \frac{N_T^2}{N_{EY}^2} + 2 \left(\frac{a^2}{b^2} - 1 \right) \left(1 - a^2 \right)^2 \frac{N_T}{N_{EY}} + \left(1 - a^2 \right)^4} \right] \dots\dots\dots 2.18$$

For fixed arches

$$k_a = \frac{1}{2} \left[- \left(1 + \frac{a^2}{b^2} \right) \frac{N_T}{N_{EY}} - \left(1 - a^2 \right)^2 - \sqrt{\left(1 + \frac{a^2}{b^2} \right)^2 \frac{N_T^2}{N_{EY}^2} + \left(\frac{a^2}{b^2} - 1 \right) \left(1 - a^2 \right)^2 \frac{N_T}{N_{EY}} + \left(1 - a^2 \right)^4} \right] \dots\dots\dots 2.19$$

Whith N_{EY} minor axis buckling load of a column of length S , $N_{EY} = \frac{\pi^2 E I_y}{(S/c)^2}$ where $c=1$ for hinged and $c=2$ for fixed, $a = \frac{S}{c} / \pi R$, and $b = \frac{\pi M_{yz}}{N_{EY} (S/c)}$. the torsional buckling load N_T of a column and lateral-torsional buckling moment M_{yz} For beam in uniform bending given by

$$N_T = \frac{A}{I_x + I_y} \left(GJ + \frac{\pi^2 E I_w}{(s/c)^2} \right) \dots\dots\dots 2.20$$

$$M_{yz} = \sqrt{N_{EY} \left(GJ + \frac{\pi^2 E I_w}{(s/c)^2} \right)} \dots\dots\dots 2.21$$

2.5.2.1. Elastic Buckling of Circular arches in uniform moment

Uniform Moment an arch is loaded in uniform bending when equal couples are applied about the x-axis and the ends are fixed against translation in the x-direction but are free to rotate about the x-and y-axes. Although this load case rarely exists in practice, it is useful as a reference load. Uniform bending can cause buckling out of the yz plane if the flexural stiffness about the x-axis is large in comparison to both the flexural stiffness about the y-axis (=EI_y)and the St.-Venant torsional rigidity of the cross section about the z –axis (=GJ). (Ziemain, 2010)

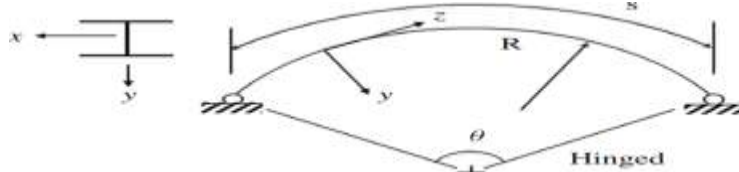


Figure 2. 7: Geometry of arch (Ziemain, 2010)

The most recent solutions are given by

$$M_{ays} = k_{as}M_{yz} \dots\dots\dots 2.22$$

Where ,for honged arches (pi and Trahair 1998)

$$k_{as} = -ab - \frac{a}{2b} + \frac{a^3b}{2} + \sqrt{\left(-ab - \frac{a}{2b} + \frac{a^3b}{2}\right)^2 + (1-a^2)^2} \dots\dots\dots 2.23$$

For fixed arches(Pi and Bradford 2005),

$$k_{as} = -\frac{ab}{2} - \frac{a}{2b} + \sqrt{\left(\frac{ab}{2} + \frac{a}{2b}\right)^2 + (1-a^2)^2} \dots\dots\dots 2.24$$

The parameters *a* and *b* are the same as those defined in above equation


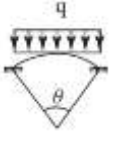
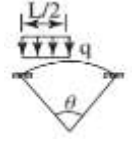
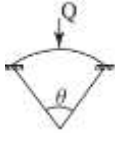
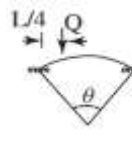
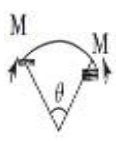
2.5.2.2. Design criteria for out-of-plane stability

Pi and Trahair (1998, 2000) and Pi and Bradford (2005) studied the out-of-plane stability of freestanding circular arches of I-sections including imperfections, residual stresses, and inelasticity. The support conditions studied included in- and out-of-plane hinged arches, which are prevented to twist about the longitudinal axis at the supports, and in- and out-of-plane fixed arches. And have proposed lower bound equation with modification factor given in table 2.4 to check the out-of-plane stability,

$$\frac{N^*}{\alpha_{any} \cdot N_{acys}} + \frac{M^*}{\alpha_{amy} \cdot M_{amys}} \leq \phi \dots\dots\dots 2.25$$

Where N*and M*are the maximum axial compression moments based on a First-order elastic analysis, α_{any} – axial compression and α_{amy} – moment modification factors (Table 2.4), ϕ the capacity reduction factor with a value of 0.9. $N_{acys} = \alpha_{acys} N_y$, $N_{acys} = \alpha_{acys} N_y$ -out of pane strength for uniform compression for hinged and fixed arch respectively. α_{acys} -Arch slenderness reduction factor, N_y -the axial yield (squash) load of cross-section, M_{amys} -the out of plane strength under uniform bending given by $M_{amys} = \alpha_{says} M_{px}$, $M_{amys} = \phi \alpha_{says} M_{px}, \leq M_{px}$, -for hinged and Fixed arch respectively, M_{px} , -full major axis plastic moment capacity. (Ziemain, 2010)

Table 2. 4: Factors for the out -of plane design of circular arches

Arch with loading condition							
α_{any}	1.0	1.1	1.5	1.4	2.7	-	
$\alpha_{amy.}$	-	1.1	1.1	1.2	1.2	-	
α_{any}	-	1.2	1.6	1.4	2.2	-	
$\alpha_{amy.}$	-	2.2	2.2	1.5	1.8	1	

2.6. Behavior of cellular beam

Due to the presence of the significant number of web openings, cellular beams cannot be treated as solid-web members or members with web openings. These structural members are highly indeterminate elements, which do not lend themselves to a simple method of analysis. The presence of web openings introduces many additional failure modes not present in solid web members. (Sameer S.Fares, John Coulson, 2016)

(Kerdal and Nethercot, 1984) were the first authors who have described the possible six main failure modes of castellated beams, which are beams with uniformly distributed hexagonal openings. These failure modes can be categorized in to global and local. The global failure modes are similar to those of full web beams such as the lateral torsional buckling, the global shear failure or the bending failure. The local failure modes are specific to the beams with web openings.

The predominant local failures modes specific to the beam of repeating circular web openings are the Vierendeel yielding, the web-post buckling and the web-post welding fracture.

2.6.1. Vierendeel yielding of cellular beam

Vierendeel bending is caused by the transfer of shear force across the openings in order to be consistent with the rate of change of bending moment along the beam. Vierendeel failure occurs by the formation of plastic hinges at four locations around the opening in the regions of high shear. The global shear force passing through the opening creates a localized bending moment in

the top and bottom tees, known as the Vierendeel moment. The global bending moment and shear forces change along the length of the beam; consequently, it is necessary to examine the interaction of the global shear and moment at each web opening along the entire length of the beam. By examining the interaction of the global moment and shear at each opening, a critical opening can be identified. The global shear and moment interact to produce an overall stress; therefore, the most efficient use of the beam is in a situation where the maximum global shear and moment occur away from each other such as a simply supported beam with a uniform load. (Sameer S.Fares, John Coulson, 2016)

The flexural capacity of the upper and lower tees under Vierendeel bending is critical. The transfer of shear forces across a single web opening causes secondary bending stresses. The Vierendeel bending stresses around the hole may be calculated using Olander's approach. Olander utilizes a circular section for the position of the critical section and the ultimate resistance of the tees. For asymmetrical sections, the shear force is resisted by the upper and lower web sections in proportion to their depth squared. For symmetrical sections, the shear force is divided equally between upper and lower web sections. (Durif, Bouchaïr and Vassart, 2013).



Figure 2. 8: Vierendeel yielding mechanism (Durif, Bouchaïr and Vassart, 2013) and (Warren, 2001)

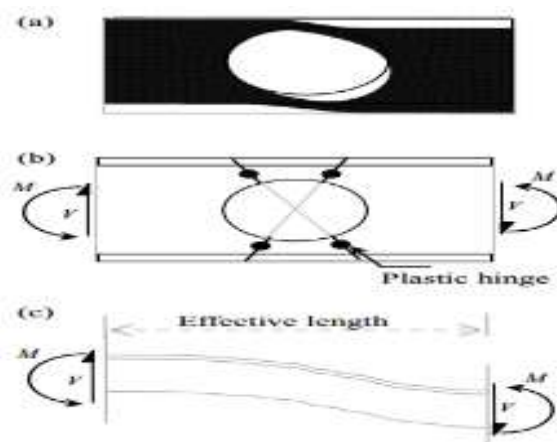


Figure 2. 9: Vierendeel mechanism of a steel beam with a circular opening: (a) Vierendeel failure, (b) plastic hinges and (c) Vierendeel bending and effective length(Panedpojaman and Rongram, 2014).

2.6.2. Web post buckling (yielding) of cellular beam

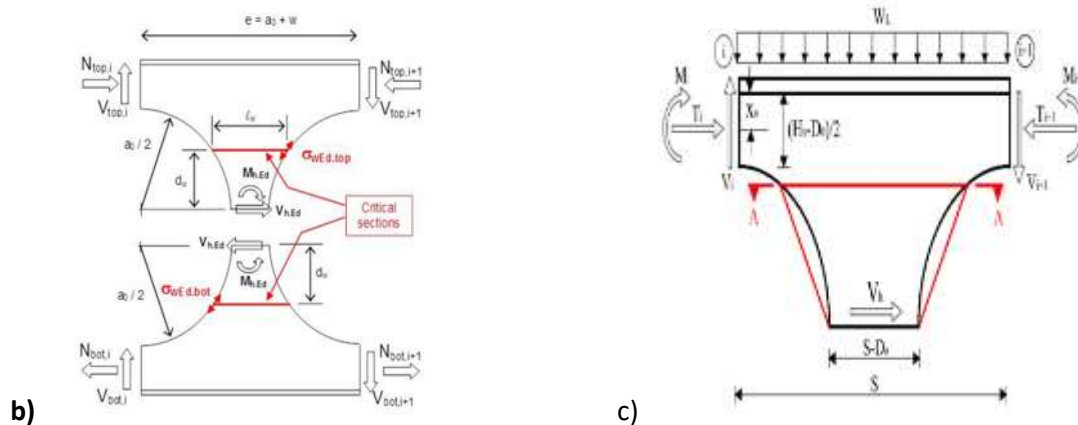
Web-post buckling is the loss of stability of the web-post caused by compression stresses due to the horizontal shear force passing through the web post. The ultimate strength of the web post is governed by one of two modes of Flexural failure caused by the development of a plastic hinge in the web post and buckling failure of the web post. During this phenomenon, the web-post twists over its vertical axis, assuming the shape shown. In Figure 2.9(a, b). The forces equilibrium due to shear is shown in Figure 2.9(c).

Web post buckling of cellular beam is dependent on the geometry and the thickness of the web post. Separate checks are made for the top and bottom tees, which may have different thicknesses and available strengths.

The web-post buckling is one of the predominant failure mode of cellular beams, regardless of the ratio between depth and span. (Figueiredo *et al.*, 2018)



(a)



b)

c)

Figure 2. 10: a) web post buckling failure mode and b) local forces and position of the critical sections in the intermediate web-post C) horizontal shear in the web post of cellular beam (Durif, Bouchaïr and Vassart, 2013)

2.6.3. Rupture of the welded joint

Rupture of a welded joint in a web-post can result when the width of the web-post or length of welded joint is small. This mode of failure is caused by the action of the horizontal shearing force in the web-post, which is needed to balance the shear forces applied at the points of contra flexure at the end of the upper I section.

2.7. Analysis and design of cellular beam

The ultimate state design of a steel beam necessitates check of its strength and serviceability. The computation of the strength of a beam with web openings is determined by considering the interaction of flexure and shear at the openings. Consequently the constraints to be considered in the design of a cellular beam include the displacement limitations, overall beam flexural capacity, beam shear capacity, overall beam buckling strength, web post flexure and buckling, Vierendeel bending of upper and lower tees, local buckling of compression flange and practical restrictions for cell diameter and the spacing between cells (Erdal and Polat, 2013)

The design procedure given here is taken from The Steel Construction Institute (SCI) Publication No: 100 titled “Design of Composite and Non-composite Cellular Beams The design methods are consistent with BS5950 parts 1 and 3, the basic geometry and notations used for these beams are shown in Figure.2.11. Although the diameter of holes and spacing between their centers are left to the designer to select the following ratios are required to be observed

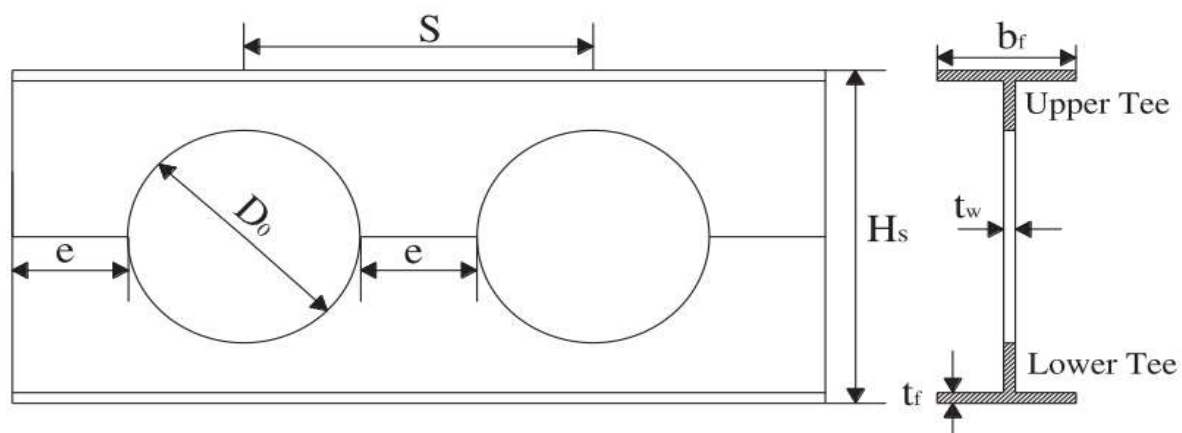


Figure 2. 11: Geometrical parameters of cellular beam

2.7.1. Guidelines for web perforations

The dimensions were chosen according to the BS: 5950 part 1, part 3.1 and SCI publication 100. The depth of the circular web opening (D_o), total depth of beam (H_s) and center to center spacing of cellular opening (S) are limited to the interval given in equation 2.26 and 2.27 to prevent Vierendeel effects before web post buckling failure.

$$1.08 < \frac{s}{D_o} < 1.5 \text{ --- --- --- --- --- 2.26}$$

$$1.25 < \frac{H_S}{D_o} < 1.75 \text{ --- --- --- --- --- 2.27}$$

2.7.2. Overall beam flexural capacity

Under favorable applied load combinations the cellular beam should have sufficient flexural capacity to be able to resist the external loading. That is the maximum moment MU under applied load combinations should not exceed plastic moment capacity MP of the cellular beam.

$$M_U = A_{LT} P_Y H_U \leq M_P \text{-----2.28}$$

Where A_{LT} is the cross sectional area of lower tee, P_Y is the design strength of steel and H_U is distance between centrals of upper tee and lower tee

2.7.3. Beam shear capacity

2.7.3.1. Vertical shear failure

It is necessary to check two shear failure modes in cellular beams. The first one is the vertical shear capacity check in the beam. The sum of the shear capacities of the upper and lower tees gives the vertical shear capacity of the beam. The factored shear force in the beam should not exceed P_{VY}

$$P_{VY} = 0.6P_Y(0.9A_{WUL}) \text{ --- --- --- --- --- 2.29}$$

Where A_{WUL} is the total cross sectional areas of webs of tees.

2.7.3.2. Horizontal shear failure

The other check is for the horizontal shear failure. The horizontal shear is developed in the web post due the change in axial forces in the tee as shown in Figure.2.12. The horizontal shear in the web post of beam should not exceed nominal shear capacity P_{VH} where:

$$P_{VH} = 0.6P_Y(0.9A_{WP}) \text{ --- --- --- --- --- 2.30}$$

Where $A_{WP} = e * t_w$, $e = s - D_0$ (mm²) the minimum area of the web-post. Neglecting the effect of the applied load and considering the vertical equilibrium and the rate of the variation of

bending moment as shown in Figure. 2.12, then the following equations can be written for cellular beams.

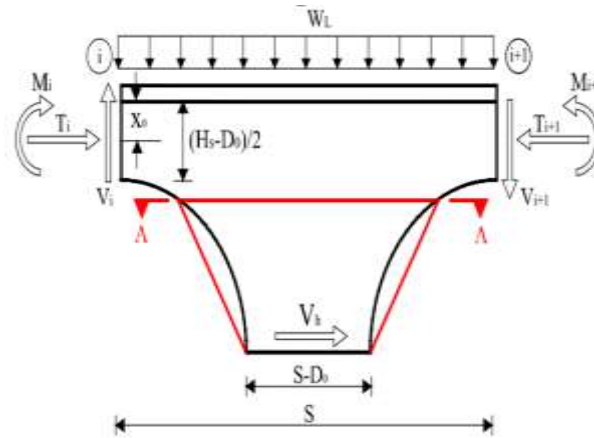


Figure 2. 12 :Horizontal shear in the web post of cellular beam (Erdal and Polat, 2013)

$$V_{i+1} = V_i$$

$$M_i = T_i \times (H_s - 2X_o)$$

$$V_{i+1} = \frac{dM}{dX} = \frac{M_{i+1} - M_i}{S} = (T_{i+1} - T_i) \times \left(\frac{H_s - 2X_o}{S}\right)$$

For horizontal equilibrium

$$V_h = T_{i+1} - T_i = V_{i+1} \frac{S}{H_s - 2X_o} \dots\dots\dots 2.31$$

Where V is shear force, T is axial force and M is bending moment at the cross section of the cellular beam, S is distance between circular opening centers, X_o is the distance between the axial forces to flange.

2.7.4. Flexural and buckling strength of web-post

For cellular beams, a similar set of equations was developed through destructive testing by the Steel Construction Institute of the United Kingdom (Ward, 1990). There are three values (C1, C2 and C3), which are functions of the properties of the web post that are used to calculate the buckling capacity of the web post as a function of the web post elastic capacity at a critical section 0.9R as shown in Figure 2.12. The equations given below are the result of detailed

nonlinear finite element studies, and only applicable for $1.08 \leq S/D_o \leq 1.50$ and $1.25 \leq d_g/D_o \leq 1.75$.(Sameer S.Fares, John Coulson, 2016).

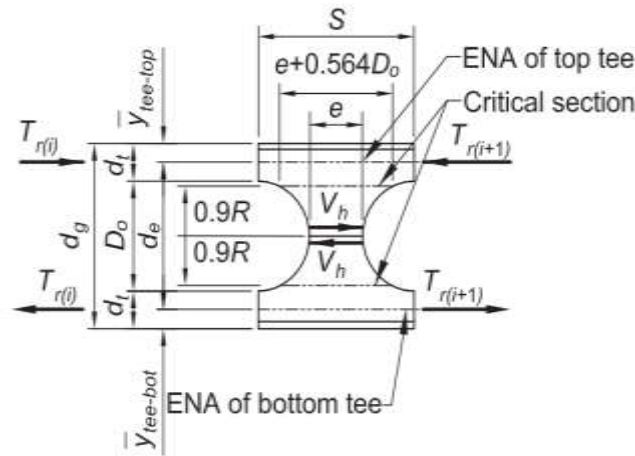


Figure 2. 13: Location of critical buckling section of cellular beam

The required flexural strength in the web post can then be determined by:

The elastic bending moment M_e , at $0.9R$ is given by

$$M_e = \frac{t_w(S-D_o+0.564D_o)^2}{6} F_y \dots\dots\dots 2.32$$

$$\frac{M_{MAX}}{M_E} = \left[C_1 \left(\frac{S}{D_o} \right) - C_2 \left(\frac{S}{D_o} \right)^2 - C_3 \right] \dots\dots\dots 2.33$$

where , M_{MAX} = maximum allowable web post moment

M_E = elastic bending moment

And $C_1 C_2 C_3$ = are constants evaluated as follows

$$C_1 = 5.097 + 0.1464 \left(\frac{D_o}{t} \right) - 0.00174 \left(\frac{D_o}{t} \right)^2 \dots\dots\dots 2.34$$

$$C_2 = 1.41 + 0.0625 \left(\frac{D_o}{t} \right) - 0.000683 \left(\frac{D_o}{t} \right)^2 \dots\dots\dots 2.35$$

$$C_3 = 3.645 + 0.0853 \left(\frac{D_o}{t} \right) - 0.00108 \left(\frac{D_o}{t} \right)^2 \dots\dots\dots 2.36$$

2.8. Factors determine structural performance of cellular beam

It has been observed from the experiments that stiffness and ultimate load of the steel beam with web openings decrease with an increase in the opening area (i.e. decrease in the S/Do ratio). Rectangular openings were found to be very critical as they show very high stress concentration around the corner regions. It is also seen that the deformations of the rectangular openings are large compared to the other type of web openings. (Morkhade and Gupta, 2015).

(Krishnachandran, 2016) found that on their Experimental and Analytical Investigations of Cellular Steel Beams Value of deflection is minimum for circular web opening of same section of beam compared to other shapes of cuts. Also the load carrying capacity is high for cellular beams. Therefore it is concluded that cellular beam is best for structural applications also concludes from parametric study of cellular The parametric study of cellular beam shown that the deflection decreases with increase of spacing ratio due to the increase of stability with spacing and deflection increases with increase of aspect ratio of cellular steel beams

According to study of (Nimmi and Krishnachandran, 2016) provision of transverse stiffeners and ring stiffeners improve the buckling resistance of cellular beam .when come to comparison transverse stiffeners are structurally efficient than ring stiffeners in resisting buckling of cellular beam in addition transverse stiffeners is economic and easily manufactured.

(Madjour, Soltani and Harkati, 2018) numerically investigate the effect of beam to column connection on the structural performance of cellular beam and found that Large circular and sinusoidal web beam openings located close to the beam to column joint have little effects on the characteristics of the connection. Thus, the characteristics of the endplate connections with perforated beams can be calculated by the same methods used for joints with solid beams in addition, in their studies they figure out that The adoption of flush endplate or extended endplate cellular beam to column joints improves significantly the ultimate load and deflection of cellular beams when compared to simply supported ones and The adoption of extended endplate cellular beam to column joints instead of flush endplate does not improve either the ultimate load or the stiffness of cellular beams.

CHAPTER THREE
METHODOLOGY

These research was correlational research aimed to explore the relation of selected dependent variable on in plane structural performance and behavior of arched cellular steel beam using commercial finite element simulation software Abaqus 6.14 by using previously reported experimental report as a bench mark for analysis and results validation. Figure 3.1 shows the steps followed to achieve set goal.

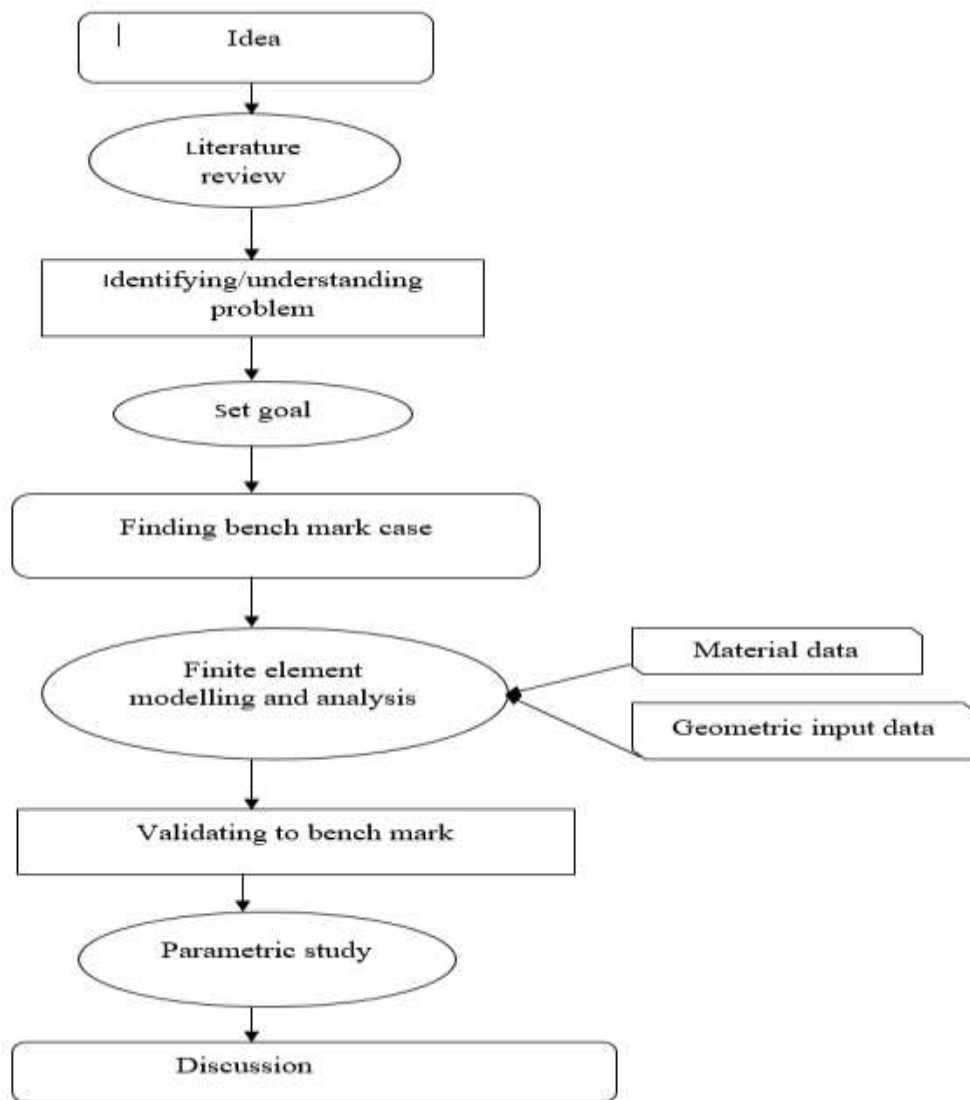


Figure 3. 1: Research design chart

3.1. Population

The Population in this research is a fully laterally restrained vertically curved (arch) I- section hot rolled steel cellular beam with differing the selected parameters that assumed to affect the structural performance, failure mode and structural response of curved cellular beam.

3.2. Sampling size and sampling procedure

3.2.1 Section geometry selection

For these studies cellular steel arches formed from double-symmetric welded I –section with sectional dimension of the I-section is $H_s \times b_f \times t_w \times t_f = 250\text{mm} \times 120\text{ mm} \times 8\text{ mm} \times 12\text{ mm}$, classified as class 1 as shown in Appendix-E. Where h , b , t_w , and t_f are the overall height and width, the thicknesses of web, and the thicknesses of flange of the cross Section, respectively as described in Figure 3.2.

The web post length(S) and opening diameter(D_o) were chosen according to the BS EN 1-1 as described in the literature review of these paper .To avoid vierendeel effect before web post buckling the opening diameter and web post length of cellular beam should be within range of $1.25 < \frac{H_s}{D_o} < 1.75$, and $1.08 < \frac{S}{D_o} < 1.5$

To meet this criteria $D_o = 160\text{mm}$, $S = 220\text{mm}$ and end post length 400 mm used for these studies.

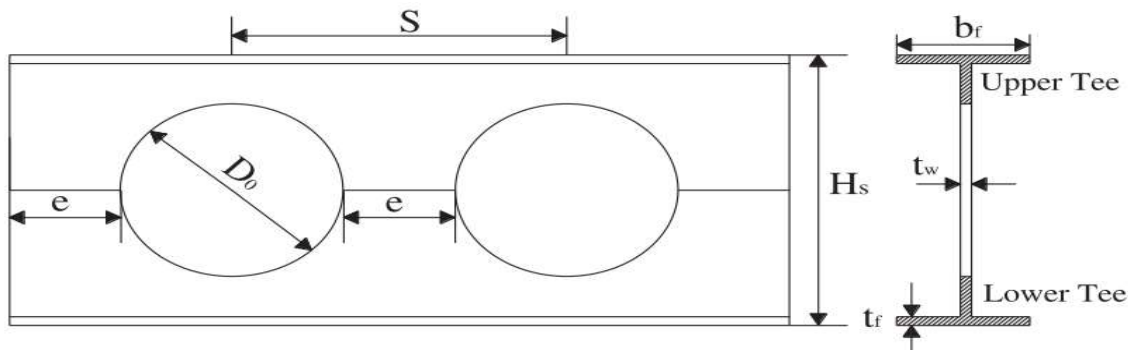


Figure 3. 2: Parameters of cellular beam

3.2.2. Sampling

To represent all possible type of cellular steel arch used in real structure these studies were used a criteria for classification of arched steel structure such as arch geometry (circular and parabolic), deep and shallow arch depending on included angle and loading condition as described briefly in literature review of this paper.

Table 3. 1: Selected sample parameters

specimen	Rise to span ratio(H_s/L)	Included angle in degree	Arch radius(mm)	Arch rise(mm)	Opening diameter(mm)	Span length(m)	Load case-1	Load case-2
Circular arch geometry								
SCC-1	0.099	45	3280.316	247.5	160	2500	MSPL	URDVL
SCC-2	0.133	60	2515.87	332.5	160	2500	MSPL	URDVL
SCC-3	0.207	90	1768.41	517.5	160	2500	MSPL	URDVL
DCC-1	0.283	120	1457.99	707.5	160	2500	MSPL	URDVL
DCC-2	0.35	140	1330.35	875	160	2500	MSPL	URDVL
DCC-3	0.419	160	1269.57	1047.5	160	2500	MSPL	URDVL
DCC-4	0.5	180	1250	1250	160	2500	MSPL	URDVL
SCC-3000	0.207	90	2122.09	621	160	3000	MSPL	URDVL
DCC-3000	0.35	140	1596.42	1050	160	3000	MSPL	URDVL
specimen	Rise to span ratio(H_s/L)	Arch radius(mm)	Arch rise(mm)	Opening diameter(mm)	Span length(m)	Load case-1	Load case-2	
Parabolic geometry								
PSC-1	0.099	3280.316	247.5	160	2500	MSPL	URDVL	
PSC-2	0.133	2515.87	332.5	160	2500	MSPL	URDVL	
PSC-3	0.207	1768.41	517.5	160	2500	MSPL	URDVL	
PDC-1	0.283	1457.99	707.5	160	2500	MSPL	URDVL	
PDC-2	0.35	1330.35	875	160	2500	MSPL	URDVL	
PDC-3	0.419	1269.57	1047.5	160	2500	MSPL	URDVL	
PDC-4	0.5	1250	1250	160	2500	MSPL	URDVL	
PSC-3000	0.207	2122.094	621	160	3000	MSPL	URDVL	
PDC-3000	0.35	1596.42	1050	160	3000	MSPL	URDVL	

*MSPL-mid span concentrated (point) load

*URDVL-uniform radially distributed vertical load

3.3. Study variable

Dependent and independent variables that are closely related with the structural behavior of cellular steel beam are discussed and identified on the phase of literature review. The variables expected to affect the behavior of arched cellular steel beam and focused on to see the effects are listed as follows.

3.3.1. Independent variables

- ✓ Rise-to-span ratio
- ✓ Radius of curvature
- ✓ Loading case
- ✓ Geometry of arch.

3.3.2. Dependent variables

- ❖ Structural behavior of arched cellular I- section steel beam.
 - ✓ Buckling Load to mid-span deflection of the beam
 - ✓ The ultimate load carrying capacity of the beam
 - ✓ Buckling load to out of plane deflection
 - ✓ Failure mode

3.4. Finite element modelling

This research was numerical investigation using commercial finite element simulation software package ABAQUS for modelling and analysis of three dimensional geometry of arched cellular steel beam to achieve the proposed objective .the section below explain the modelling and analysis process of arched cellular steel beam to figure out its behavior under static loading condition.

Finite element analysis (FEA) is a process, which predicts deflection and other effects of stress on a structure. FEA divides the structure into a grid of elements, which forms a model of the real structure. Each of the elements is a simple shape (such as square or a rectangular) for which the finite element program has information to write the governing equation in the form of a stiffness matrix. The unknowns for each element are the displacements at the node points, which are the points at which elements are connected. The finite element program will assemble the stiffness

matrices for the simple elements together to form the global stiffness matrix for the entire model. This stiffness matrix is solved for the unknown displacement at the nodes and the stress at each element can be calculated.

3.5. Modelling and analyzing of arched cellular beam

As described above these research rely on the result extracted from commercial FEA simulation software ABAQUS/standard version 6.14.1, so for convenience the result of the simulation of related experimental work reported on published paper validated to the physical experimental work .the procedure from modelling to parametric investigation of arched cellular steel beam described in Figure 3.3.

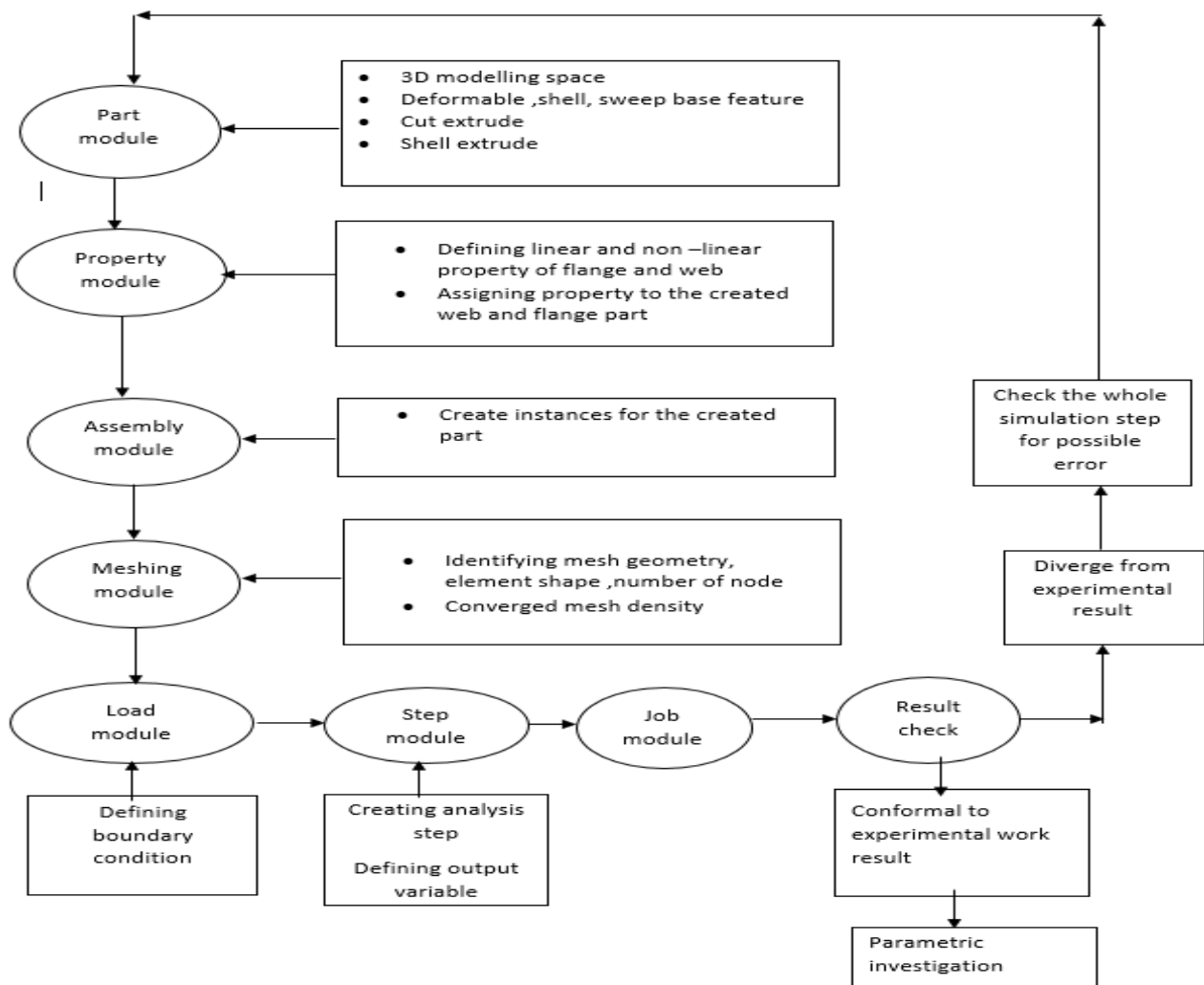


Figure 3. 3: Modelling and analyzing flow chart

3.5.1 Modelling geometry of arched cellular beam

The three dimensional geometry of arched cellular beam and solid arched I-section beam was created using 3D-modelling space, deformable type, shell shape and sweep type base feature using the tools available in part module.

A part created using the Part module tools is called a native part and has a feature-based representation. A feature captures your design intent and contains geometry information as well as a set of rules that govern the behavior of the geometry.

3.5.1.1. Modelling space

Three-dimensional model

Abaqus/CAE embeds the part in the X , Y , and Z coordinate system. A three-dimensional part can contain any combination of solid, shell, wire, cut, round, and chamfer features. ABAQUS allow three-dimensional part using three-dimensional solid, shell, and beam, truss, or membrane elements.

3.5.1.2. Base feature

Sweep

To model three-dimensional parts of arched cellular beam I had sketched two shapes: a sweep path and a sweep profile. The profile is then swept along the path to create the feature using arch through three points for circular arch and spline through points for parabolic arch.

Part type Deformable

Any arbitrarily shaped axisymmetric, two-dimensional, or three-dimensional part that created should be specified as a deformable part. A deformable part represents a part that can deform under load; the load can be mechanical, thermal, or electrical. By default, Abaqus/CAE creates parts that are deformable.

Shell feature

A shell feature is an idealization of a solid in which thickness is considered small compared to the width and depth.



Figure 3. 4: Modelled parts of cellular arched steel

3.5.2 Mechanical material properties

The mechanical properties of structural steel such as stress-strain relation, density, elastic modulus under static load is important in modelling and analyzing steel structure on simulation finite element software. The important mechanical properties of steel used in these research were extracted from the published previous experimental research work carried by (Dou *et al.*, 2015) and (Zaher *et al.*, 2018), on their research report they under taken tensile test coupon to found out the stress-stress relation of the steel member used for their investigation.

3.5.2.1. Stress-strain relation of structural steel

The important mechanical properties of most structural steels under static load are obtained from tensile test coupon. These test methods cover the tension testing of metallic materials in any form at room temperature, specifically, the methods of determination of yield strength, yield point elongation, tensile strength, elongation, and reduction of area. (AASHTO No T68, 2016)

Initially the steel has a linear stress–strain curve whose slope is the Young’s modulus of elasticity E . The values of E vary in the range 200 000–210 000 N/mm², and the approximate value of 205 000 N/mm² is often assumed (EC3 uses 210 000 N/mm²). The steel remains elastic while in this linear range, and recovers perfectly on unloading. The limit of the linear elastic behavior is often closely approximated by the yield stress f_y and the corresponding yield strain $\epsilon_y = f_y/E$. Beyond this limit the steel flows plastically without any increase in stress until the strain-hardening strain ϵ_{st} is reached. This plastic range is usually considerable, and accounts for the ductility of the steel. The stress increases above the yield stress when the strain-hardening strain ϵ_{st} is exceeded, and this continues until the ultimate tensile stress f_u is reached. After this, large

local reductions in the cross-section occur, and the load capacity decreases until tensile fracture takes place. The yield stress f_y is perhaps the most important strength characteristic of a structural steel. This varies significantly with the chemical constituents of the steel, the most important of which are carbon and manganese, both of which increase the yield stress.

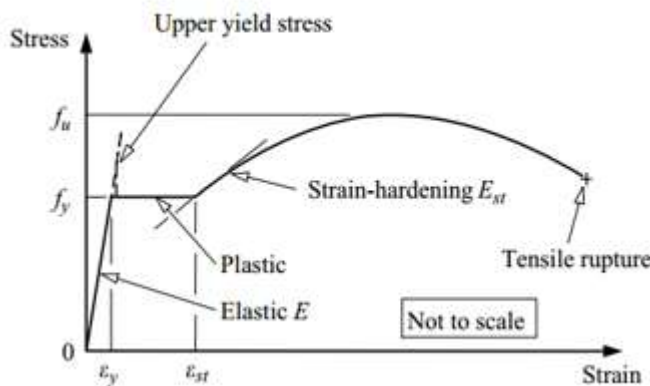


Figure 3. 5: Idealized stress-strain relationship for structural steel. (N.S.Trahair et al, 2008)

For this studies the structural steel properties used for parametric investigation were taken from exipermental data reported by (Dou *et al.*, 2015). according to their research paper on an experimental inestigation into flexural-torsional ultimate resistance of steel circular arches they performed Six tensile test coupons were cut from the flange and web plates of the I-section in the arch segment during manufacturing and were tested through a standard procedure to obtain the engineering stress-strain curves of materials, as shown in Figure. 3.6. For the three coupons from the web plates and flanges mechanical properties obtained were very close to each other with average values of yield stress f_y , modulus of elasticity and ultimate tensile strength f_u . Tabulated as below.

Table 3. 2: Mechanical properties of steel used for parametric investigation

Plate origin	Plate thickness(mm)	yield strss f_y (N/mm ²)	modulus of elasticity E_s (MPa)	ultimate stress f_u (N/mm ²)
Web	8	315	213×10^3	430
Flange	12	285	202×10^3	440

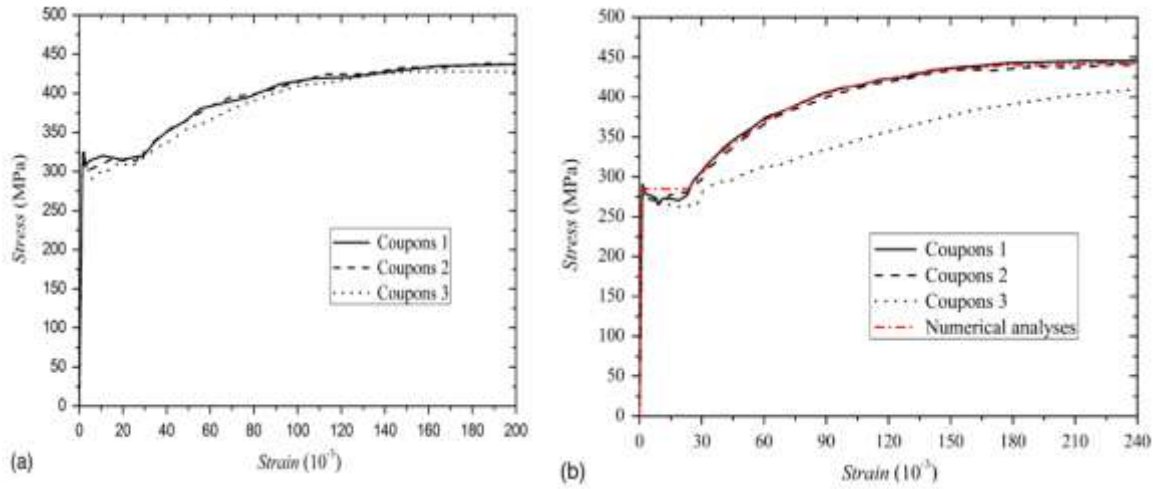


Figure 3. 6: Stress-strain relation test from a)web and b)flange (Dou et al., 2015)

For validation the material properties used is as reported by (Zaher *et al.*, 2018) on theirs report of experimental investigation on the structural behavior of arched cellular beam.

Table 3. 3: Steel material properties used for validation

parts	Plate thickness (mm)	Yield stress f_y (N/mm ²)	Modulus of elasticity E_s (MPa)	Ultimate stress f_u (N/mm ²)
web	4	242	205×10^3	290
Flange	8	233	199×10^3	315

- Shear modulus $G = \frac{E}{2(1+\nu)} \approx 80\text{GPa}$
- Poisson’s ratio in elastic range $\nu=0.3$
- Unit mass $\rho = 7850 \text{ kg/m}^3$
- Coefficient of linear thermal expansion $\alpha = 12 \times 10^{-6} \text{ per } ^\circ\text{C}$
- Engineering strain hardening ensuring ductility $\epsilon_u = 0.023$ (EN,EBCS 2013)

3.5.3. Part assembly

Created part geometry exists in its own coordinated system, independent of other parts in the model, to assembly each part relative to each other in a global coordinate system assembly module used to create instances of part .for this research dependent part instances used to assemble parts of model.

3.5.4. Model meshing

Finite element analysis (FEA) is a process of discretization of the continuum into nodes and grid of element to predict deflection and other effects of stress on a real structure. The process of discretizing a real model into nodes and grid elements is called meshing. Meshes of solids play an important role in finite element analysis, which includes the shape of the element and its size.

A wide range of elements is available in Abaqus/Standard. Each element behaves differently depending on five aspects (family, degrees of freedom, number of nodes, formulation, and integration). Each element has a unique name that identifies each of these five aspects of an element.

The major distinction between different elements is the geometry type that each family assumes. The Figure 3.7 below shows the families of shapes commonly used in stress analysis.

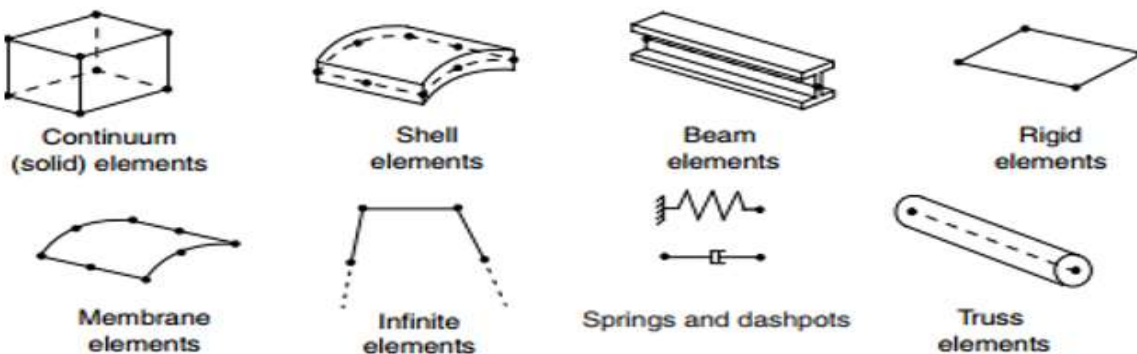


Figure 3. 7: Commonly used element families (ABAQUS, 2014).

Shell element (S) type geometry is used in this investigation because many of the previous numerical investigations on steel structures with shell elements show good conformity to experimental works.

The Mesh module can generate meshes containing the element shapes shown in Figure 3.8. Most elements in Abaqus/Standard, Abaqus/Explicit, and Abaqus/CFD correspond to one of the shapes shown; a shell mesh region typically has a quadrilateral and a triangular element type assigned to it by default. However, you can change the element assignment for any Abaqus

element that is topologically equivalent to the element shape assigned to the region. As a result, you can choose to mesh a shell region with only all triangular elements, and Abaqus/CAE ignores the quadrilateral element assignment.

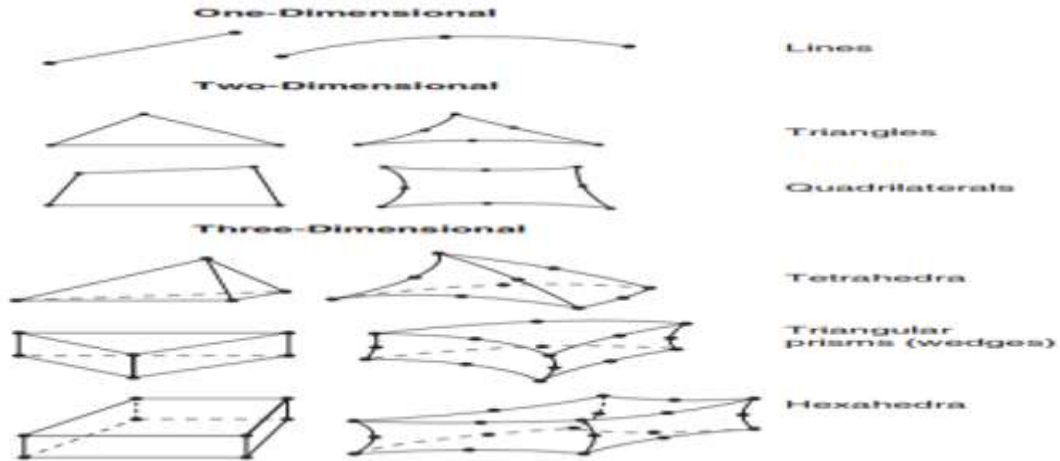


Figure 3. 8: Element shape (ABAQUS, 2013)

In Finite element the degrees of freedom (displacement and rotation) calculated only at the nodes of the element. At any other point in the element, the displacements are obtained by interpolating from the nodal displacements. Usually the interpolation order is determined by the number of nodes used in the element, Elements that have nodes only at their corners, such as the 8-node brick shown in Figure 3–9(a), use linear interpolation in each direction and are often called linear elements or first-order elements, Elements with mid-side nodes, such as the 20-node brick shown in Figure 3–9(b), use quadratic interpolation and are often called quadratic elements or second-order elements Modified triangular or tetrahedral elements with mid-side nodes, such as the 10-nodetetrahedron shown in Figure 3–9(c), use a modified second-order interpolation and are often called modified elements or modified second-order elements.

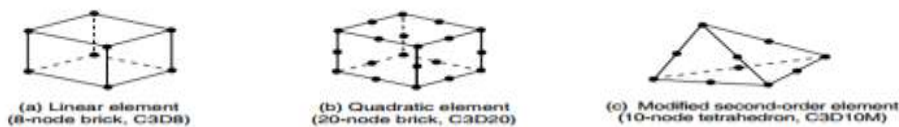


Figure 3. 9: Linear brick, quadratic brick and modified tetrahedral elements. (ABAQUS, 2013)

Abaqus/Standard offers a wide selection of both linear and quadratic elements, for this investigation shell element of four node with six degree of freedom associated with reduced integration numerical techniques to integrate various quantities over the volume of each element (S4R) and S3 were used. The S4R shell element dominantly, having four nodes each with six degrees of freedom, was used to model the tested specimens for calibration to experimental work and parametric investigation.

The initial step in finite element analysis is meshing of model means the model is discretized in to a number of small element and nodes. After the application of the load, the stress and the strain are calculated at integration point of these elements .an important step in finite element modelling is the selection of mesh density (size). A convergence of result is obtained when adequate number of elements used in a model, this achieved when an increase in mesh density has a negligible effect on analysis result. For this particular research the models are meshed with 35 mm mesh size of elements shows converged result as shown in Figure 3.10.



Figure 3. 10: Meshing of model B-3

Table 3. 4: Mesh detail for B-3 cellular steel arch

Details					Details				
By Part					By Element Type				
Part Name	Element Type	Elements	Nodes		Element Type	Element Shape	Geometric Order	Elements	
1	B-3	1316	1449		1	S4R	quadrilateral	linear	1285
2		S4R	1285		2	S3	triangular	linear	31
3		S3	31						

3.5.5. Boundary condition and loading

These research mainly focused on the in plane structural behavior of arched cellular beam to ensure that adequate lateral support provided to prevent lateral torsional buckling in addition to both side pinned support.

Loading of beam is dependent on the step analysis. For linear analysis linear perturbation is used unit load to found minimum eigenvalue (critical linear buckling load).the critical buckling load obtained applied to the beam using general static risk to obtain inelastic buckling load of cellular steel arch under consideration by taking account material, geometrical nonlinearities and large deformation. The whole analysis procedure used for this research is described in the analysis step.

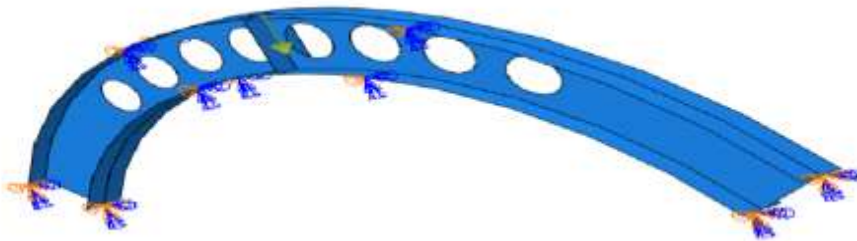


Figure 3. 11: Boundary and loading of model

Table 3. 5: Boundary condition.

Support type	U_x	U_y	U_z	θ_x	θ_y	θ_z
Pinned	1	1	1	1	1	0
Out of plane	0	0	1	1	1	0

1=restrained, 0=unrestrained U=deflection, θ =rotation

3.5.6. Analysis step

All analyses are load-controlled. As material and geometric imperfection are dominated by non-linear behavior the load is applied gradually in these analyses. As the primary objective is to find the ultimate load with post-buckling behavior the arc-length method procedure was selected in preference to Newton–Raphson to solve the non-linear equilibrium equations. For the linear buckling analysis linear perturbation buckle step with the subspace to extract the Eigen mode method is used for the eigenvalue extraction.

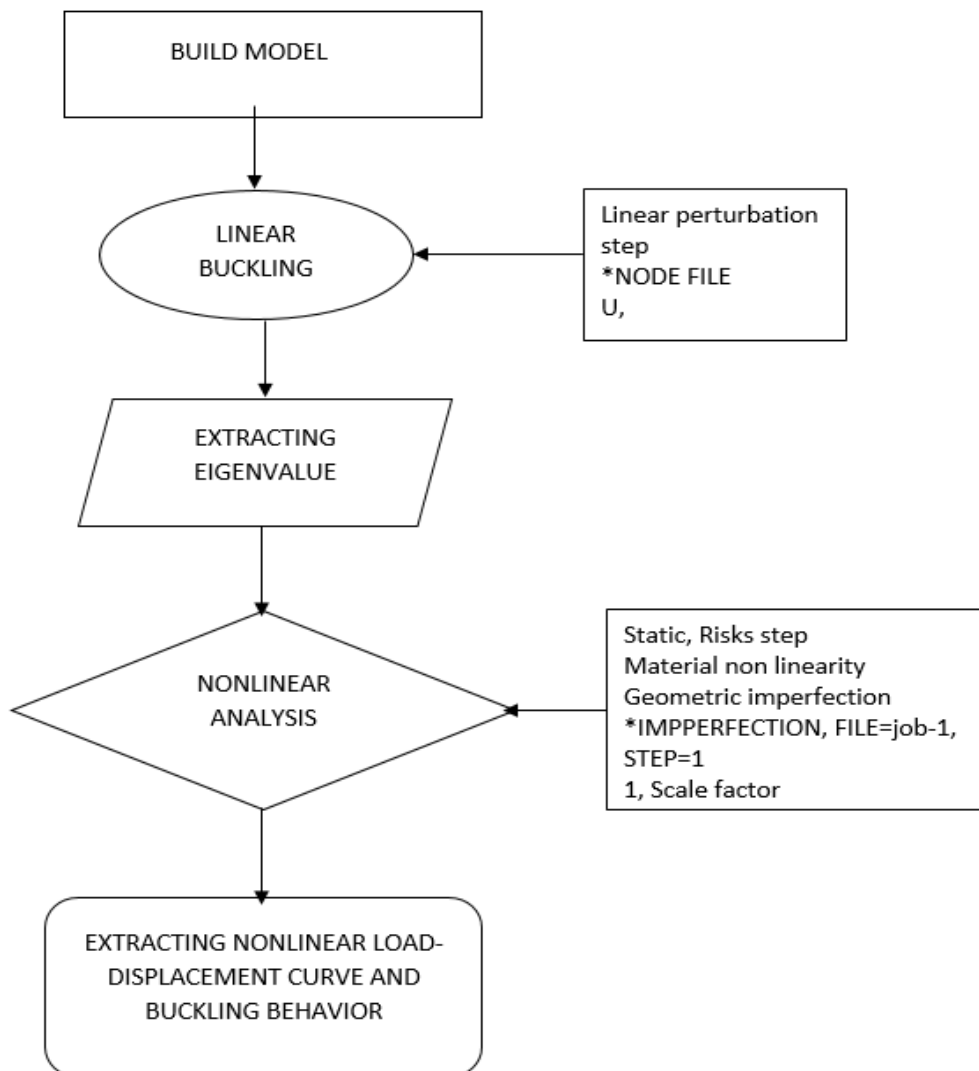


Figure 3. 12: Analysis step procedure

3.5.6.1. Linear buckling analysis

In these research the bilinear stress- strain curve with linear strain hardening was used to account for material imperfection and initial local geometric imperfection as a result of fabrication and transportation process are typically found in beams also considered. Therefore, superposition of local buckling mode with measured magnitude was recommended for accurate finite element analysis to investigate the sensitivity of these imperfection. Eigenvalue buckling prediction of purely linear perturbation analysis step which the response can be linear only was used as reference load to extract critical buckling load of the model in general nonlinear analysis.

Abaqus/Standard offers the Lanczos and the subspace iteration eigenvalue extraction methods. The Lanczos method is generally faster when a large number of Eigen modes is required for a system with many degrees of freedom. The subspace iteration method may be faster when only a few (less than 20) Eigen modes are needed. For this particular research subspace eigenvalue extraction method was used by specifying desired number of eigenvalue. For this particular study three eigenvalue were required with 300 maximum number of iteration used. Among the result minimum Eigen value were taken as maximum linear buckling load of the model.

3.5.6.2. The solution of nonlinear problems

The objective of the nonlinear analysis is to determine nonlinear load –displacement response curve as shown in Figure 3.13. In a nonlinear analysis the solution cannot be calculated by solving a single system of linear equations, as would be done in a linear problem. Instead, the solution is found by specifying the loading as a function of time and incrementing time to obtain the nonlinear response. Therefore, Abaqus/Standard breaks the simulation into a number of time increments and finds the approximate equilibrium configuration at the end of each time increment. Using the Newton method, it often takes Abaqus/Standard several iterations to determine an acceptable solution to each time increment.

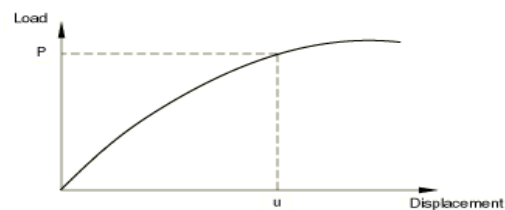


Figure 3. 13: Non linear load displacement curve(ABAQUS, 2013)

Abaqus /standard program able to compute iteration until equilibrium net force acting at every node must be zero .For the body to be in equilibrium, the net force acting at every node must be zero. Therefore, the basic statement of equilibrium is that the internal forces, I , which is caused by stress in the element attached to that node and the external applied forces on structure, P , must balance each other. (ABAQUS, 2013)

$$P - I = 0 \dots\dots\dots 3.1$$

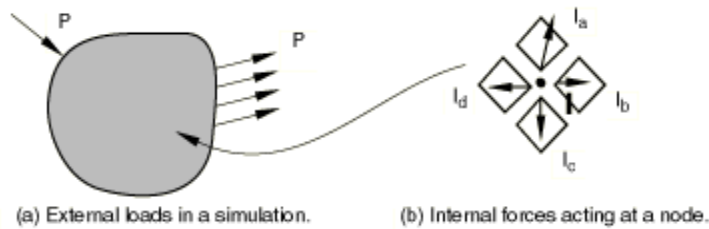


Figure 3. 14: Internal and External loads on a body. (ABAQUS, 2013)

The nonlinear response of a structure to a small load increment ΔP , is shown in Figure 3.15. Abaqus/Standard uses the structure's tangent stiffness, K_0 which is based on its configuration at u_0 , and ΔP to calculate a displacement correction, c_a , for the structure. Using c_a the structure's configuration is updated to u_a .

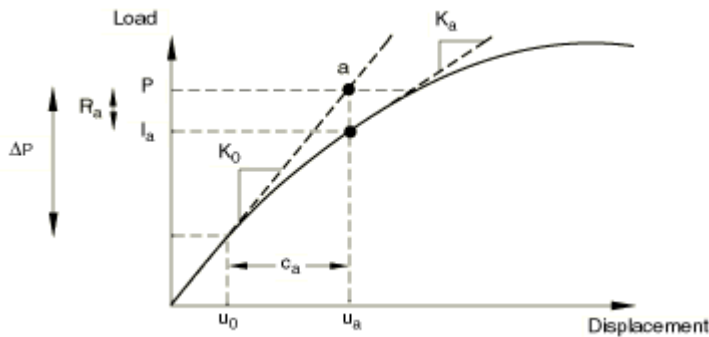


Figure 3. 15: First iteration (ABAQUS, 2013)

Abaqus/Standard then calculates the structure's internal forces, I_a in this updated configuration. The difference between the total applied load, P , and I_a can now be calculated as

$$R_a = P - I_a \dots\dots\dots 3.2$$

Where R_a is the force residual for the iteration.

If R_a is zero at every degree of freedom in the model, point a in Figure 3.15 would lie on the load-deflection curve and the structure would be in equilibrium. In a nonlinear problem R_a will never be exactly zero, so Abaqus/Standard compares it to a tolerance value. If R_a is less than this force residual tolerance at all nodes, Abaqus/Standard accepts the solution as being in equilibrium. By default, this tolerance value is set to 0.5% of an average force in the structure, averaged over time. Abaqus/Standard automatically calculates this spatially and time-averaged force throughout the simulation.

If R_a is less than the current tolerance value, P and I_a are considered to be in equilibrium and u_a , is a valid equilibrium configuration for the structure under the applied load. However, before Abaqus/Standard accepts the solution, it also checks that the last displacement correction, c_a , is small relative to the total incremental displacement, $\Delta u_a = u_a - u_o$. If c_a , is greater than a fraction (1% by default) of the incremental displacement, Abaqus/Standard performs another iteration. Both convergence checks must be satisfied before a solution is said to have converged for that time increment.

If the solution from an iteration is not converged, Abaqus/Standard performs another iteration to try to bring the internal and external forces into balance. First, Abaqus/Standard forms the new stiffness, k_a for the structure based on the updated configuration u_a , This stiffness, together with the residual R_a , determines another displacement correction, c_b , that brings the system closer to equilibrium point b in as shown in Figure 3.16 .

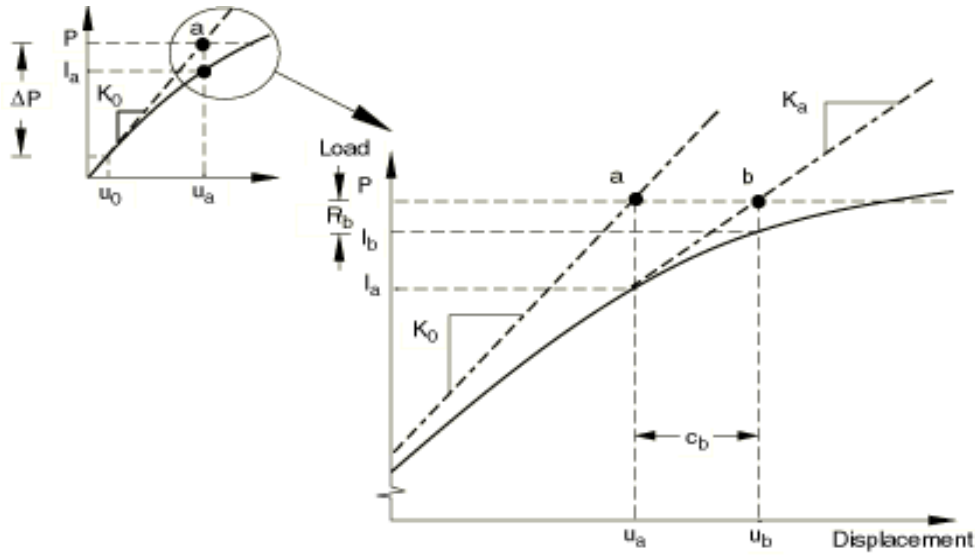


Figure 3. 16: Second iteration. (ABAQUS, 2013)

Abaqus/Standard calculates a new force residual, R_b using the internal forces from the structure's new configuration u_b . Again, the largest force residual at any degree of freedom, R_b , is compared against the force residual tolerance, and the displacement correction for the second iteration, c_b , is compared to the increment of displacement, Δu_b . If necessary, Abaqus/Standard performs further iterations until convergence criterion for the out-of-balance load vector is equal 0.5% of average force in structure.

For each iteration in a nonlinear analysis Abaqus/Standard forms the model's stiffness matrix and solves a system of equations. Therefore, the computational cost of each iteration is close to the cost of conducting a complete linear analysis. (ABAQUS, 2013)

3.5.6.3. The Riks method

It is often necessary to obtain nonlinear static equilibrium solutions for unstable problems, where the load-displacement response can exhibit the type of behavior sketched in Figure 3.17. that is, during periods of the response, the load and/or the displacement may decrease as the solution evolves. The modified Riks method is an algorithm that allows effective solution of such cases.

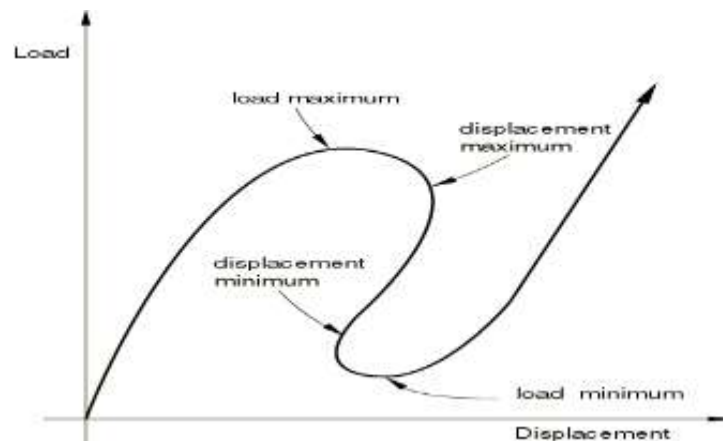


Figure 3. 17: Proportional loading with unstable response. (ABAQUS, 2013)

In simple cases linear eigenvalue analysis may be sufficient for design evaluation; but if there is concern about material nonlinearity, geometric nonlinearity prior to buckling, or unstable post buckling response, a load-deflection (Riks) analysis must be performed to investigate the problem further.

The Riks method uses the load magnitude as an additional unknown; it solves simultaneously for loads and displacements. Therefore, another quantity must be used to measure the progress of the solution; Abaqus/Standard uses the “arc length,” l , along the static equilibrium path in load-displacement space. This approach provides solutions regardless of whether the response is stable or unstable. (ABAQUS, 2013)

3.5.6.4. Proportional loading

A load whose magnitude is defined in the Riks step is referred to as a “reference” load. The loading during a Riks step is always proportional. The current load magnitude, is defined by

$$P_u = \lambda P_{ref} \dots \dots \dots 3.3$$

Where, P_{ref} is the reference load vector, and λ is the “load proportionality factor.” The load proportionality factor is found as part of the solution. Abaqus/Standard prints out the current value of the load proportionality factor at each increment.

Incrementation

Abaqus/Standard uses Newton's method (as described in to solve the nonlinear equilibrium equations. The Riks procedure uses only a 1% extrapolation of the strain increment.

You provide an initial increment in arc length along the static equilibrium path, Δl_{in} , when you define the step. The initial load proportionality factor, $\Delta \lambda_{in}$ is computed as

$$\Delta \lambda_{in} = \frac{\Delta l_{in}}{l_{period}} \dots \dots \dots 3.4$$

Where l_{period} a user-specified total arc length scale factor (typically set equal to 1). This value of $\Delta \lambda_{in}$ is used during the first iteration of a Riks step. For subsequent iterations and increments the value of λ is computed automatically, so you have no control over the load magnitude. The value of λ is part of the solution. Minimum and maximum arc length increments, Δl_{min} and, Δl_{max} can be used to control the automatic incrimination. (ABAQUS, 2013)

CHAPTER FOUR

RESULT AND DISCUSSION

Under this chapter the validity of the proposed simulated finite element model is checked through extensive comparisons between identical simulated models with its experimental results of cellular arched steel beam under concentrated load applied at the mid span. The load deflection curve for finite element model compared to the result that has been presented by (Zaher,et al 2018) experimental investigation on structural behavior of arched steel beam with cellular opening under concentrated load applied at mid span length of cellular arched beam with simply pinned at both end support condition.

After relevance and reliability of the software result to physical experimental work checked and assured that the proposed method of analysis and modelling step proposed capable of predicting the critical buckling load and displacement with expected mode of failure of arched cellular beam parametric investigation result and discussion presented in sub section 4.4 .

4.1. Bench mark experiment

To check conformity of proposed finite element analysis experimental work reported on structural performance of arched steel beam with cellular opening published by (Zaher,et al 2018) was used for comparison to its identical simulated finite element model on Abaqus/standard package.

4.1.1. General description on the genesis of data used in the experiment

4.1.2. Geometrical property

The geometry of experimentally tested solid arched I-section (B1) and cellular arched I-section (B2-B4) used was within the range of cellular beam geometry recommendation of BS EN 1993-1-1 as described in literature review and class 1 section and covers a significant range of beams used primarily used as roof beam and dimensions of tested specimens tabulated as Table 4.1.

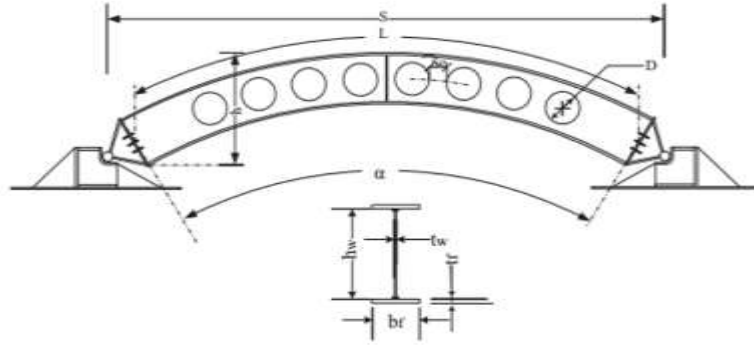


Figure 4. 1:Deimension of tested specimen(Zaher,et al 2018)

Table 4. 1: Dimensions of expermintally tested speceimens

Specimen	Web height(mm)	Web thickness t_w (mm)	Flange width b_f (mm)	Flange thickness t_f (mm)	Develop arch length L (mm)	Span S (mm)	Arch rise (mm)	Subtended angle	Holes diameter D (mm)
B-1	170	4	120	8	2451	2590	472	60	-
B-2	240	4	120	8	2451	2590	538	60	160
B-3	240	4	120	8	2651	2590	699	90	160
B-4	240	4	120	8	2032	2190	484	60	160

4.1.3. Material property

Material property of tested specimens obtained from tensile coupon test of web and flanges palates are presented in table 4.2 as the average yield stress (f_y), the modulus of elasticity (E_s), and ultimate stress (f_u).

Table 4. 2: Steel properties of tested specimens

Parts	Plate thickness (mm)	Yield stress f_y (N/mm ²)	Modulus of elasticity E_s (MPa)	Ultimate stress f_u (N/mm ²)
Web	4	242	$205 \cdot 10^3$	290
Flange	8	233	$199 \cdot 10^3$	315

4.1.4. Test setup and loading

A vertical load was applied at the mid span on the top flange of the arch using a hydraulic jack of 1000kN capacity, as shown in Fig 4.2. The load on the beam was gradually applied in increments of approximately 5kN steps, and it was monotonically increased until the end of the test after a number of unloading-reloading cycles at the beginning of the elastic domain. The lateral

displacement of the web and the vertical displacement of the tested specimens were measured using linear variable differential transformers (LVDTs) at specific location. (Zaher *et al.*, 2018)

For this studies the vertical deflection with respect to ultimate buckling load recorded below the applied load used for validation of proposed analysis step and modelling procedure of arched cellular beam using Abaqus standard finite element simulation software .



Figure 4. 2: Complete test set up (Zaher et al., 2018)

4.1.5. Experimental result

According to (Zaher et al., 2018) stability observation of tested specimens The web post buckling initiated when the applied load attained the critical load (P_{cr}) When the applied loads approached its ultimate value (P_u), the web post buckling failures were clearly visible. The critical and ultimate load with its respective vertical deflection below applied load are shown in Table 4.3.

Table 4. 3: Experimental result

Tested specimens	Ultimate load P_u (Exp) (kN)	Critical load P_{cr} (Exp) (kN)	Ultimate deflection $\delta_{u(Exp)}$ (mm)	Failure mode
B-1(solid beam)	253	204	44	Flexure
B-2	124	121	24	Web post buckling
B-3	137	133	18	Web post buckling
B-4	130	129	17	Web post buckling

4.2. Finite element simulation result of experimentally tested models

To check the capability and result coherence of the method of analysis and simulation (Abaqus packages) described in chapter three of this paper, all the experimentally tested cellular specimens reported on the paper published by (Zaher *et al.*, 2018) were simulated and analysed using commercial finite element software package Abaqus standard version 6.14.1. The result of finite element with respect to experimentally reported result were described as below.

Here below Figure 4.3, 4.4 and 4.5 shows buckling load to in plane deflection curve contour from Abaqus analysis output presented for specimen B-2, B-3 and B-4 respectively. Ultimate inelastic buckling load was obtained by multiplying load proportionality factor by buckling load extracted using linear perturbation.

Printed using Abaqus/CAE on: Thu Jan 02 10:28:46 Pacific Standard Time 2020

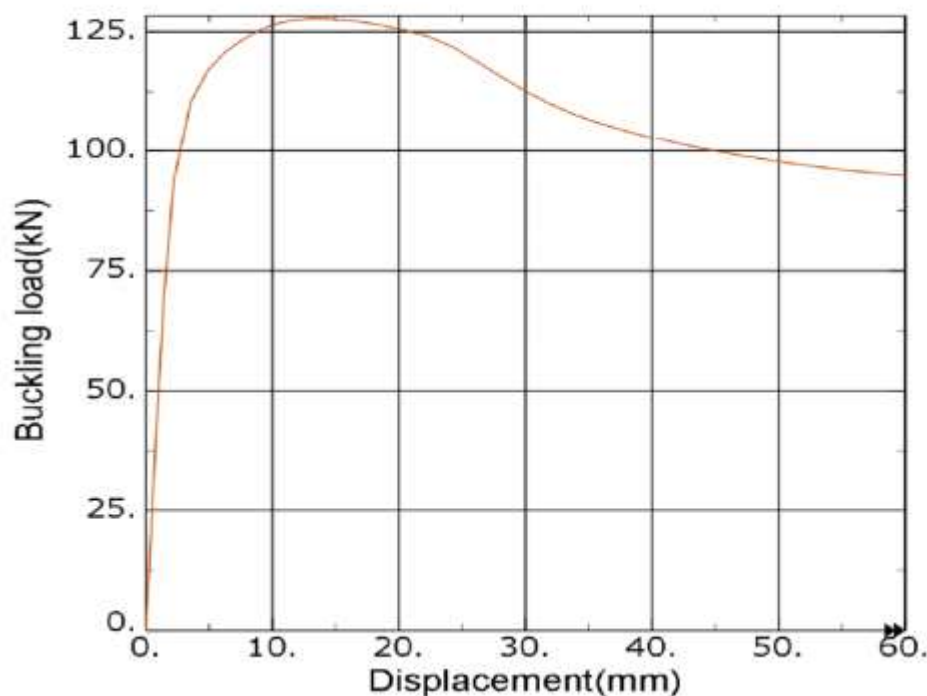


Figure 4. 3:Abaqus result of buckling load to displacement contour of B-2

Printed using Abaqus/CAE on: Thu Jan 02 10:37:45 Pacific Standard Time 2020

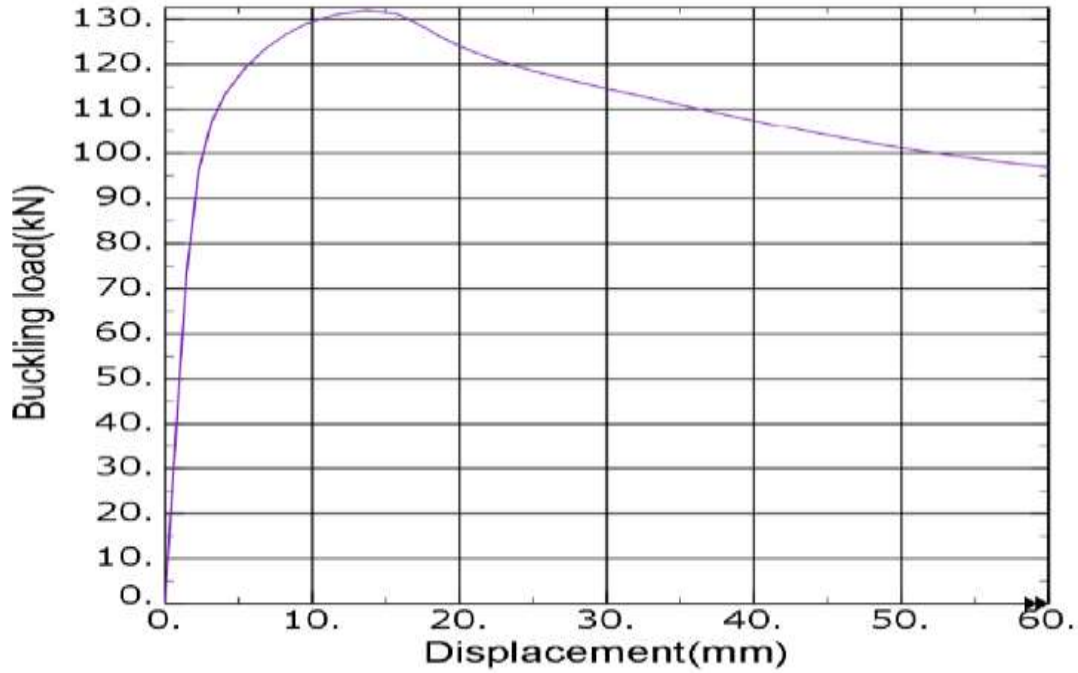


Figure 4. 4:Abaqus result of buckling load to Displacement contour for specimen B-3

Printed using Abaqus/CAE on: Thu Jan 02 10:46:27 Pacific Standard Time 2020

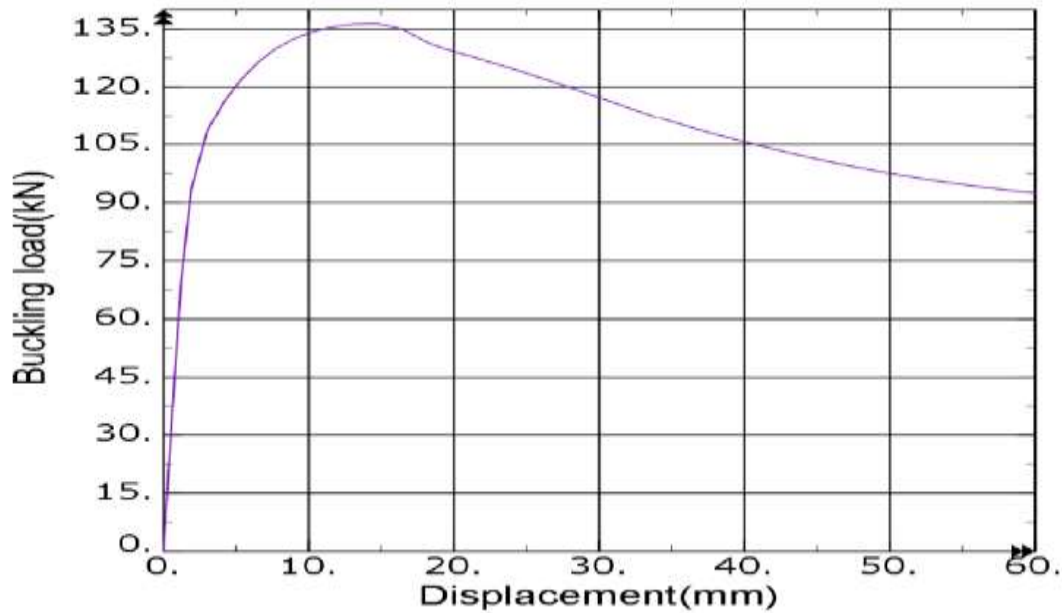
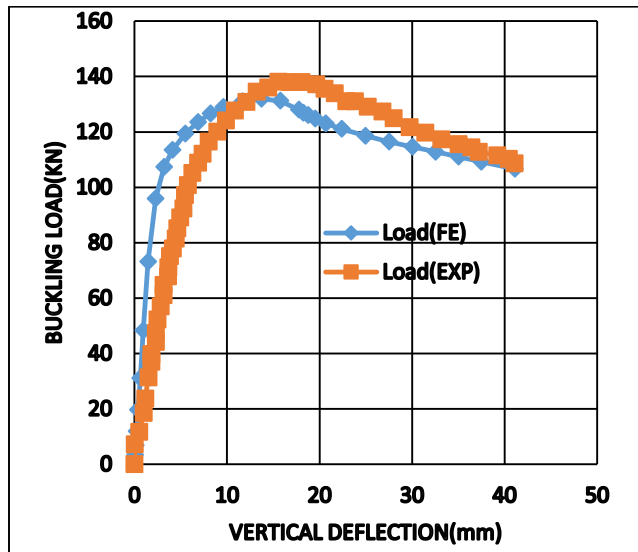


Figure 4. 5: Abaqus buckling load to displacement contour result for B-4

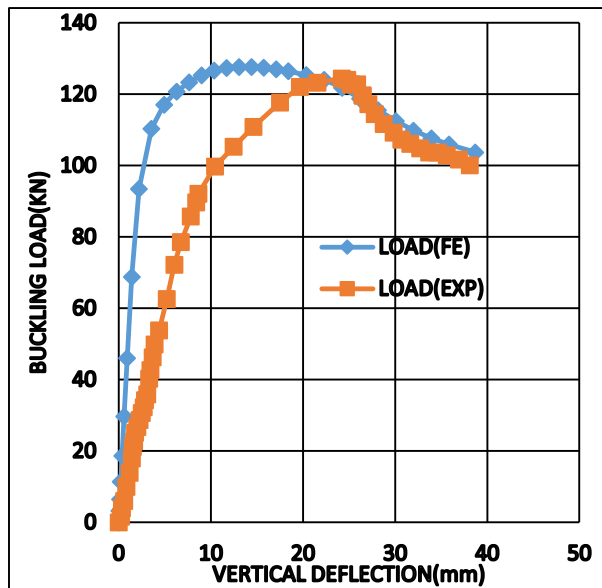
1. Tested specimens B-3



Critical	LOAD(kN)	DISPL(mm)
FE	131	17.76
Exp	137	18
RATIO (EXP/FE)	1.04	1.013514
% difference	4.37	1.33

Figure 4. 6: Load to in plane vertical deflection of FE and EXP of B-3

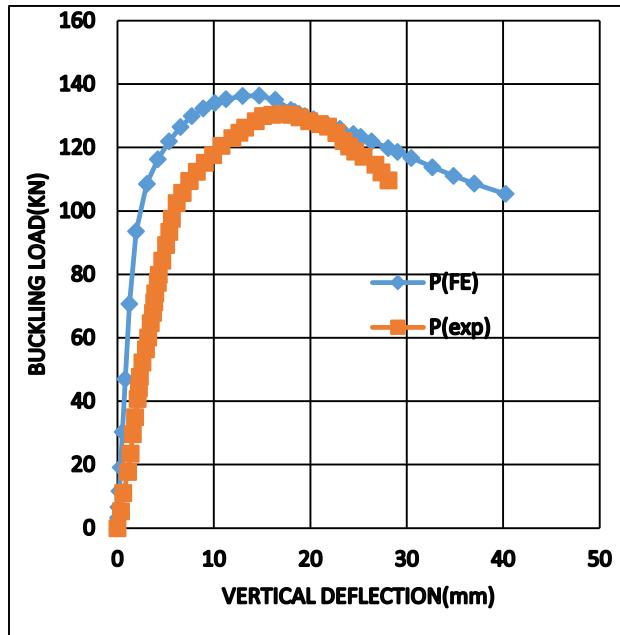
2. Tested specimens B-2



critical point	LOAD(KN)	DISP(mm)
FE	127	20.37
EXP	124	24
RATIO (EXP/FE)	0.98	1.18
% DIFFERENCE	2.36	15.125

Figure 4. 7: Buckling load to in plane vertical deflection of B-2

3. Tested specimens B-4



critical pt	LOAD	DEFLECTION
FE	136	16.34
EXP	130	17
Ratio	0.955882	1.040392
% difference	4.411765	3.882353

Figure 4. 8: Buckling load to vertical deflection of FE and EXP for B-4

4.3. Comparison of finite element and experimental result

As shown in the Fig 4.3-4.5 and corresponding tables three arched cellular steel beam of different subtended angle and span length modelled and analyzed using proposed nonlinear finite element software Abaqus 6.14.1. The finite element model gives acceptable results for the ultimate buckling load and maximum in plane deflection with values slightly less than 5% difference to the experimental values reported. These slight difference between finite element and experimental results can be due to the difference between the real material behavior and bilinear property used for modelling, inaccuracy of geometric imperfection scaling and unconsidered residual stress. Generally, the result of finite element simulation shows the proposed modelling and analysis step can predict buckling load, deflection and failure modes of arched cellular beam.

4.4. The result of FE analysis and simulation.

To study the elastic -plastic structural performance and in plane structural stability of arched cellular beam under mid span concentrated load and uniform radially distributed vertical load with varied span to rise ratio, geometry of arch and radius of curvature for all the samples specified in research methodology of this paper were modelled and analyzed.

The ultimate buckling load to in plane deflection and the ultimate buckling load to the out of plane deflection were presented below to show the effect of dependent variable of this research ,while the individual sample analysis result and simulation were presented in Appendix-A-D.

4.5. Structural behavior of arched cellular beam under mid span vertical load

4.5.1. Effect of rise to span ratio on shallow circular arched cellular steel

Specimens SCC-1, SCC-2 and SCC-3 were shallow circular arched cellular beams had the same cross sections with the same bilinear material property and same span length but with varied span to rise ratio altered with subtended angle. The curve shown in Figure 4.9 and Table 4.4 indicate that the ultimate buckling load of the specimens increased with the increased span to rise ratio .The buckling load to insignificant (very small less than 1mm) out of plane deflection curve of Figure 4.10 and with the 3-D simulation result in Appendix-A clearly figure out that shallow circular arched cellular beam failure type were local web post buckling.

Table 4. 4: Ultimate buckling load and maximum deflection of shallow circular cellular

Specimens	Ultimate buckling load(kN)	Maximum vertical deflection (mm)	% of ultimate load increment	Failure mode
SCC-1	330.32	17.58		WPB
SCC-2	346.23	18.34	4.59	WPB
SCC-3	395.89	25.38	12.54	WPB

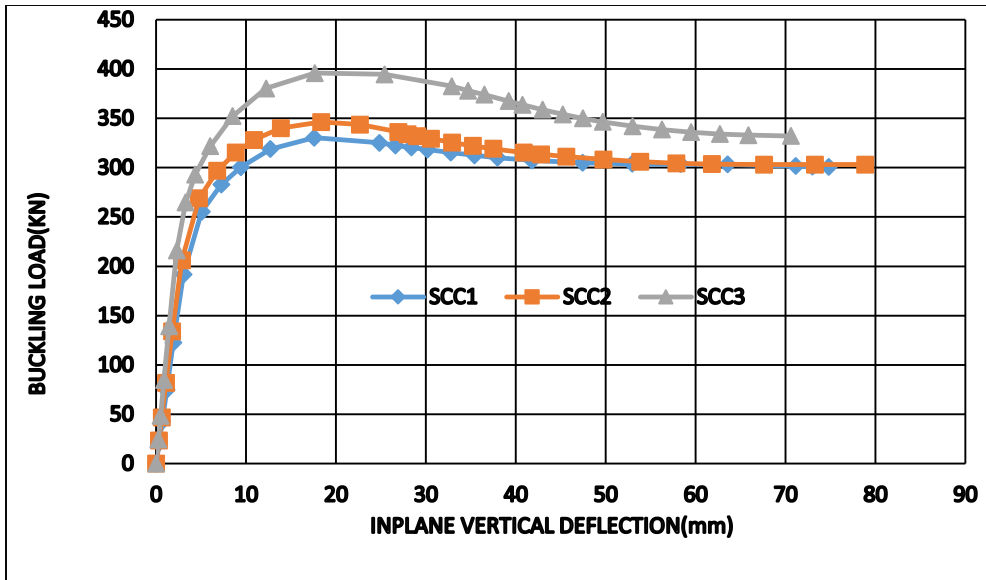


Figure 4. 9: Buckling load to in plane vertical deflection of shallow circular arched

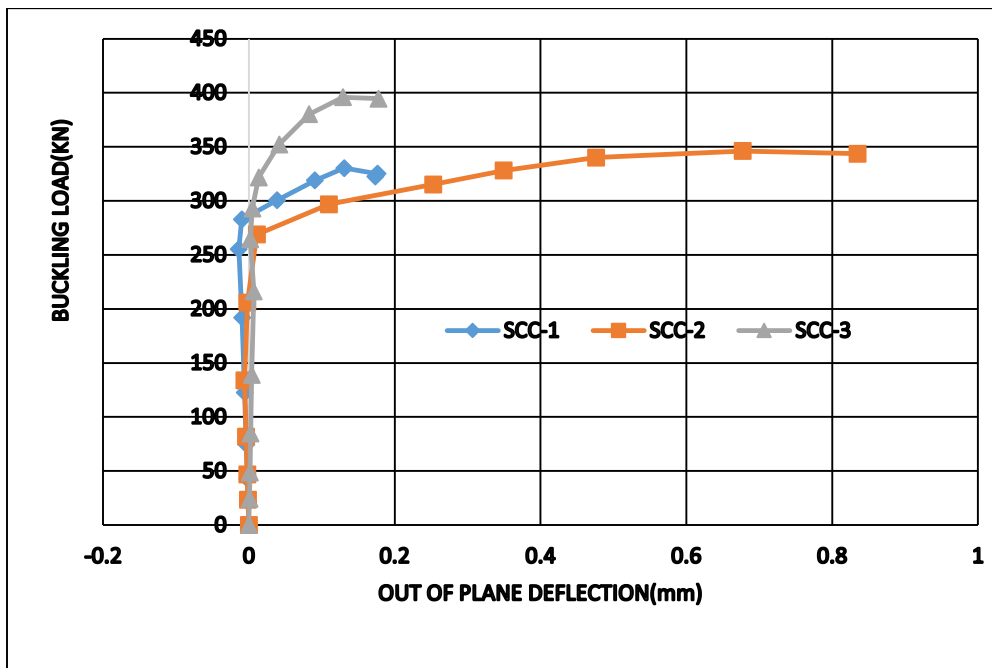


Figure 4. 10: Buckling load to out of plane deflection

4.5.2. Effect of rise to span ratio on shallow parabolic arch

Shallow Parabolic arched specimens PSC-1, PSC-2 and PSC-3 had the same cross section with the same bilinear material property and same span length but with varied span to rise ratio altered with subtended angle. The buckling load to in plane vertical deflection curve shown in Figure 4.11 and Table 4.5 indicate that the ultimate buckling load of the specimens increased with the increased span to rise ratio and the buckling load to insignificant (less than 1mm) out of plane deflection curve of Figure 4.12, with the 3-D simulation result in Appendix-B clearly figure out that shallow parabolic arched cellular beam failure type were local web post buckling under mid span point load.

Table 4. 5: Shallow parabolic arch ultimate buckling load variation to rise –to-span ratio

specimens	Ultimate buckling load(kN)	Maximum vertical deflection (mm)	% of buckling load increment	Failure mode
PSC-1	308.69	19.29		WPB
PSC-2	345.55	17.17	10.66	WPB
PSC-3	425.027	24.05	18.699	WPB

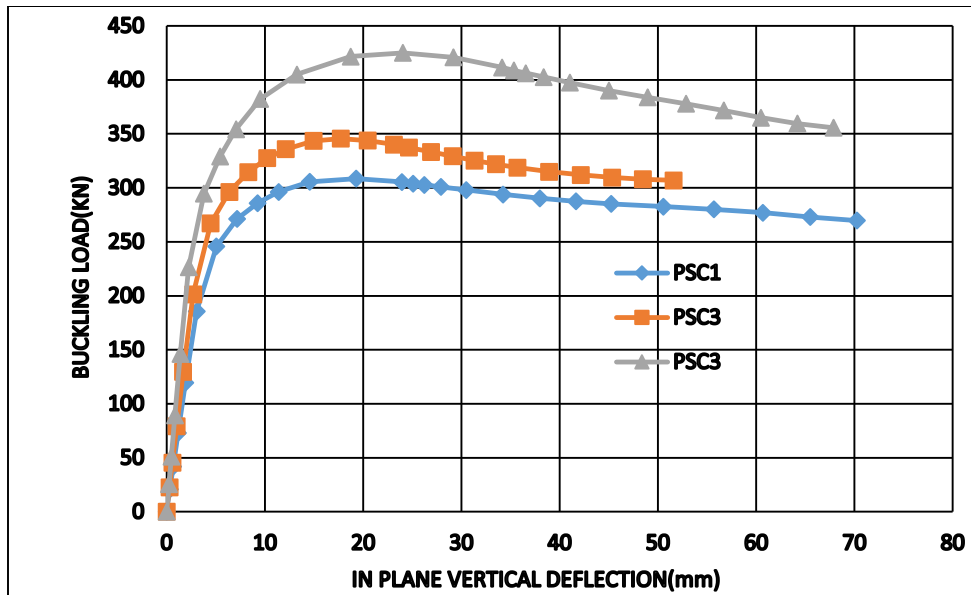


Figure 4. 11 : Buckling load versus in plane vertical deflection shallow arched parabola

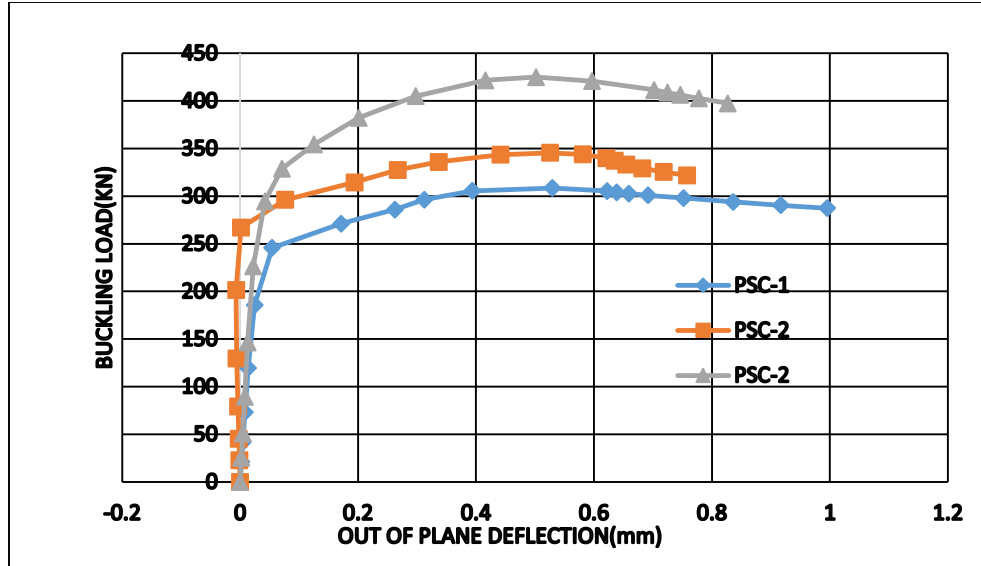


Figure 4. 12: Buckling load versus out of plane deflection of parabolic shallow arch

4.5.3. Effect of rise to span ratio on deep circular cellular arch

Deep circular cellular arch with subtended angle greater than 90° specimens DCC-1, DCC-2 and DCC-3 with the same cross-section and span length but different rise to span ratio altered with subtended angle. The buckling load versus in plane vertical deflection shown in Figure 4.13 and Table 4.6 indicate the structural performance circular arched cellular beam increases with rise-to- span ratio but with less variation to the increment of rise- to- span ratio. The ultimate load to out of plane deflection curve of Figure 4.14 elucidate that the out of plane deflection of deep circular curve increases significantly beyond DCC-1 which, rise to span ratio 0.283(subtended angle 120°) with insignificant out of plane deflection and appendix-A verify that deep circular curve failed in plane manner with web post buckling and more susceptible to out of plane deflection than shallow circular curve.

Table 4. 6: Ultimate buckling load and maximum vertical deflection of deep circular curve

specimens	Ultimate buckling load(kN)	Maximum vertical deflection(mm)	% buckling load increment	Mode of failure
DCC-1	416.752	24.34	5.0	WPB
DCC-2	429.97	22.56	3.04	WPB
DCC-3	430.01	29.49	0.23	WPB
DCC-4	435.89	35.08	1.34	WPB

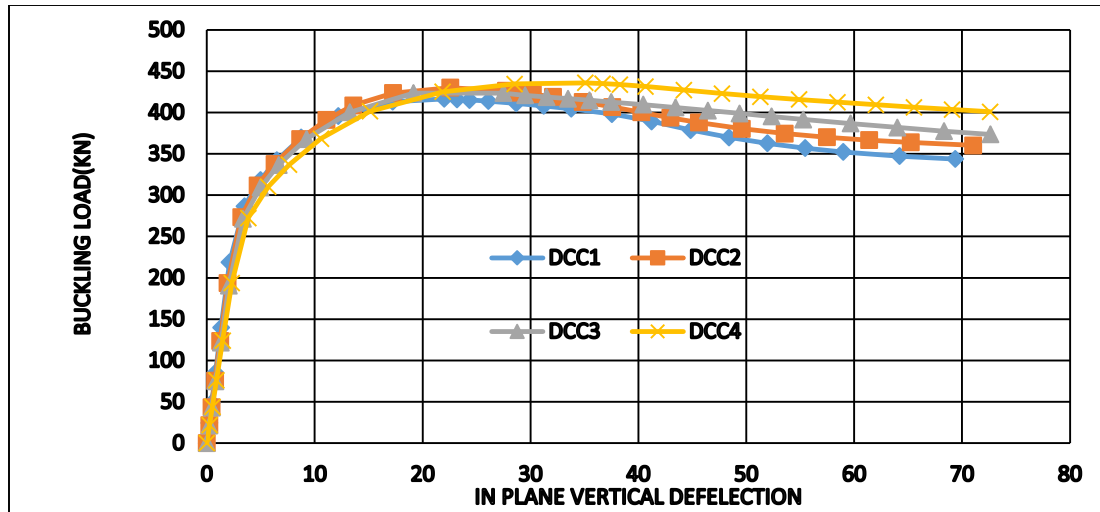


Figure 4. 13: Buckling load to in plane vertical deflection of deep circular arched

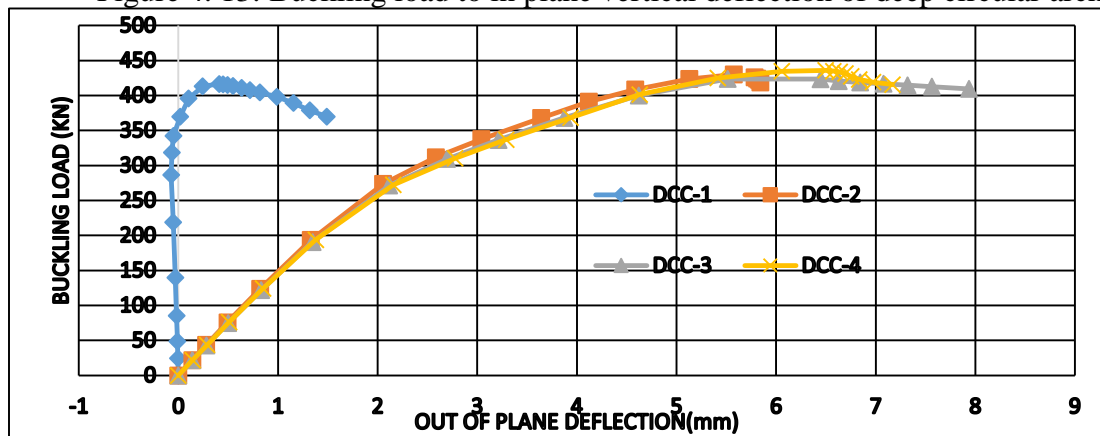


Figure 4. 14: Buckling load to out of plane deflection curve of deep circular arch.

4.5.4. Effect of rise to span ratio on deep parabolic arch

Specimens PDC-1, PDC-2, PDC-3 and PDC-4 deep arches with subtended angle greater than 90^0 with parabolic geometry with equivalent cross-section and identical material property, the same span length studied under mid span point load. The output result clearly shows that the ultimate buckling load of parabolic arches increases with span to rise ratio as described in Figure 4.15 and Table 4.7 below. The buckling load to out of plane deflection curve Figure 4.13 indicate that parabolic deep cellular arch PDC-1 and PDC-3 out of plane deflection is nearly zero (insignificant) compared to arch PDC-2 and PDC-4 because of uneven bending and shear distribution characteristics of arched structure and Appendix-B shows the arch failure mode were symmetric in plane web post buckling type.

Table 4. 7: Ultimate buckling load and maximum vertical deflection of deep parabolic arch

Specimens	Ultimate buckling load(KN)	Maximum in plane vertical deflection(mm)	% buckling load increment	Failure mode
PDC-1	460.31	26.79	7.66	WPB
PDC-2	491.60	22.99	6.36	WPB
PDC-3	506.98	26.44	3.03	WPB
PDC-4	570.38	30.37	11.11	WPB

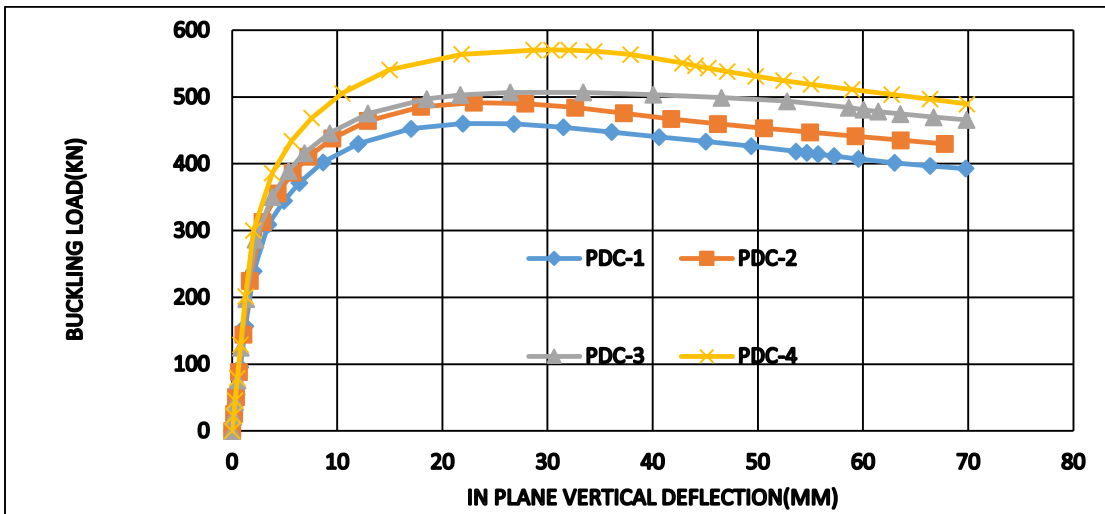


Figure 4. 15: Buckling load to vertical deflection of parabolic deep arch

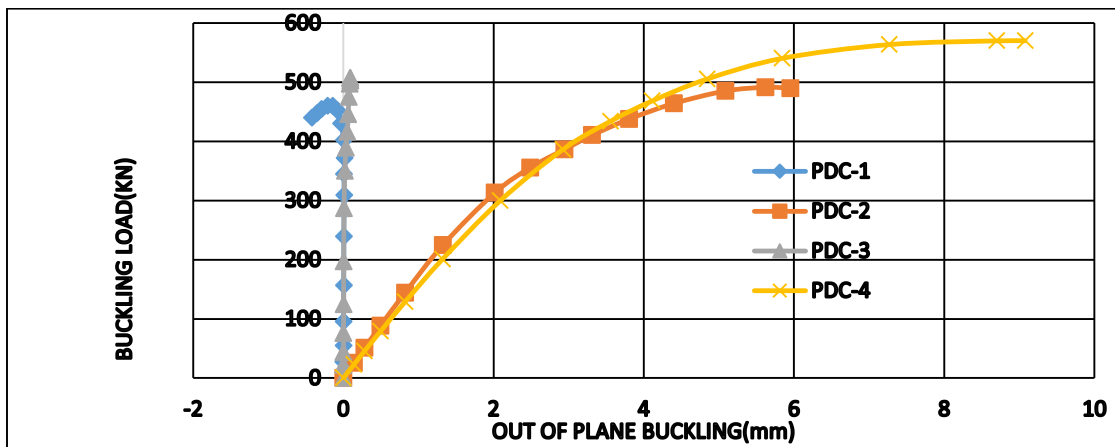


Figure 4. 16: Buckling load versus out of plane deflection parabolic deep arch

4.6. Effect of arch geometry under mid span point load

In the above discussion samples of different rise-to-span ratio with the same cross-section, material property and span length under mid span point load with circular and parabolic arch geometry are presented. The effect of arch geometry on structural performance of arched cellular beam under mid span concentrated load compared and discussed as below.

Table 4. 8: Shallow arch geometry buckling load comparison under MSPL

Samples		Ultimate buckling load (kN)		% difference	Efficient geometry
Circular	parabolic	Circular	Parabolic		
SCC-1	PSC-1	330.32	308.69	6.548	circular
SCC-2	PSC-2	346.23	345.55	0.19	Nearly equal
SCC-3	PSC-3	395.89	425.02	6.853	parabolic

Table 4. 9: Ultimate buckling load comparison of deep arch geometry under MSPL

Samples		Ultimate buckling load (kN)		%difference	Efficient geometry
Circular	parabolic	circular	parabolic		
DCC-1	PDC-1	416.52	460.31	9.51	Parabolic
DCC-2	PDC-2	429.97	491.60	12.53	parabolic
DCC-3	PDC-3	423.48	506.98	16.47	parabolic
DCC-4	PDC-4	435.89	570.38	23.57	parabolic

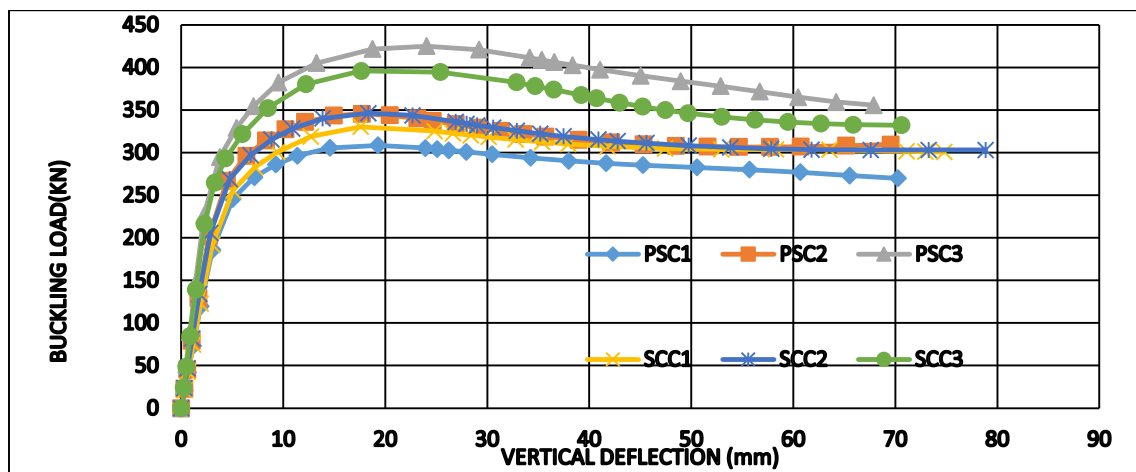


Figure 4. 17 : Buckling load to deflection curve comparison of shallow arch geometry

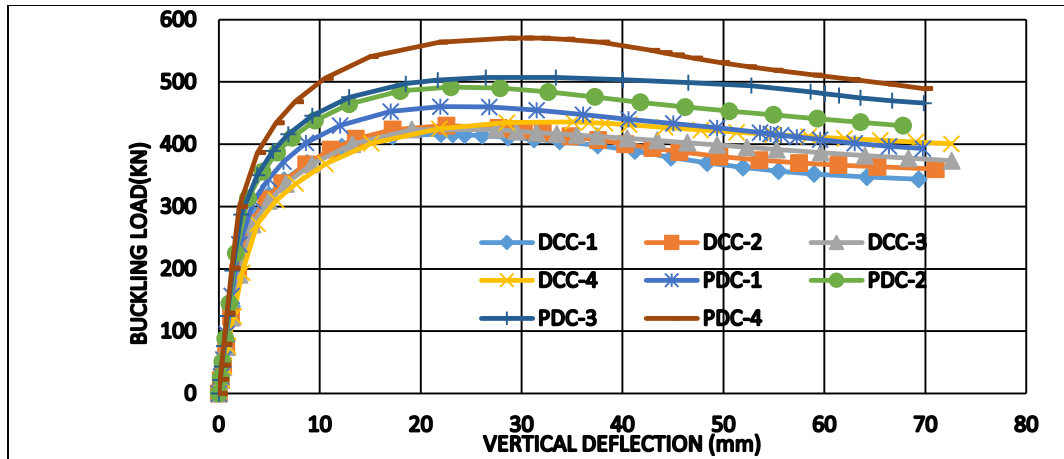


Figure 4. 18: buckling load to deflection curve comparison of deep arch geometry

The above numeric result Table 4.8 and 4.9 buckling load to deflection curve of Figure 4.17 and 4.18 shows that the with increase of span to rise ratio specifically for arches with subtended angle greater than 90° cellular parabolic deep arches were structurally efficient than equivalent deep circular cellular arches of identical span to rise ratio under mid span point load.

4.7. Structural behavior of arched cellular beam under uniform radially distributed vertical load.

4.7.1. Effect of rise to span ratio on shallow circular cellular arch

Specimens SCC-1, SCC-2 and SCC-3 under applied uniformly distributed load had the same cross section means equal flange thickness, web thickness and depth with the same bilinear material property and same span length but with varied span to rise ratio altered with subtended angle. The curve shown below in Figure 4.19 and Table 4.10 indicate that the ultimate buckling load of the specimens increased with the increased span to rise ratio.

The buckling load to out of plane deflection curve of Figure 4.19 and with the 3-D simulation result in appendix-A clearly shows that shallow circular arched cellular beam under radially distributed vertical load were more prone to out of plane deflection than identical arch under mid span point load with increase of rise- to-span ratio.

Table 4. 10: Ultimate load and maximum vertical deflection of SCC under URDVL

Model	Ultimate buckling load(kN)	Max vertical deflection (mm)	% increment of buckling load	Failure mode
SCC-1	62.84	21.96		WPB
SCC-2	77.01	23.32	18.4	WPB
SCC-3	92.19	18.52	16.46	Out of plane buckling

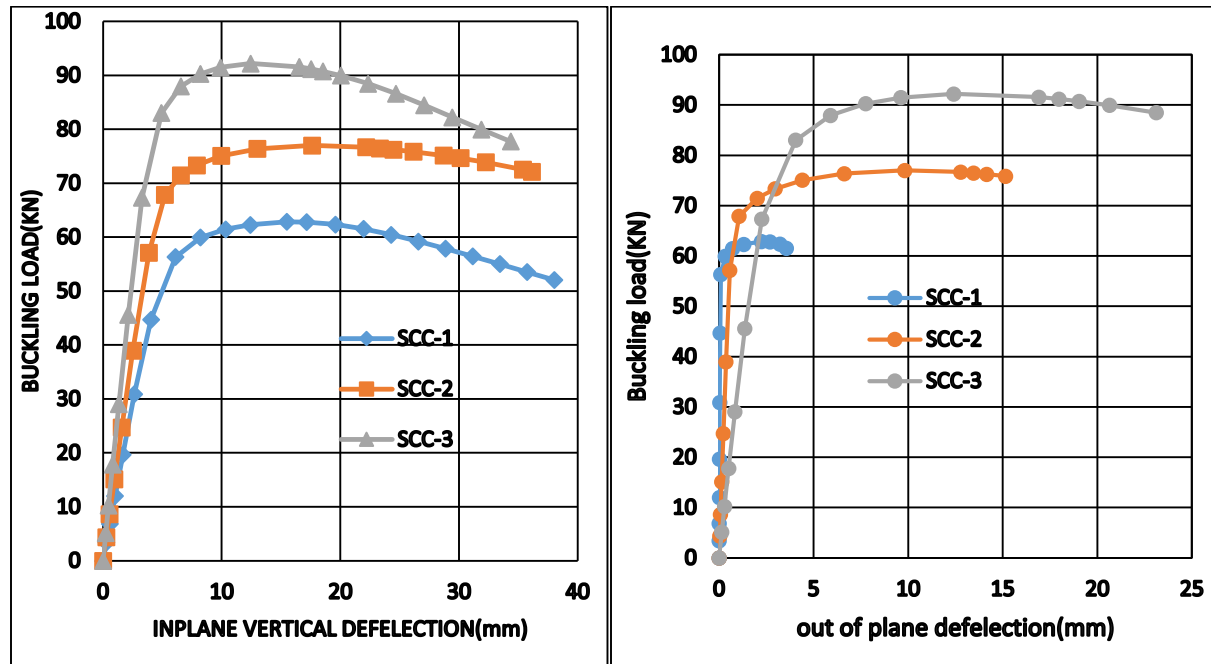


Figure 4. 19: Buckling load to deflection of shallow circular under URDVL

4.7.2. Effect of rise to span ratio on shallow parabolic cellular arch

Sample PSC-1, PSC-2 and PSC-3 had identical material property, span length and cross-section except rise to span ratio altered with subtended angle were studied under radially distributed vertical load the output result described in Figure 4.20 buckling load to in plane deflection and Table 4.11 shows that the structural performance of shallow parabolic arch increase with rise to span ratio. in addition as shown in buckling load to out of plane deflection curve Figure 4.20 as rise to span ratio increases the out of plane deflection of the curve also dominant type of failure mode.

Table 4. 11: Ultimate buckling load and maximum vertical deflection PSC under URDVL

Model	Ultimate buckling load(kN)	Maximum vertical deflection(mm)	% buckling load increment	Mode of failure
PSC-1	61.50	19.50		WPB
PSC-2	76.45	18.05	19.55	Out of plane buckling
PSC-3	97.24	11.04	21.3	Out of plane buckling

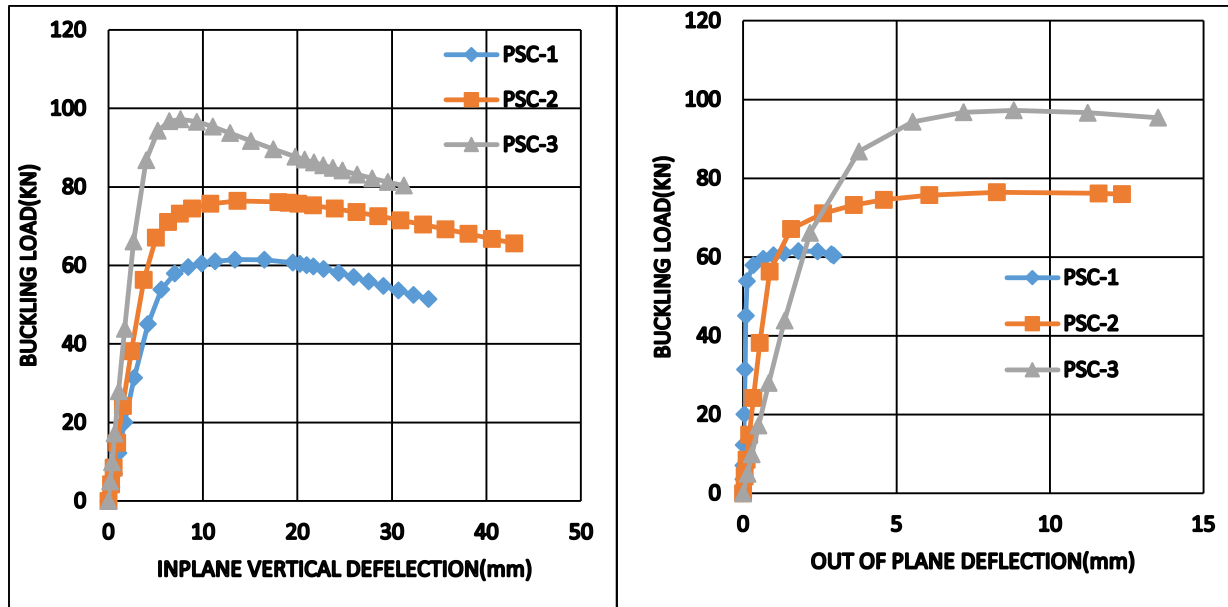


Figure 4. 20: Buckling load to deflection of PSC

4.7.3. Effect of rise to span ratio on deep parabolic arched cellular steel beam

Samples of deep parabolic arches PDC-1, PDC-2, PDC-3 and PDC-4 with identical cross-section, span length and material property but only different span to rise ratio under uniform radially distributed vertical load shows that ultimate buckling load of deep parabolic arch increase with rise- to -span ratio up to PDC-3 of 0.419 rise-to-span ratio, beyond this ratio ultimate buckling load is not directly proportional to rise -to -span ratio as described on Table 4.12 and Figure 4.21.

Figure 4.21 out of plane deflection to buckling load with 3D-simulation result presented on Appendix-B indicate that under uniform radially distributed load deep parabolic arches susceptible to out of plane deflection.

Table 4. 12: Ultimate buckling load variation to rise-to span ratio of deep parabola under URDVL

Model	Ultimate buckling load(Kn)	Maximum vertical deflection(mm)	% buckling load increment	Mode of failure
PDC-1	124.34	8.99	21.79	Out of plane buckling
PDC-2	171.43	10.22	27.4	Out of plane buckling
PDC-3	180.73	7.34	5.1	Out of plane buckling
PDC-4	159.50	6.03	-10.7	Out of plane buckling

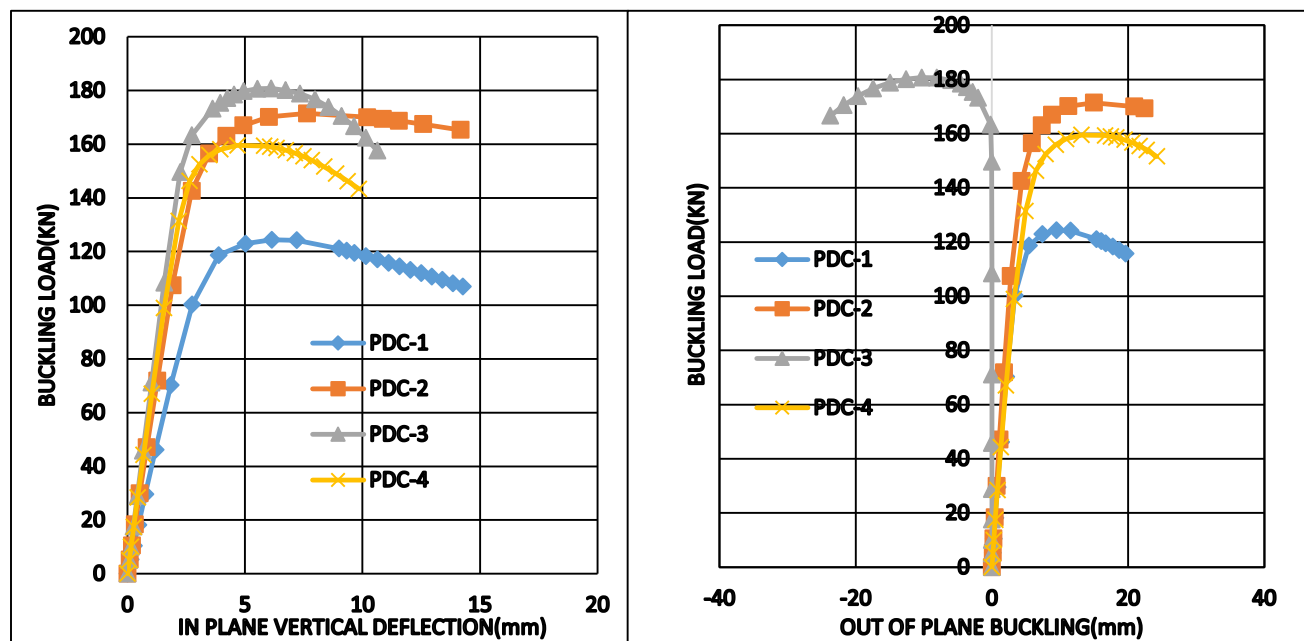


Figure 4. 21: Buckling load to deflection PDC

4.7.4. Effect of rise to span ratio on deep circular arched cellular steel beam

The buckling load to deflection curve show in Figure 4.22 below and Table 4.13 assures that the effect of rise- to- span ratio on structural performance deep circular arched cellular beam under uniform radially distributed vertical load increases with rise to span ratio increment up to sample DCC-2 which, subtended angle is 140⁰ beyond this the ultimate buckling load decrease inversely with rise to span ratio under uniform radially distributed vertical load.

The buckling load to out of plane deflection curve Figure 4.23 and 3-D simulation on Appendix-A shows that the failure mode of sample DCC-1 and DCC-2 are similar fail in symmetric out of

plane deflection, while sample DCC-4 and DCC-3 fail in the unsymmetrical out of plane mode . Generally, the failure mode of deep circular arched cellular beam under uniform radially vertical load is quite different from its deep circular arched cellular beam under mid span point load.

Table 4. 13: Buckling load variation with span to rise ratio under URDVL

model	Ultimate buckling load	Vertical deflection (mm)	% buckling load increment	Mode of failure
DCC-1	121.18	15.82		Out of plane buckling
DCC-2	129.52	12.12	6.43	Out of plane buckling
DCC-3	126.29	12.25	-2.49	Out of plane buckling
DCC-4	121.01	10.94	-4.18	Out of plane buckling

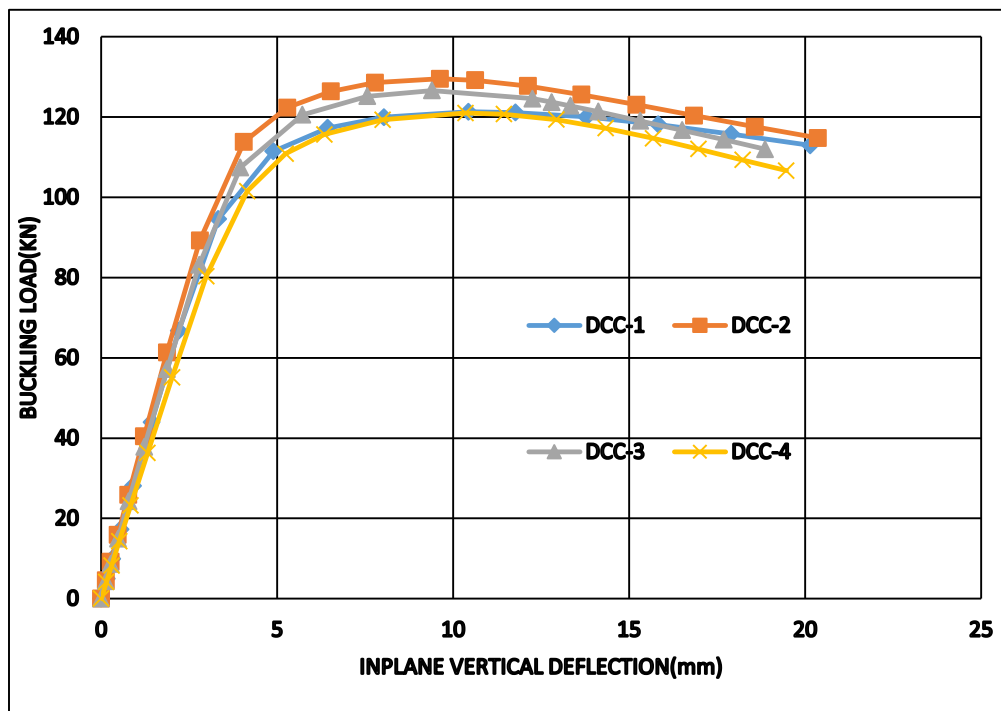


Figure 4. 22: Buckling load to inplane vertical deflection of DCC under URDVL

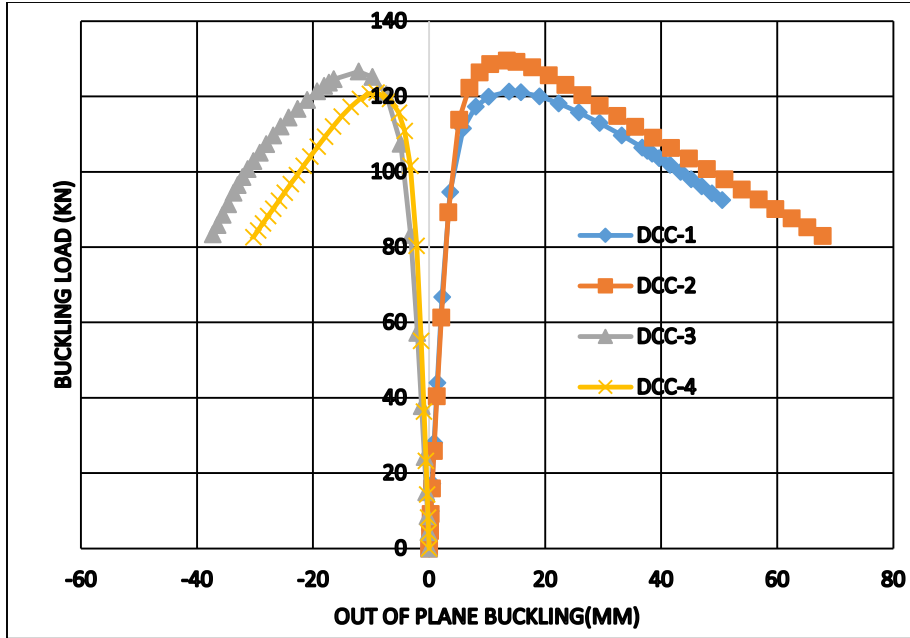


Figure 4. 23: Buckling load to out of plane deflection DCC under URDVL

4.8. Effect arch geometry under uniform radially distributed vertical load

Here shallow circular (SCC-1, SCC-2 and SCC-3) and four deep (DCC-1, DCC-2 and DCC-3) circular arch geometry compared to its three shallow parabolic arches (PSC-1, PSC-2 and PSC-3) and four deep parabolic (PDC-1, PDC-2, PDC-3 and PDC-4) counterpart respectively to figure out the effect of arch geometry .

The comparison of buckling load to in plane deflection curve of Figure 4.24 and Table 4.14 points out that deep parabolic arches had greater buckling load than the its identical circular arches these means under uniform radially distributed vertical load deep parabolic arched cellular beams are stiffer than identical deep circular arched cellular beam.

Table 4. 14 : Ultimate load comparison of deep arch geometry under URDVL

Samples		Ultimate buckling load (KN)		%difference	Efficient geometry
circular	parabolic	circular	parabolic		
DCC-1	PDC-1	121.18	124.34	2.54	Parabolic
DCC-2	PDC-2	129.52	171.43	24.27	parabolic
DCC-3	PDC-3	126.59	180.73	29.95	parabolic
DCC-4	PDC-4	121.01	159.50	24.13	parabolic

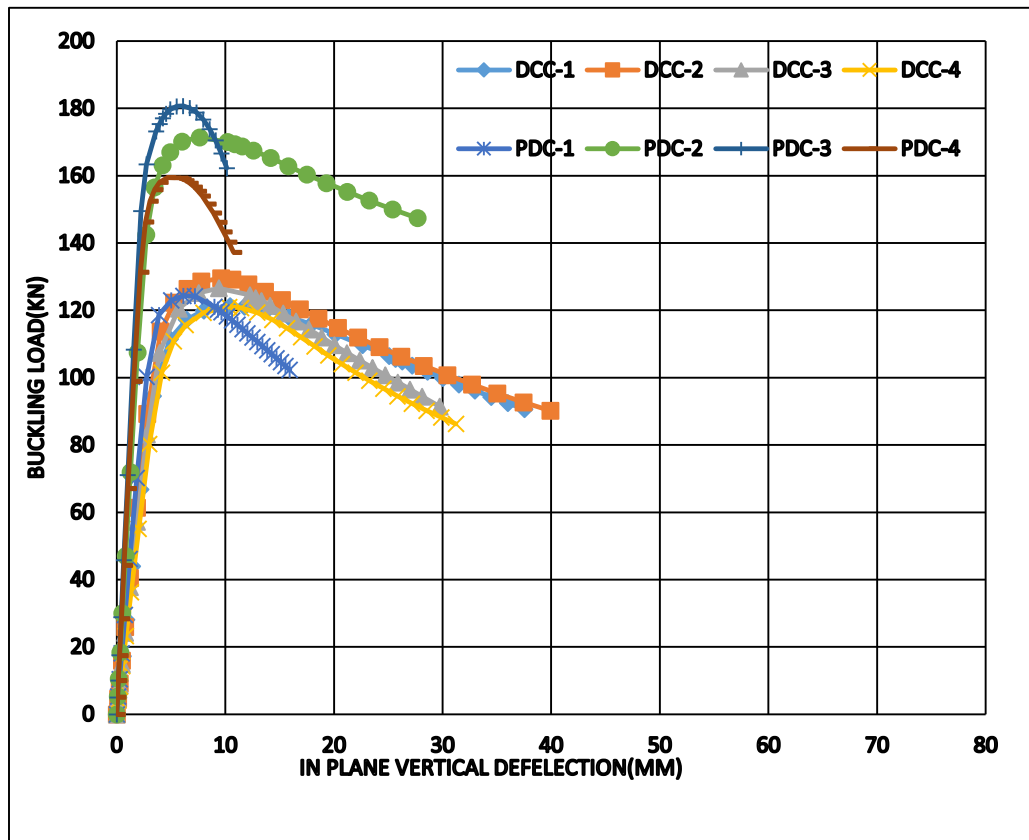


Figure 4. 24: Deep arched cellular beam geometric comparison under URDVL

For shallow arched cellular steel beam with subtended angle less than 90° parabolic and circular geometry of arch have little effect on the stiffness cellular steel arch as described on Table 4.15 and Figure 4.25 shallow arch parabolic and circular cellular arch deform and carry nearly equal buckling load under uniform radially distributed vertical load.

Table 4. 15: Ultimate buckling load comparison of shallow curve geometry under URDVL

Samples		Ultimate buckling load (KN)		% difference	Efficient geometry
Circular	parabolic	Circular	Parabolic		
SCC-1	PSC-1	62.84	61.50	2.13	circular
SCC-2	PSC-2	77.01	76.45	0.72	Nearly equal
SCC-3	PSC-3	92.19	97.24	5.19	parabolic

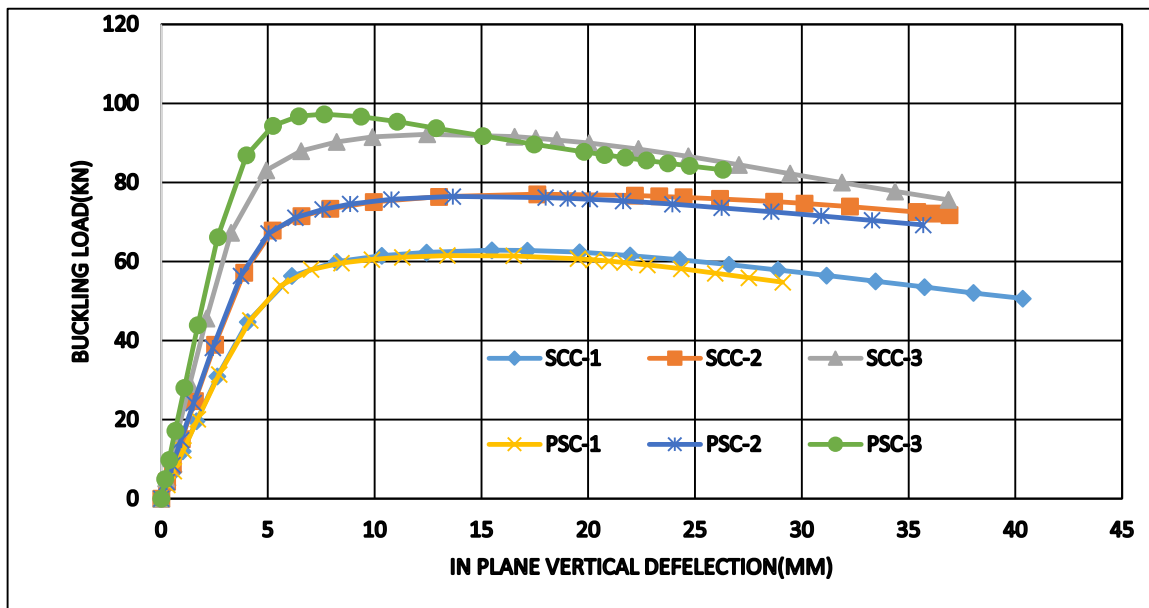


Figure 4. 25: Shallow arched cellular geometric comparison under URDVL

4.9. Effect of radius of curvature

To discuss the effect of radius of curvature on the structural performance of arched cellular beams, arched cellular beams of the same rise to span ratio with the same subtended angle but only different in span length to account radius of curvature difference randomly selected from shallow and deep arches from two arches geometry (parabolic and circular).the effect of radius of curvature on structural behavior of arched cellular beam under mid span point load and uniform radially distributed vertical load discussed as bellow.

4.9.1. Effect of radius of curvature under mid-span point load

Arched cellular beam SCC-2500($R=1768.41\text{mm}$), SCC-3000($R=2122.094\text{mm}$) and PSC-2500($R=1768.41\text{mm}$), PSC-3000($R=2122.094\text{mm}$) are shallow circular and parabolic arched cellular beams with the same rise to span ratio ($H_s/L=0.207$) and subtended angle ,but different in radius of curvature because of 2500mm and 3000m span length difference.

As shown in buckling load to in plane vertical deflection Figure 4.26 the radius of curvature of arched cellular beam inversely proportional to arch stiffness irrespective of arch geometry and shallowness under mid-point concentrated load. This result indicate that with same rise-to-span ratio and subtended angle increasing radius of curvature increases horizontal shear force which in turn increases compression stress which initiates web post buckling of cellular steel beam under mid span point load .

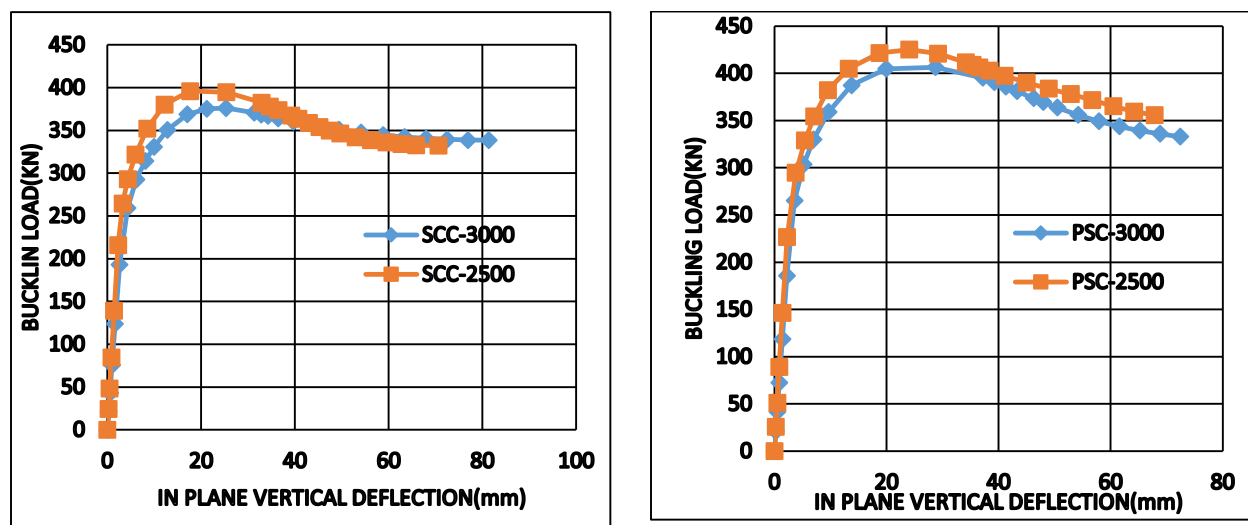


Figure 4. 26: Buckling load to deflection curve of SCC-3000, SCC-2500, PSC-3000, and PSC-2500 under MSPL

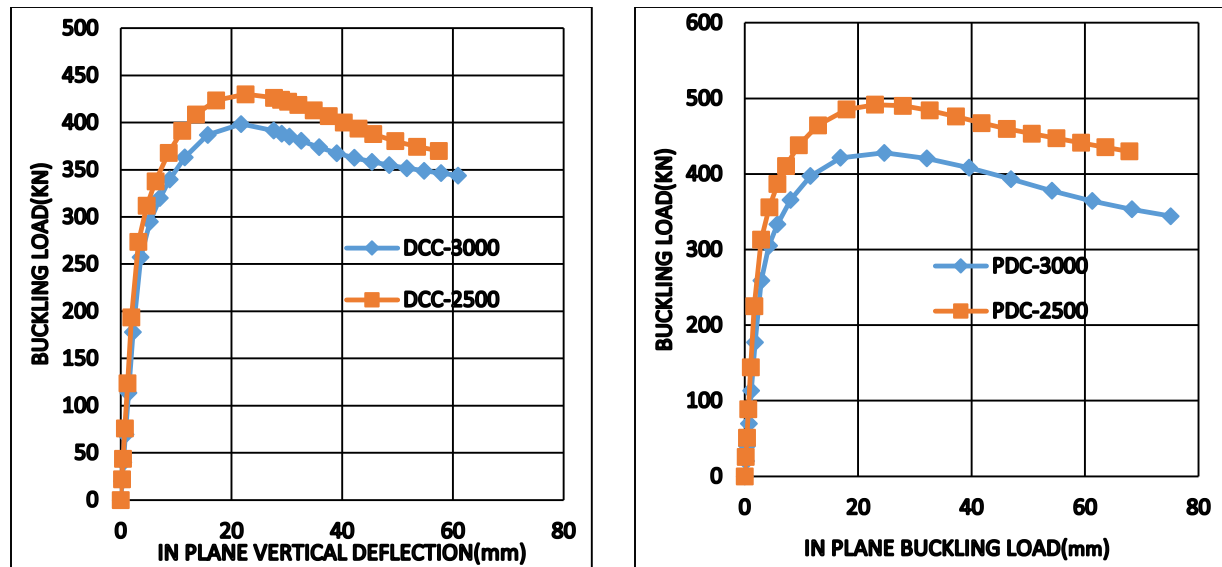


Figure 4. 27: Buckling load to deflection curve of DCC-3000, DCC-2500, PDC-3000 and PDC-2500 under MSPL

4.9.2. Effect of radius curvature under uniform radially distributed vertical load

Arched beams SCC-3000 ($R=2122.09\text{mm}$, subtended angle 90° , circular geometry, span length 3000mm and rise to span ratio=0.35) compared to its counterpart arched cell beam SCC-2500 only different by its radius of curvature due span length difference ($R=1333.35\text{mm}$, span length of 2500mm) also, parabolic arched cellular beam PSC-3000 ($R=2122.09\text{mm}$) compared to its identical except radius curvature PSC-2500 ($R=1330.35\text{mm}$) beam.

As shown on buckling load to in plane vertical deflection curve Figure 4.28 under uniform radially distributed vertical load shallow arched cellular beam deflects with same pattern with increasing radius of curvature, but increasing radius of curvature under uniform radially distributed vertical load has advantage of decreasing the horizontal shear stress which Cause web –post buckling due to this arched cellular steel beam of the same rise-to-span ratio with longer spans are stiffer than short span arched cellular steel of the same span to rise-ratio beam irrespective to arch geometry under uniform radially distributed vertical load.

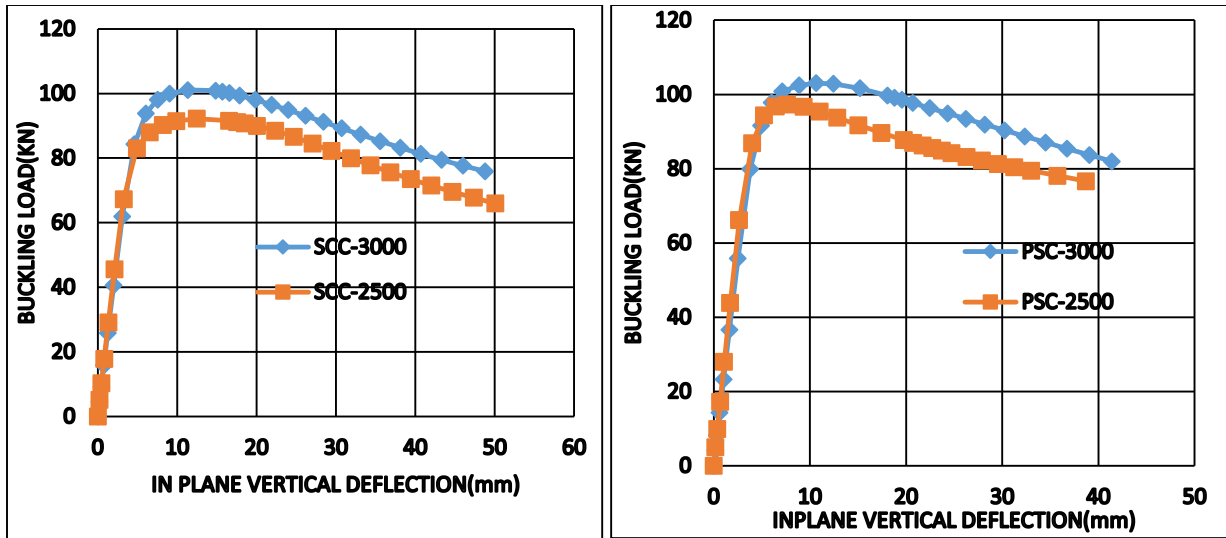


Figure 4. 28: Buckling load to deflection SCC-3000, SCC-2500, PSC-3000, PSC-2500 under URDVL

In contradiction to the above observation of the effect of increasing radius of curvature in deep arched cellular beam under uniform radially distributed vertical load reduces stiffness of arched cellular beam. As shown in Fig 4.29 in which deep parabolic and circular arch PDC-3000($R=2122.09$), DCC-3000($R=2122.09$) respectively compared to their identical counterpart except radius of curvature difference PDC-2500($R=1330.35$) and DCC-2500($R=1330.35$) of the same rise-to-span ratio ($H_s/L=0.35$). In terms of buckling load to in plane vertical deflection deep arched cellular beam with short span were structurally stiff and stronger.

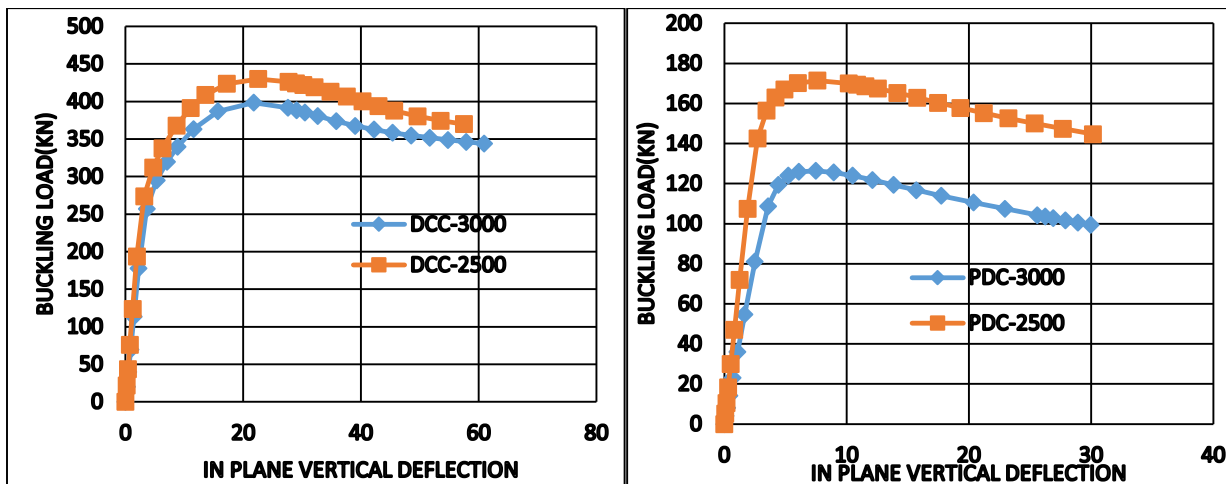


Figure 4. 29: Buckling load to deflection DCC-3000, DCC-2500, PDC-3000, and PDC-2500 under URDVL

CHAPTER FIVE

CONCLUSION AND RECOMMENDATION

Abaqus standard version 6.14 finite element program for the nonlinear elastic-plastic analysis of arches is used in this paper to investigate the in-plane elastic-plastic buckling and strength of circular and parabolic cellular steel arches pinned at both ends. The finite element program considers the effects of large deformations, material nonlinearities and initial geometric imperfection in predicting the elastic-plastic behavior of cellular steel arches under mid span concentrated and uniform radially distributed vertical loads, which induce combined bending and compression in the arch. The complex effect of rise-to-span ratio, arch geometry and radius of curvature on the in plane elastic-plastic stability and strength of cellular steel arches are included and discussed in these study.

From numerical analysis result extracted from finite element program used and three-dimensional simulation observation described under result and discussion chapter of this paper on selected samples identified in chapter three and in supportive of related literature the following conclusion were drawn on elastic-plastic in plane strength and stability of circular and parabolic arched cellular steel beam. However, caution must be taken in applying these conclusions to unsymmetrical loading condition, un-even web opening distribution and unsymmetrical section of arched cellular steel beams.

5.1. CONCLUSION

1. The proposed finite element package (ABAQUS), modelling step and method of analysis described shows good accuracy to experimental works to determine ultimate buckling load, out of plane deflection, in plane deflection and post buckling behavior of arched cellular steel beam. Can be used for large scale parametric study on this area.
2. Numerical analysis result from finite element program indicate that the structural stiffness of arched cellular beam is increased with rise-to-span ratio increment under mid span concentrated load regardless of arch geometry and degree of arch. For shallow circular arch as rise-to span ratio increases from 0.099 (subtended angle(θ) = 45^0) to 0.207(subtended angle(θ) = 90^0) ultimate buckling load increases by 12.54%, for shallow parabolic cellular arch increment of rise-to-span ratio from 0.099 to 0.207 results 18.7% increase in buckling load carrying capacity.

3. Under uniform radially distributed vertical load direct proportionality of circular arched cellular steel arch buckling load carrying capacity to rise-to-span ratio limited up to rise-to-span ratio=0.35, subtended angle 140° (DCC-2) beyond which rise-to-span ratio is inversely proportional to ultimate buckling load for circular arched cellular beam .in these case increment of rise-to-span ratio from 0.099(subtended angle(θ) = 45°) to 0.35 (subtended angle(θ) = 140°) increases ultimate buckling load by double(51.48%),but increasing rise to span ratio from 0.35 to 0.5(subtended angle(θ) = 180°) reduces buckling load by 7.03%.
4. For parabolic cellular steel arch under uniform radially distributed vertical load direct proportionality of arch buckling load carrying capacity to rise- to-span ratio limited to up to rise-to-span ratio=0.419 (PDC-3).increasing rise-to-span ratio beyond 0.419 reduces buckling load .for instance increasing rise-to span ratio from 0.099 to 0.419 increases buckling load by 65.97%. But increasing rise-to-span ratio from 0.419 to 0.5 reduces buckling load by 10.7%.
5. Ultimate buckling load comparison of arch geometry under similar rise-to –span ratio, span length and radius of curvature indicated that for cellular steel arches with rise-to-span ratio ($H_s/l \geq 0.133$, subtended angle $\geq 90^{\circ}$ for circular) parabolic arched cellular beam is structurally efficient (support larger load) than circular arched cellular beam. Comparison of arched cellular steel of the same rise-to span ratio of 0.207(subtended angle(θ) = 90° ,for circular) parabolic arched geometry shows increment of buckling load by 6.853 under mid span concentrated load and 5.19 % under uniform radially distributed vertical load. For rise to span ratio 0.283, 0.35, 0.419 and 0.5 parabolic arch buckling load greater than circular arched cellular steel of the same rise to span ratio by 9.51%, 12.53%, 16.47% and 23.57% under uniform radially distributed vertical loads.
6. Numerical finite element result extracted assured that increasing radius of curvature without altering rise-to-span ratio and subtended angle reduces ultimate buckling load carrying capacity of arched cellular beam regardless of arch geometry and degree of arch under mid span concentrated load.
7. Under uniform radially distributed vertical load increasing radius of curvature also increase ultimate buckling load of shallow arches. Conversely increasing radius of

curvature reduces ultimate buckling load of deep arched cellular beam under uniform radially distributed load.

8. Under mid span concentrated load symmetric web post buckling failure mode were expected while out of plane deflection is prominent type of failure mode in case of arched cellular beam under uniform radially distributed vertical load. In addition susceptibility to out of plane deflection of arched cellular beam increased with rise –to-span ratio.

8.2. RECOMMENDATION

In addition to structural complexity of arched structure due to non-uniform distribution of internal stress along arch length, introduction of opening on web makes analysis of arched cellular beam more complex. From point view of these study and available related literature on structural behavior of arched cellular beam the following topics requires further investigation to extend and fill gap on understanding arched cellular steel beam.

1. Developing analytical equation for buckling resistance of cellular arched webs using FE package.
2. Experimental and Numerical investigation on the out of plane inelastic buckling strength of arched cellular steel.
3. Studying the effect of support condition on strength of arched cellular beam.
4. Studying the effect of residual stress on strength of arched cellular beam.
5. Investigating effect end post length on structural behavior of arched cellular steel beam.

REFERENCES

- ABAQUS (2014) *Abaqus 6.14/CAE user's guide*. Dessault systemes, simulia corp., providence, RI, USA
- ABAQUS (2013) 'Abaqus analysis user guide' Dessault systemes, simulia corp., providence, RI, USA
- ANSI/AISC-360-10 (2010) *Specification for Structural Steel Buildings*. American Institute of steel construction.
- ArcelorMittal (2016) *The intelligent solution for long spans*. Luxembourg.
- Dou, C. (2015) 'Experimental Investigation into Flexural-Torsional Ultimate Resistance of Steel Circular Arches', *Journal of Structural Engineering*, 141(2015), pp. 1–12. doi: 10.1061/(ASCE)ST.1943-541X.0001240.
- Dowswell, B. (2018) *Curved Member Design Guide 33*. united state of America: American institute of steel construction.
- Durif, S. and Bouchair, a. (2016) 'Analytical model to predict the resistance of cellular beams with sinusoidal openings', *Journal of Constructional Steel Research*. Elsevier Ltd, 121, pp. 80–96. doi: 10.1016/j.jcsr.2016.01.015.
- Durif, S., Bouchair, A. H. and Vassart, O. (2013) 'Validation of an analytical model for curved and tapered cellular beams at normal and fire conditions', *Periodica Polytechnica Civil Engineering*, 57(1), pp. 83–95. doi: 10.3311/PPci.2144.
- EBCS EN 1993-1-1 : 2013 : 2013 Design of steel structures – Part 1-1 : General rules and rules for buildings*. Addis abeba ,Ethiopia.
- Erdal, F. and Polat, M. (2013) 'Ultimate load carrying capacity of optimally designed steel cellular beams', *Journal of Constructional Steel Research*. Elsevier Ltd, 80, pp. 355–368. doi: 10.1016/j.jcsr.2012.10.007.
- Ferreira, F. P. V., Rossi, A. and Martins, C. H. (2019) 'Lateral-torsional buckling of cellular beams according to the possible updating of EC3', *Journal of Constructional Steel Research*. Elsevier Ltd, 153, pp. 222–242. doi: 10.1016/j.jcsr.2018.10.011.
- Figueiredo, L. (2018) 'Design procedure for the web-post buckling of steel cellular beams', *Journal of Constructional Steel Research*. Elsevier Ltd, 148, pp. 525–541. doi: 10.1016/j.jcsr.2018.06.020.
- Guo, Y. (2015) 'An experimental study on out-of-plane inelastic buckling strength of fixed steel arches', *Engineering structures*. Elsevier Ltd, 98, pp. 118–127. doi: 10.1016/j.engstruct.2015.04.029.

Krishnachandran, V. N. (2016) 'Experimental and Analytical Investigations of Cellular Steel Beams', pp. 1886–1892.

Macsteel trading (2003) *Cellular beams design guide*. johannesburg: macsteel trading.

Madjour, A., Soltani, M. R. and Harkati, E. H. (2018) 'Numerical investigation into the ultimate strength of steel cellular beams with semi-rigid connections', *Periodica Polytechnica Civil Engineering*, 62(2), pp. 517–532. doi: 10.3311/PPci.11304.

McCormac, J. C. (1995) *Structural Steel Design LRFD Method*. Second edi. Harpercollins collage.

Morkhade, S. G. and Gupta, L. M. (2015) 'An experimental and parametric study on steel beams with web openings', *International Journal of Advanced Structural Engineering*. Springer Berlin Heidelberg, 7(3), pp. 249–260. doi: 10.1007/s40091-015-0095-4.

Trahair, M.A.Bradfoed, D.A.Nethercot, and L. G. (2008)" *The behaviour and design of steel structures to EC3*". Fourth edi. USA and CANADA: by Taylor and Francis.

Nimmi, K. P. and Krishnachandran, V. N. (2016) 'Buckling Analysis of Cellular Steel Beams with and', 4(Viii), pp. 609–615.

Pachpor P.D, Gupta L.M, D. n. . (2011) 'Finite element analysis and comparison of castellated & cellular beam', *Advanced Materials Research*, 264-65, pp. 694–699. doi: 10.4028/www.scientific.net/AMR.264-265.694.

Panedpojaman, P. and Rongram, T. (2014) 'Design Equations for Vierendeel Bending of Steel Beams with Circular Web Openings', *World Congress on Engineering 2014*, II(c), pp. 0–5.

Pi, Y., Bradford, M. A. and Tin-loi, F. (2008a) 'In-plane strength of steel arches', *Advanced Steel Construction*, 4(4), pp. 306–322.

Pi, Y., Bradford, M. A. and Tin-loi, F. (2008) 'In-plane strength of steel arches', 4(4), pp. 306–322.

Pi, Y., Bradford, M. A. and Uy, B. (2002) 'In-plane stability of arches', 39, pp. 105–125.

Pi, Yong-lin, Trahair, N. . (1998) 'Out-of-plane inelastic buckling and strength of steel arches By Yong-Lin', *Journal of Structural Engineering*, 124(2), pp. 174–183.

Sameer S.Fares, John Coulson, D. W. D. (2016) *AISC DESIGN GUIDE 31 Castellated and Cellular Beam Design*. united state of America: American Institute of steel construction.

Shivatare, C. V (2017) 'Comparative analysis of conventional truss system and cellular beam system', *IJARIE*, 3(4), pp. 2804–2809.

Spoorenberg, R. C. *et al.* (2012) ‘Design rules for out-of-plane stability of roller bent steel arches with FEM’, *Journal of constructional steel research*. Elsevier Ltd, 79, pp. 9–21. doi: 10.1016/j.jcsr.2012.07.027.

Warren, J. (2001) ‘ultimate load and deflection behaviour of cellular beams’, *Master of science thesis ,university of natal,DURBAN*.

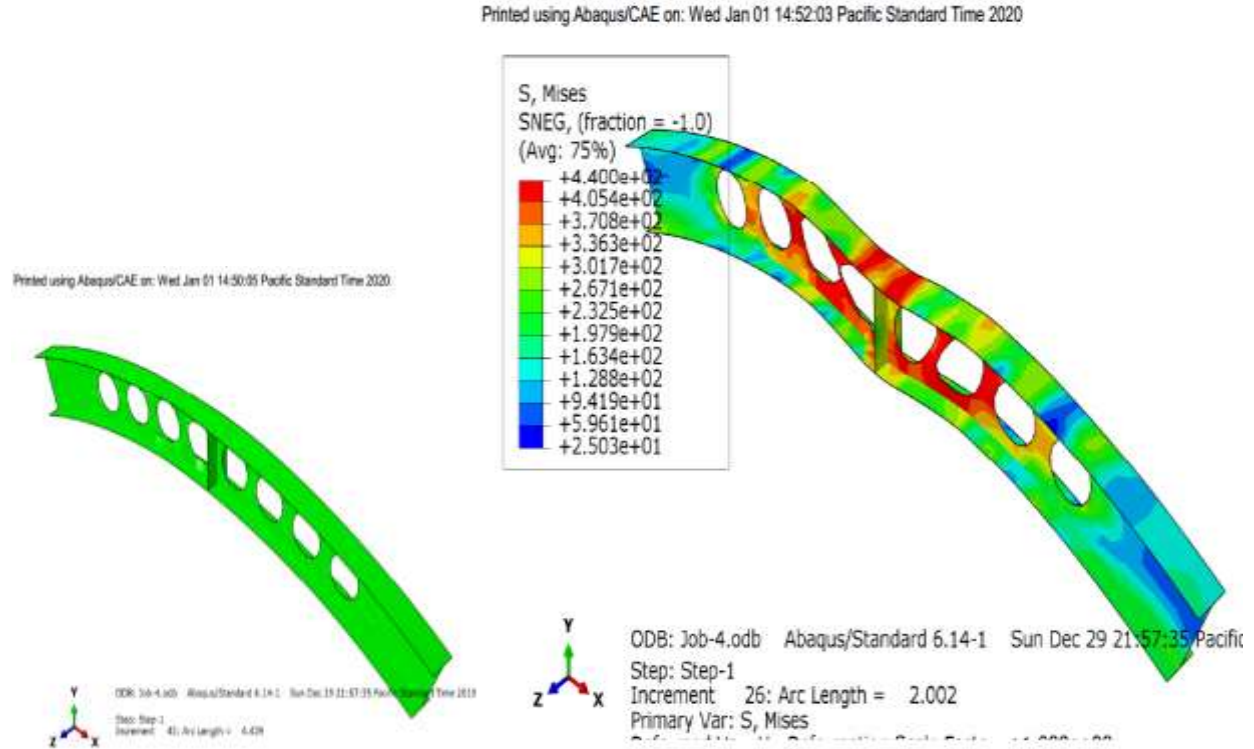
Yong -lin pi, T. N. . R. B. Y. (1999) ‘In-plane buckling and design of steel arches’, *Journal of Structural Engineering*, 125(November), pp. 1291–1298.

Zaher, O. F., Yossef, N. M. and Dabaon, M. A. (2018) ‘Structural behaviour of arched steel beams with cellular openings’, *Journal of Constructional Steel Research*. Elsevier Ltd, 148, pp. 756–767. doi: 10.1016/j.jcsr.2018.06.029.

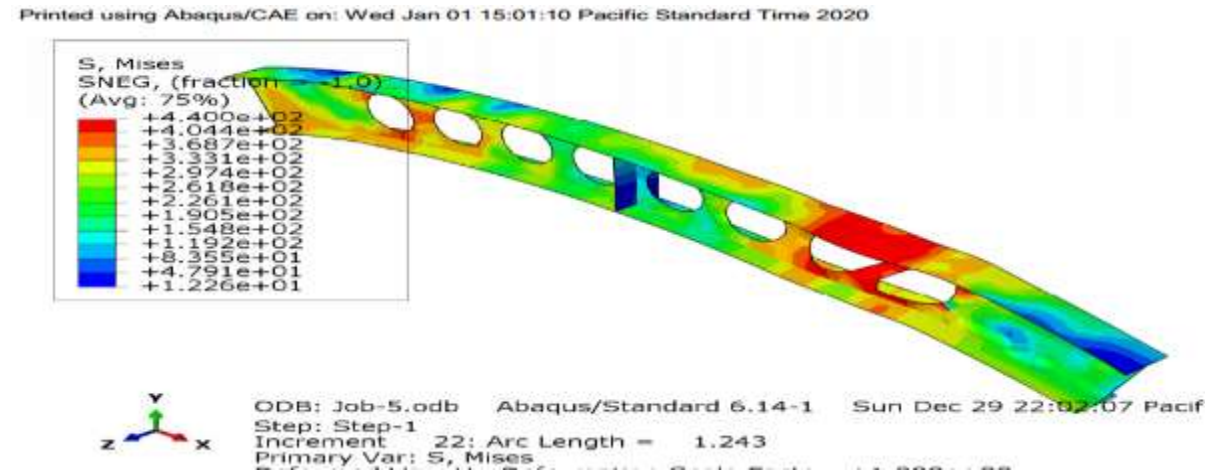
Ziemain, R. D. (2010) *GUIDE TO STABILITY DESIGN CRITERIA FOR METAL STRUCTURES*. sixth. Hoboken,New Jersey: John wiley and sons,Inc.

APPENDIX-A

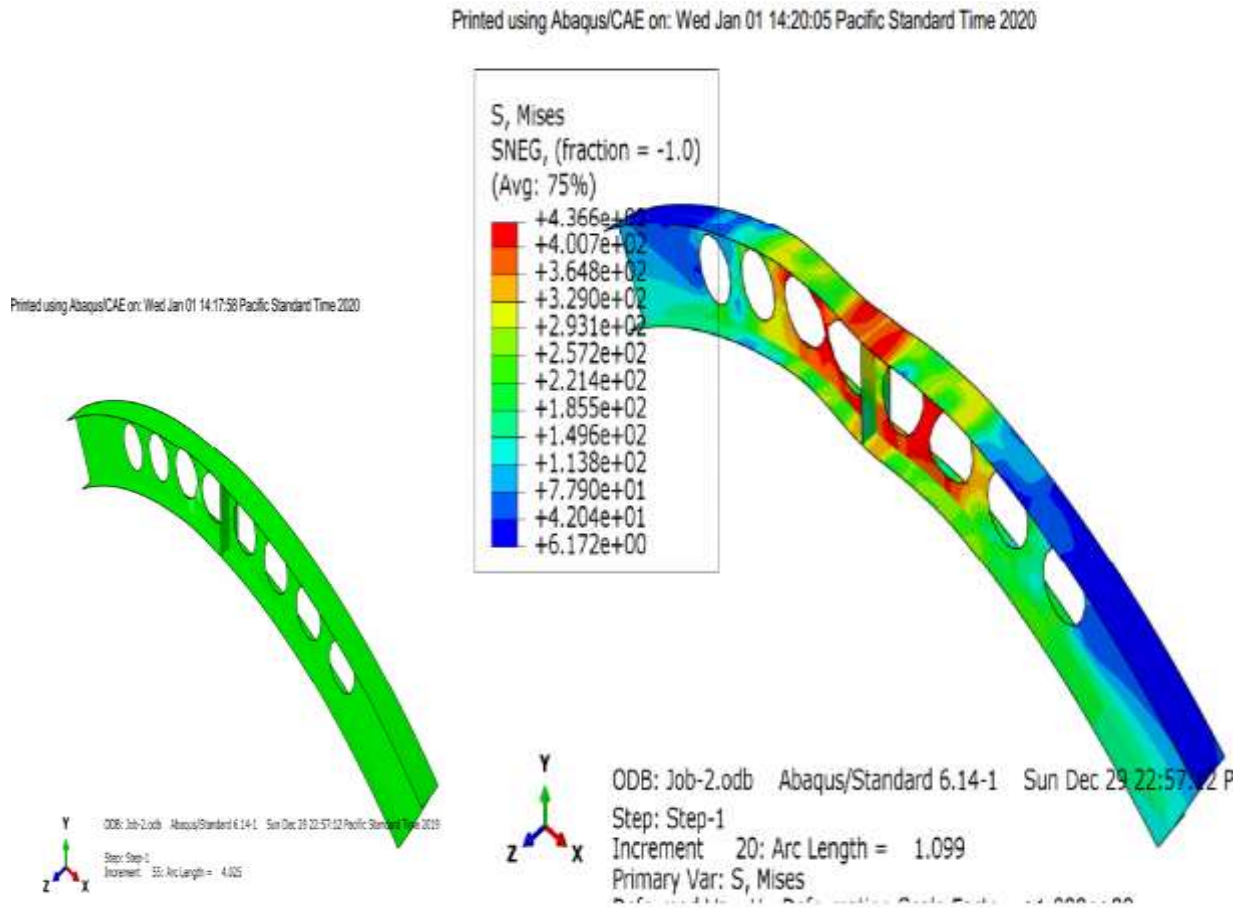
3-D DEFORMED AND UNDEFORMED CIRCULAR ARCHED CELLULAR MODEL



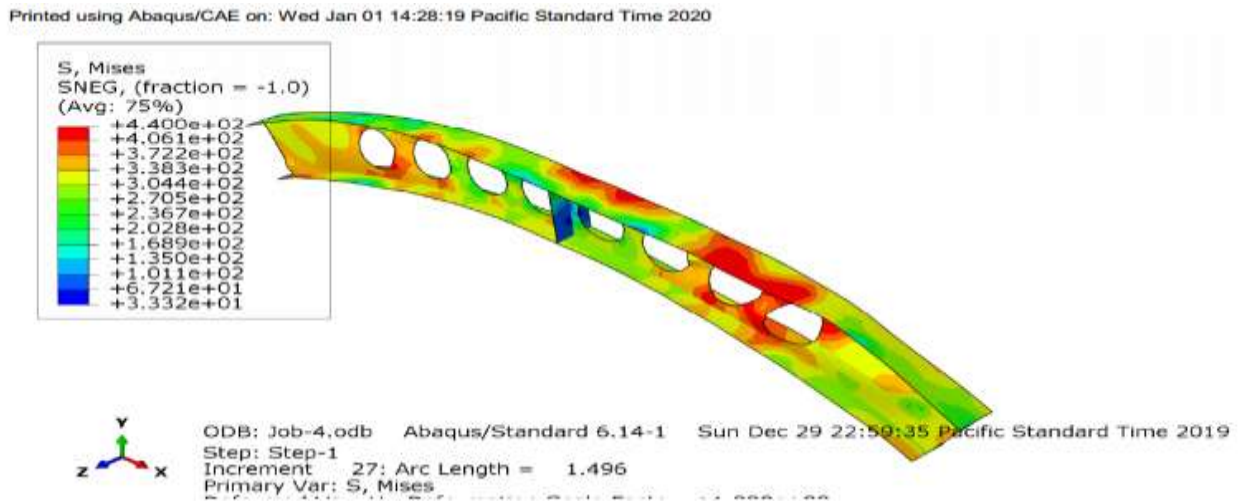
SCC-1, undeformed and deformed shape under mid span concentrated load.



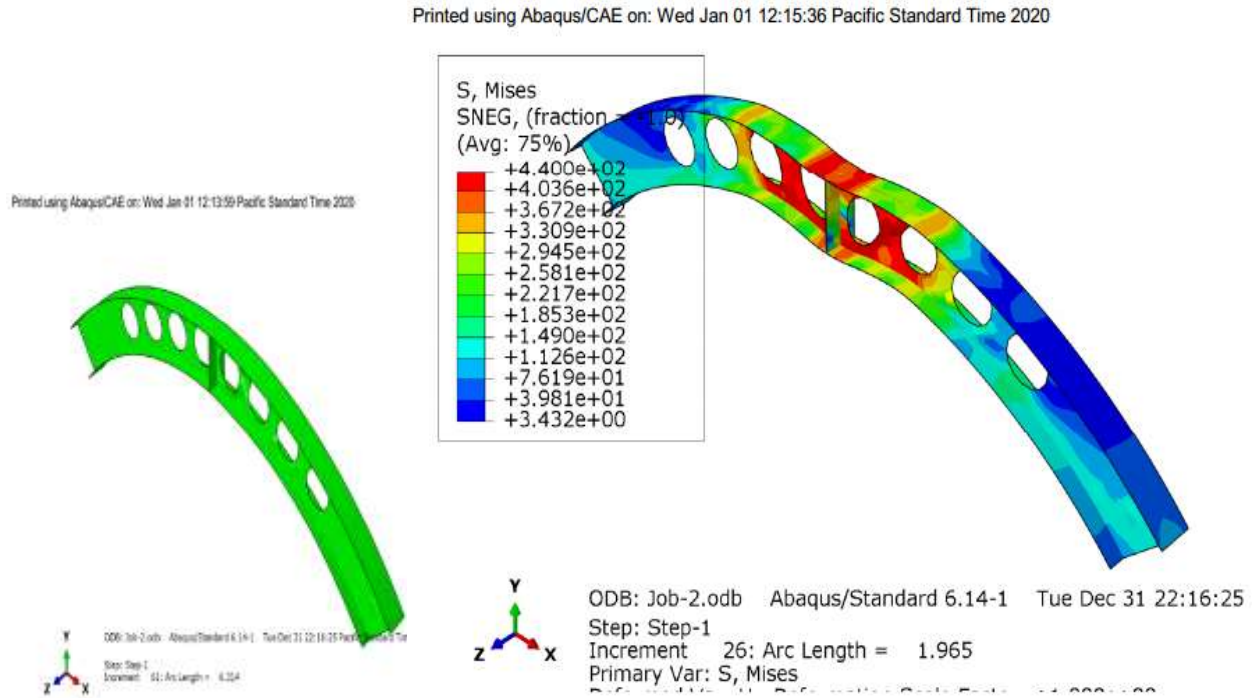
SCC-1, deformation under uniform radially distributed load



SCC-2 ,Un-deformed and deformed shape under mid-span concentrated load.

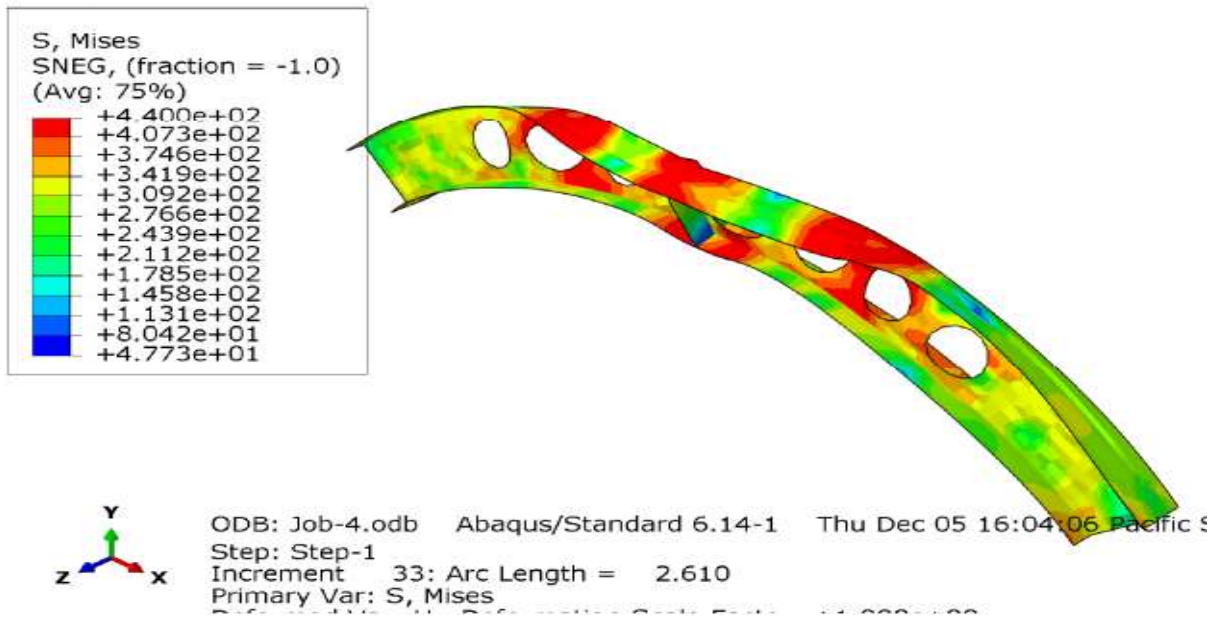


SCC-2 ,deformed shape under uniform radially disterbuted vertical load.

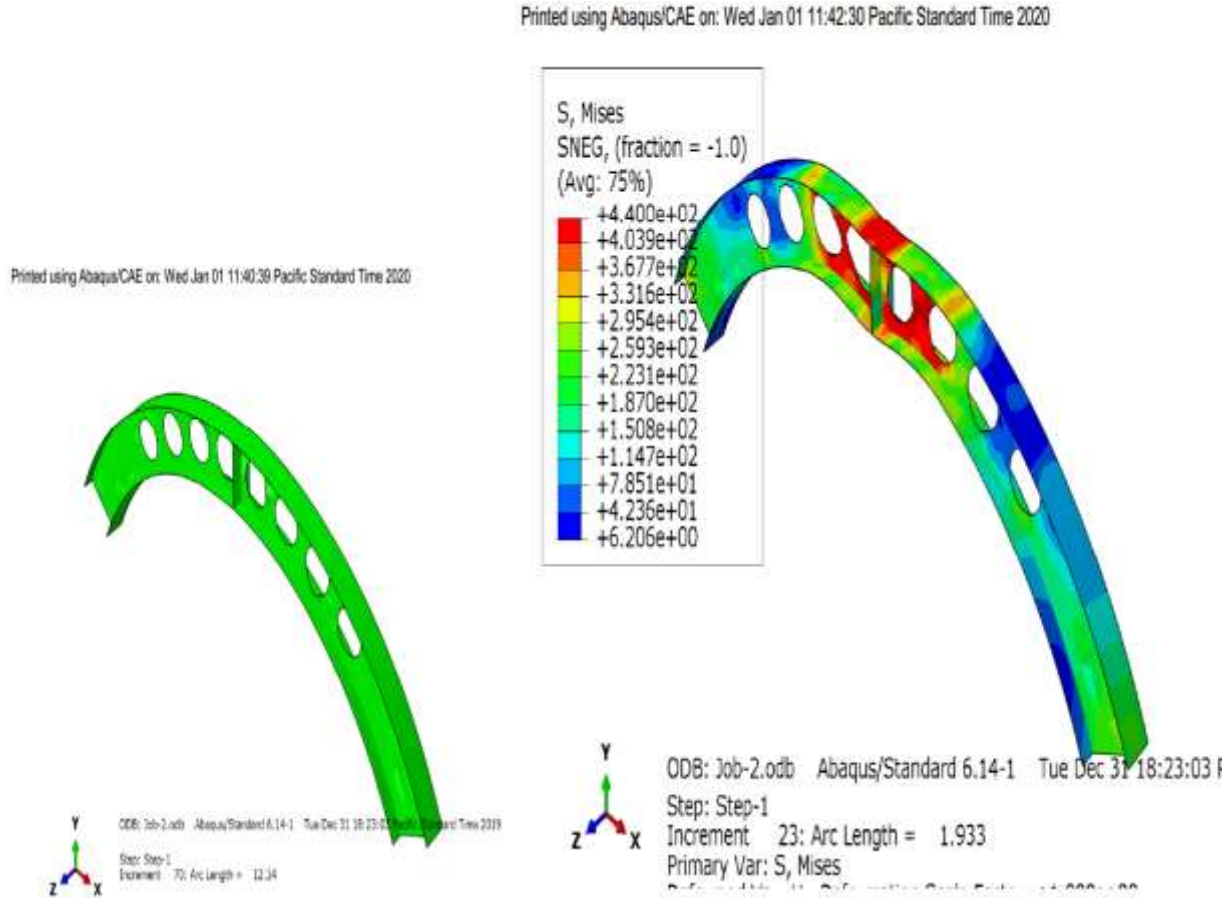


SCC-3, deformation under mid span concentrated load

Printed using Abaqus/CAE on: Wed Jan 01 12:21:53 Pacific Standard Time 2020

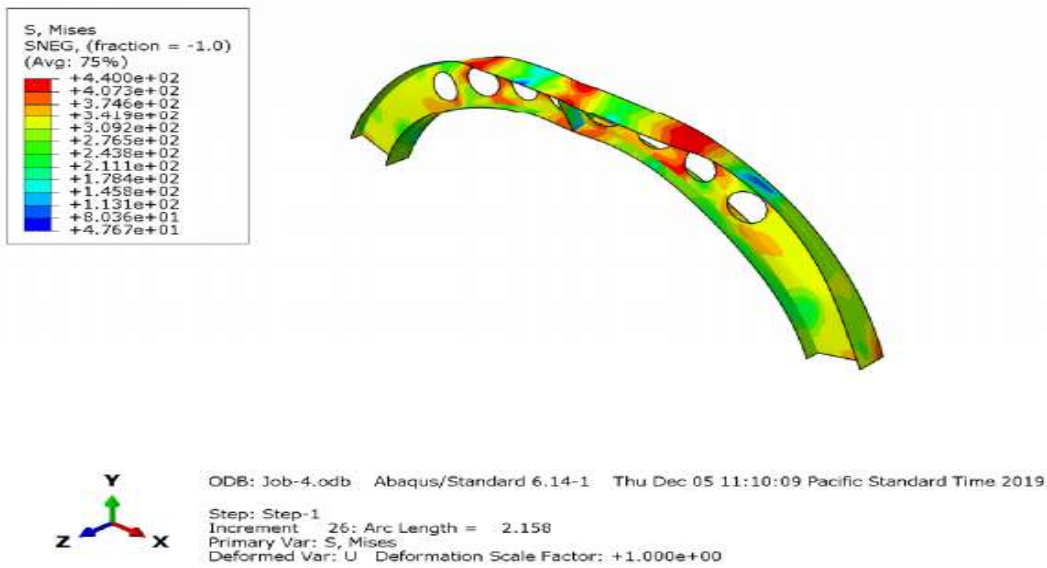


SCC-3, deformation under uniform radially distributed vertical load

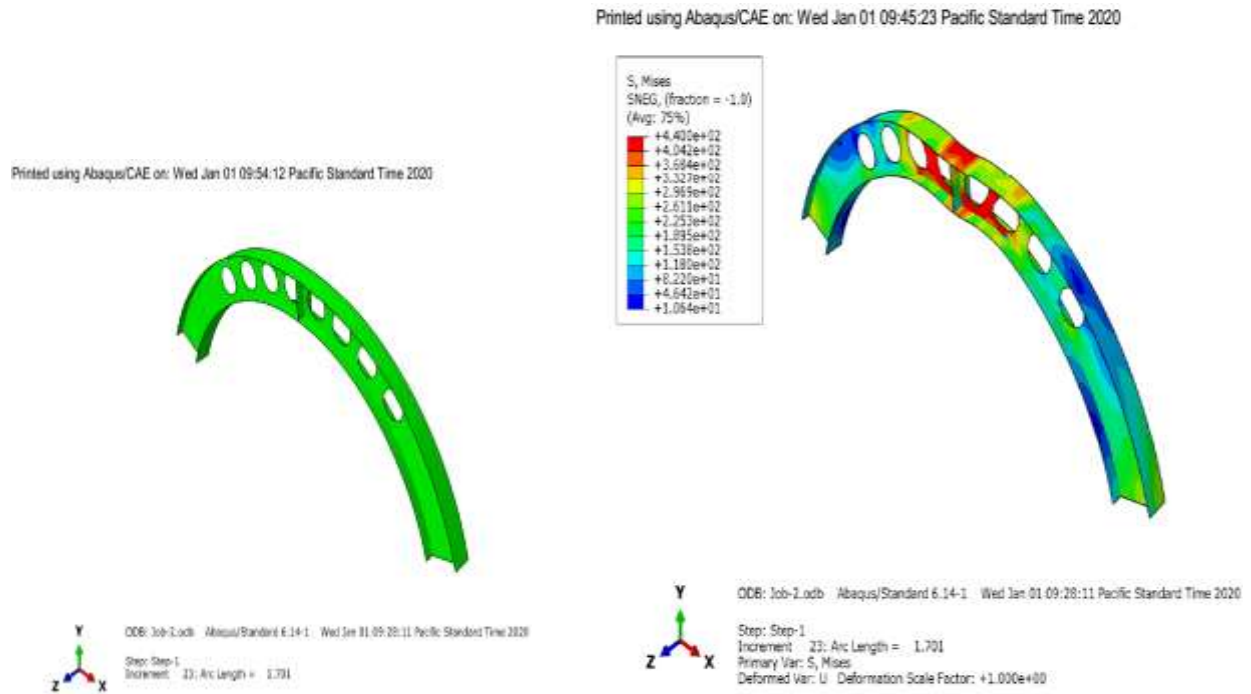


DCC-1, un deformed and deformed shape under mid span concentrated load

Printed using Abaqus/CAE on: Wed Jan 01 10:30:11 Pacific Standard Time 2020

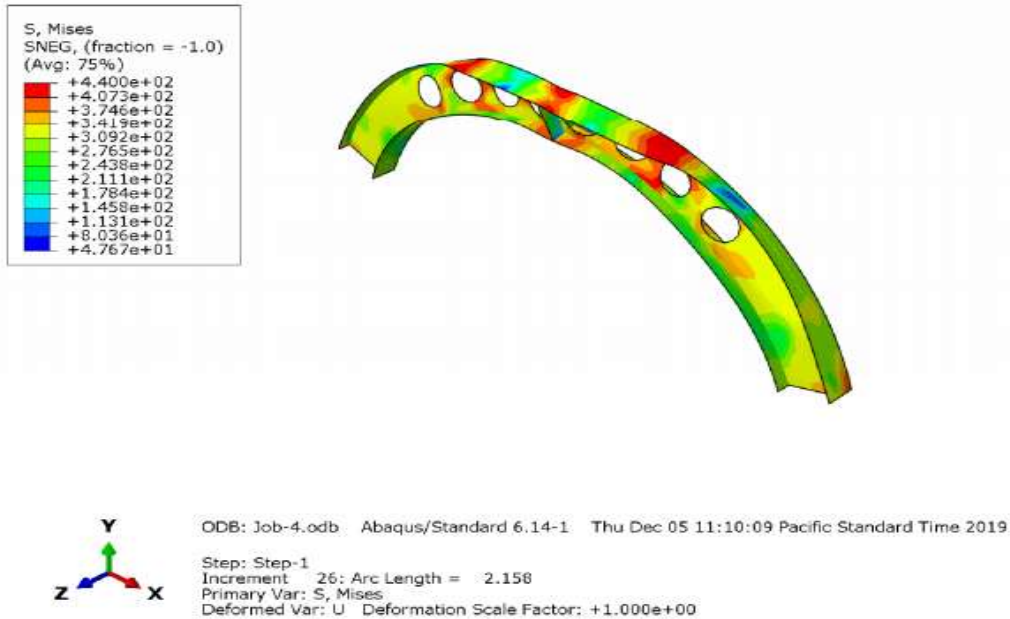


DCC-1, Defromation shape under uniform radially distributed vertical load



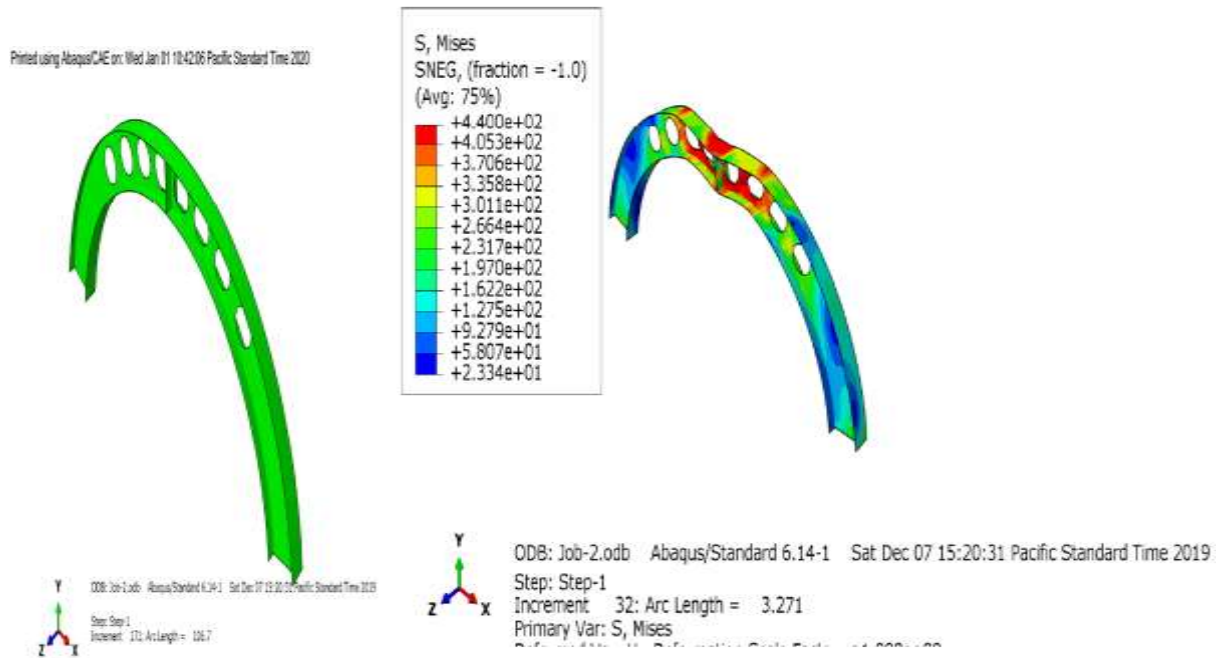
DCC-2, un- deformed and deformed shape under mid span point load

Printed using Abaqus/CAE on: Wed Jan 01 10:30:11 Pacific Standard Time 2020



DCC-2, deformed shape under Uniform radially distributed vertical load

Printed using Abaqus/CAE on: Wed Jan 01 10:52:14 Pacific Standard Time 2020

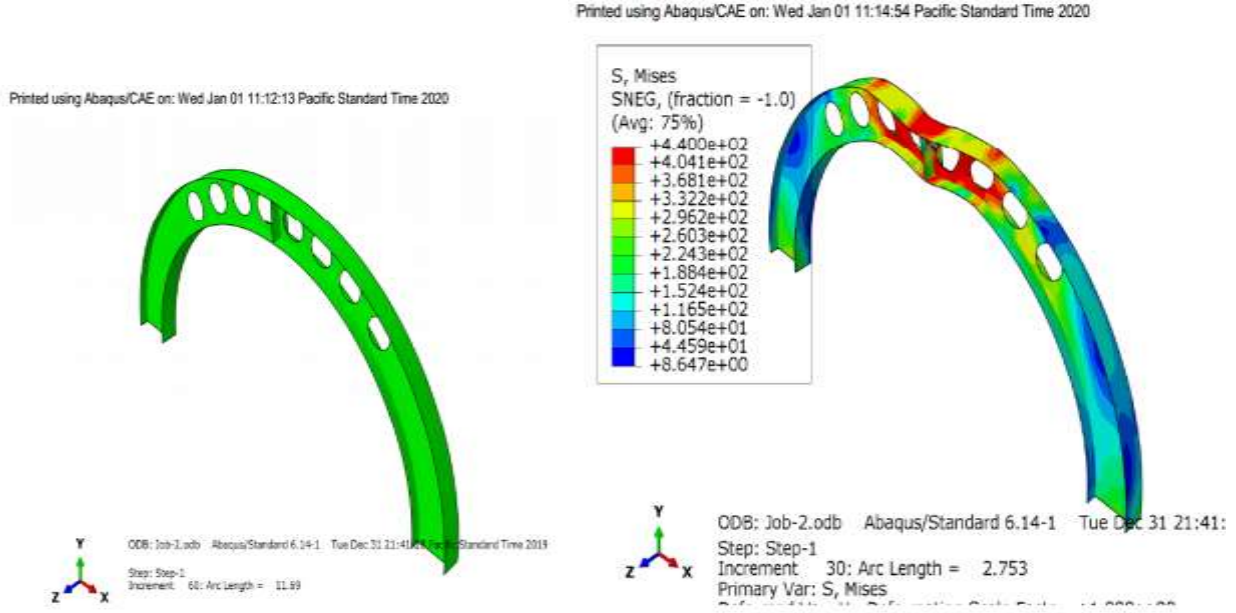


Dcc-3, un-deformed and deformed shape under midpoint load

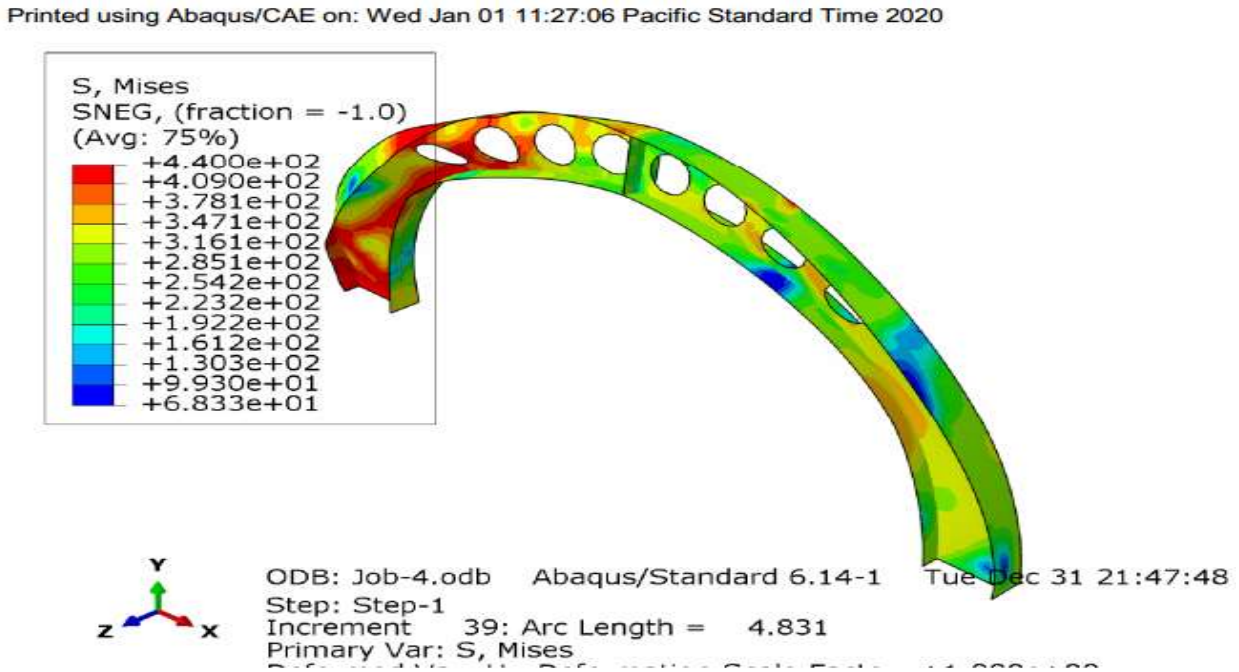
Printed using Abaqus/CAE on: Wed Jan 01 11:01:34 Pacific Standard Time 2020



Dcc-3, deformed shape under uniform radially distributed vertical load



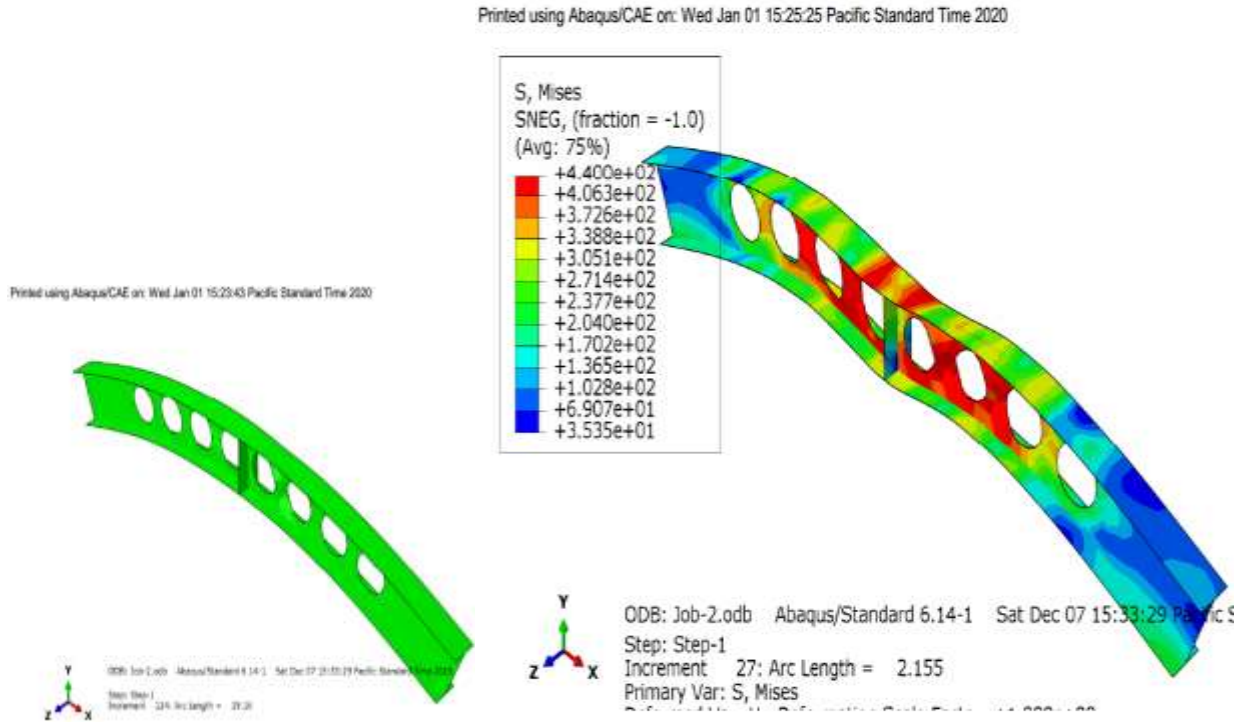
DCC-4, un-deformed and deformed shape under mid span concentrated load



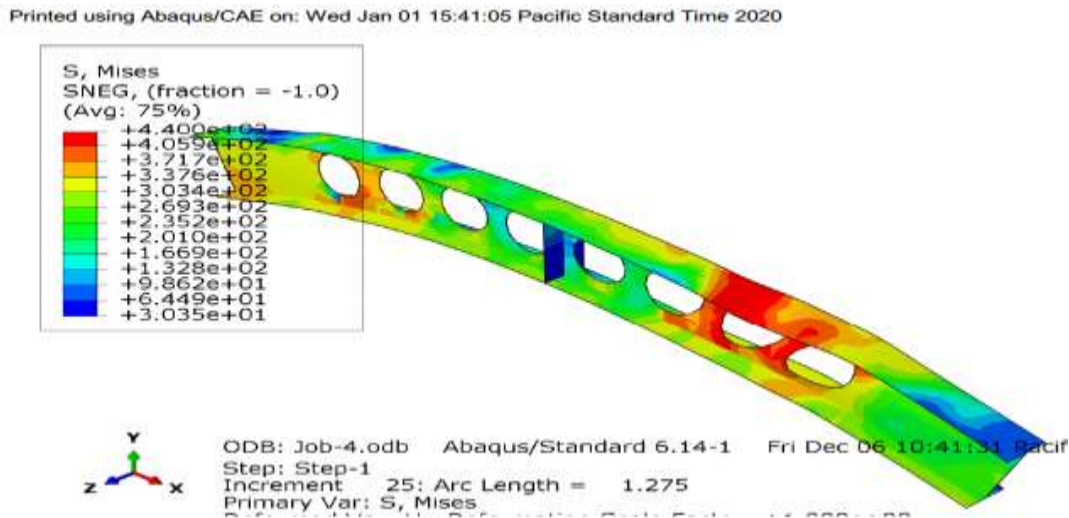
DCC-4, deformation under uniform radially distributed vertical load

APPENDIX-B

3-D UNDEFORMED AND DEFORMED SHAPE OF PARABOLIC CELLULAR ARCH MODEL

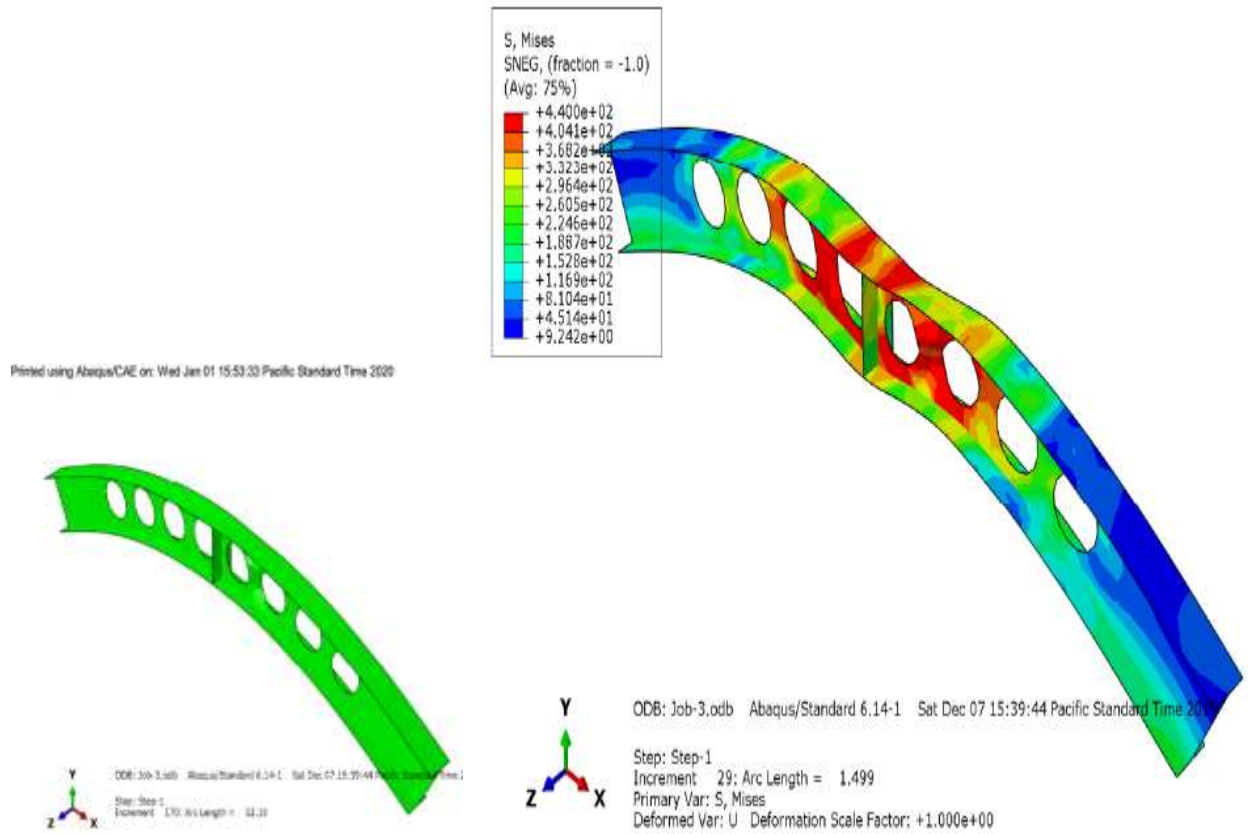


PSC-1, un-deformed and deformed shape under mid –span concentrated load



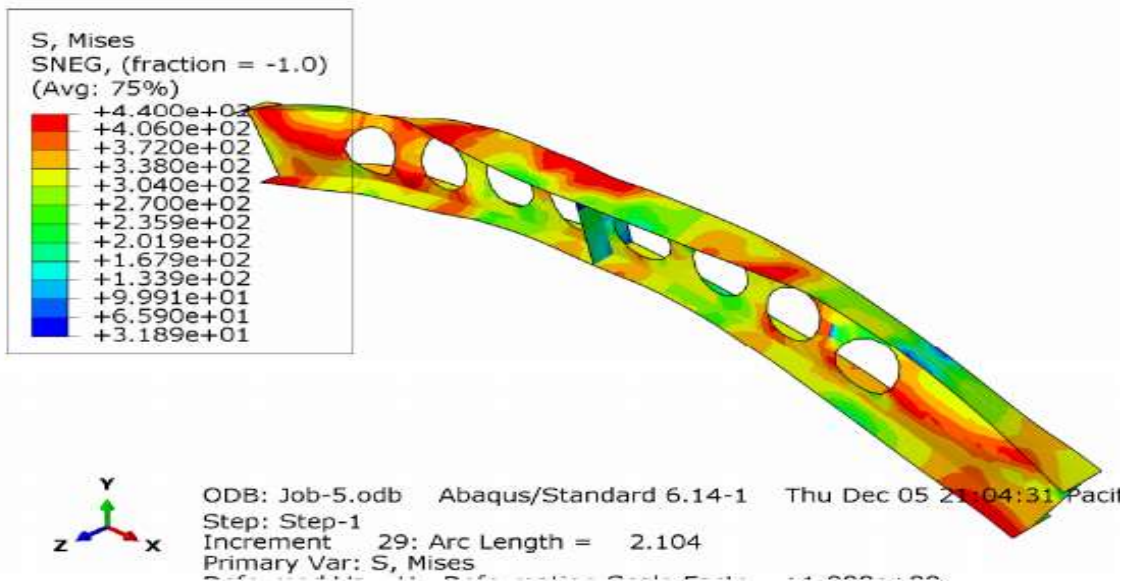
PSC-1, deformed shape under uniform radially distributed vertical load

Printed using Abaqus/CAE on: Wed Jan 01 15:55:09 Pacific Standard Time 2020



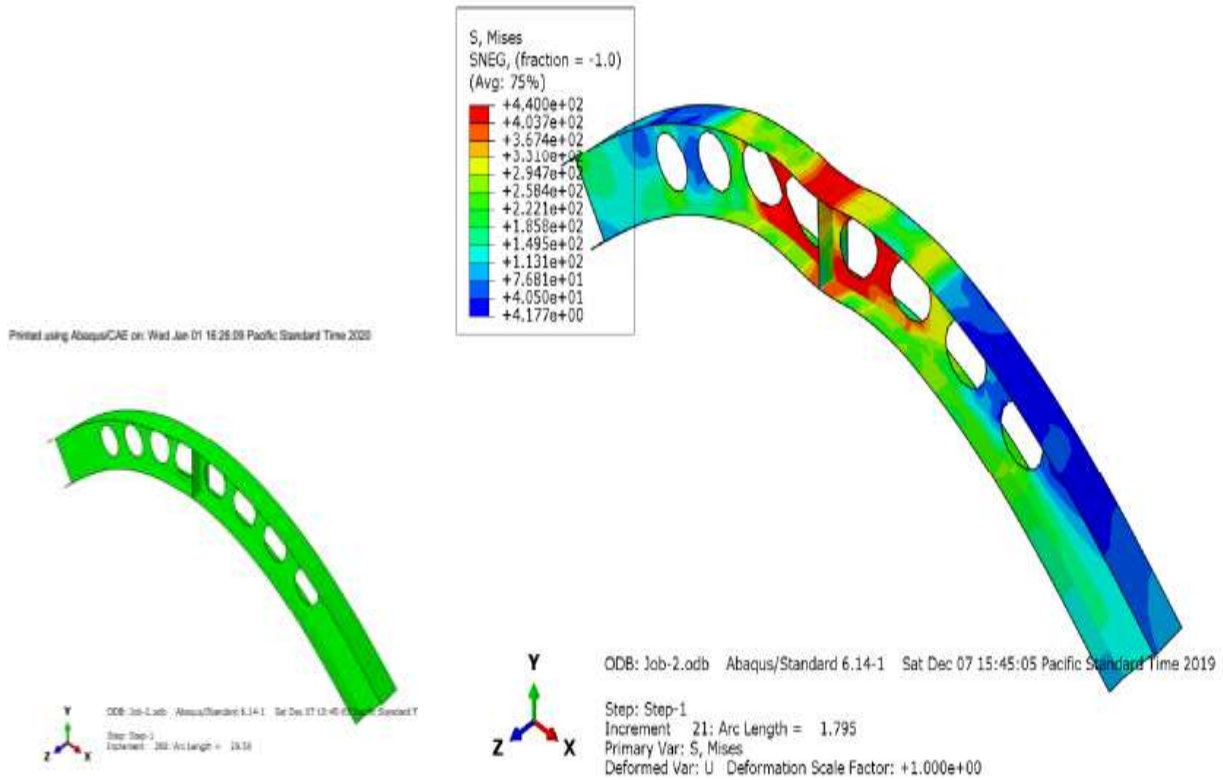
PSC-2, un-deformed and deformed shape under mid-span concentrated load.

Printed using Abaqus/CAE on: Wed Jan 01 16:16:06 Pacific Standard Time 2020



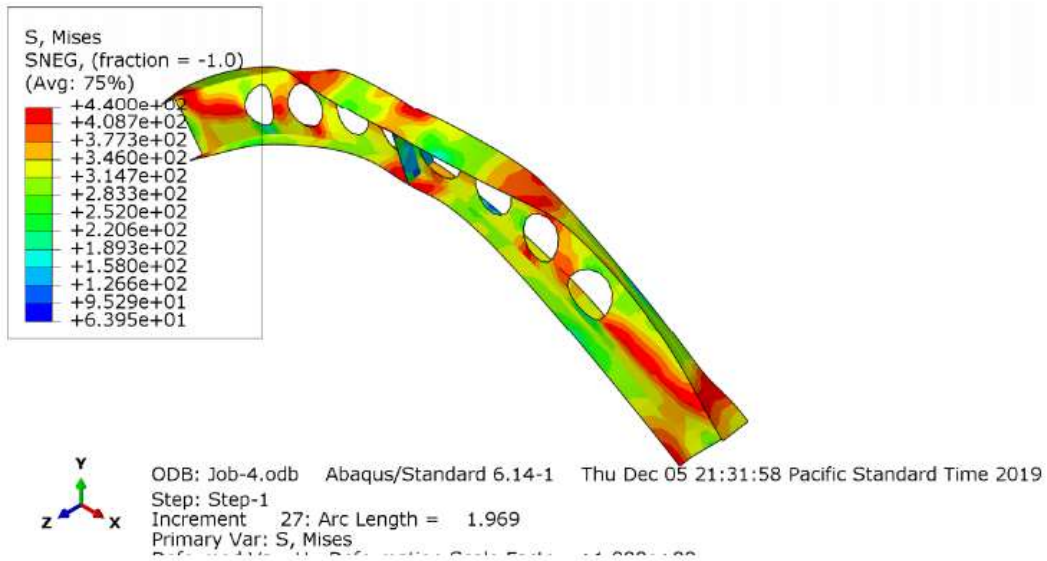
PSC-2, deformed shape under uniform radially distributed vertical load

Printed using Abaqus/CAE on: Wed Jan 01 16:27:38 Pacific Standard Time 2020



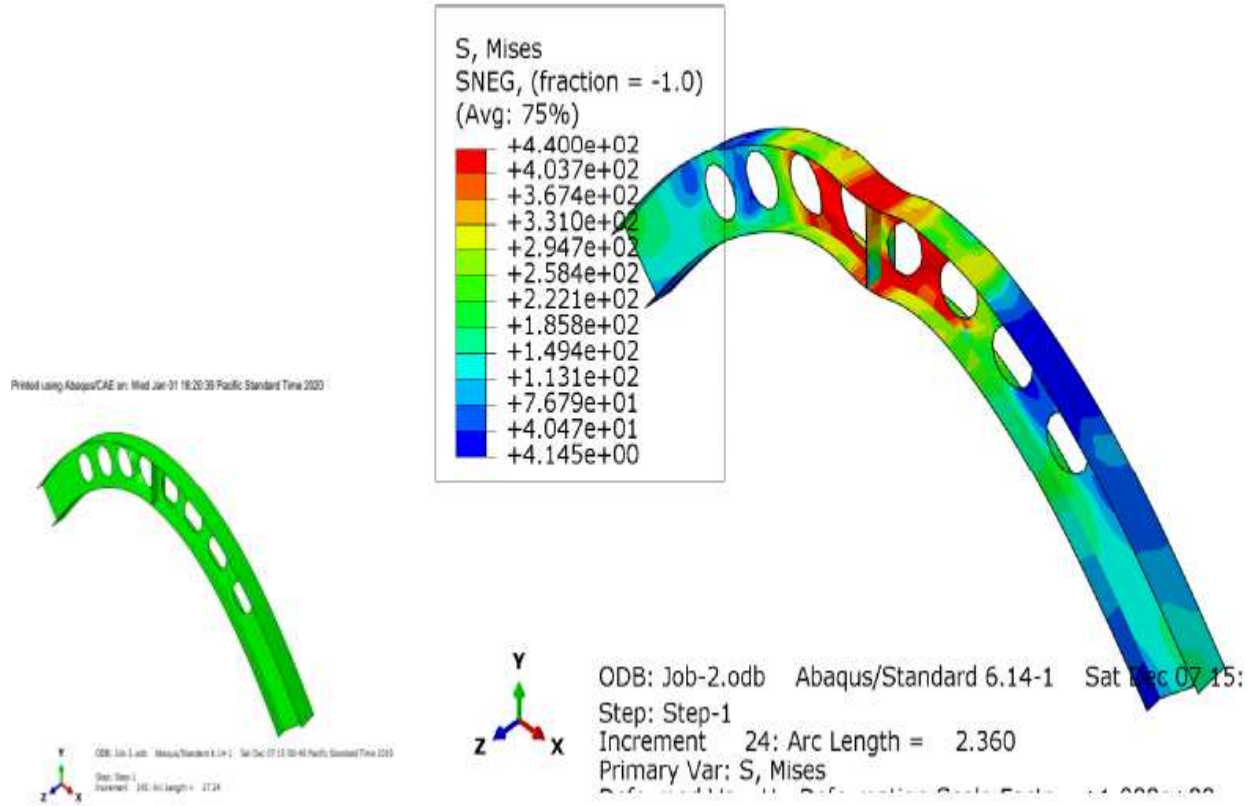
PSC-3, un-deformed and deformed under mid-span point load

Printed using Abaqus/CAE on: Wed Jan 01 16:34:12 Pacific Standard Time 2020



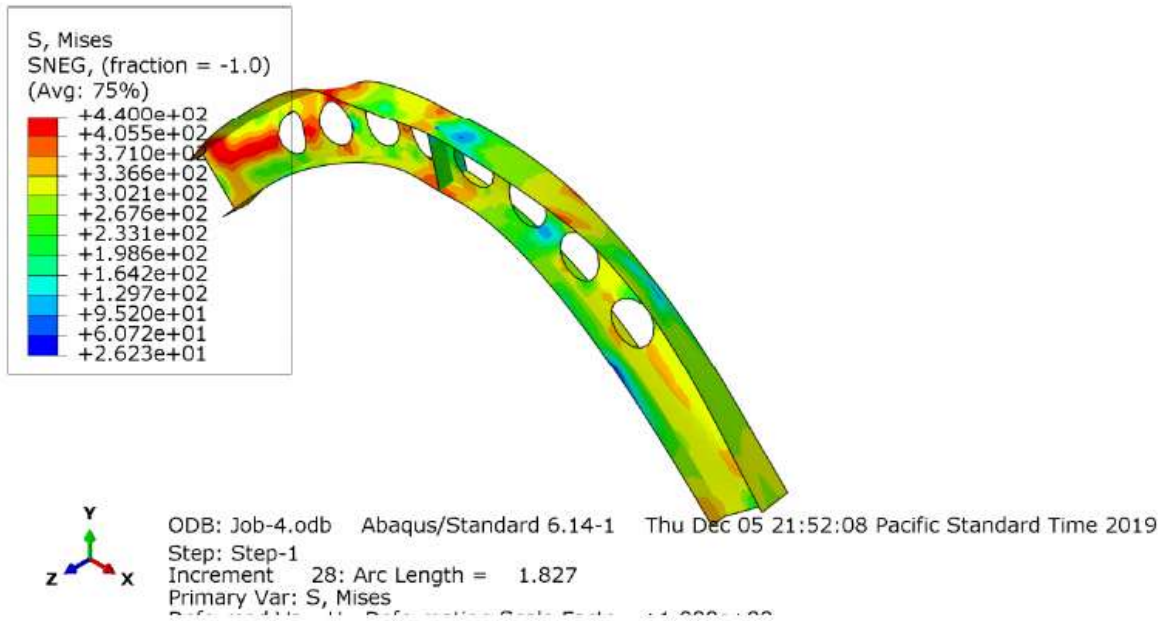
PSC-3, deformed shape under uniform radially distributed vertical load

Printed using Abaqus/CAE on: Wed Jan 01 18:22:09 Pacific Standard Time 2020

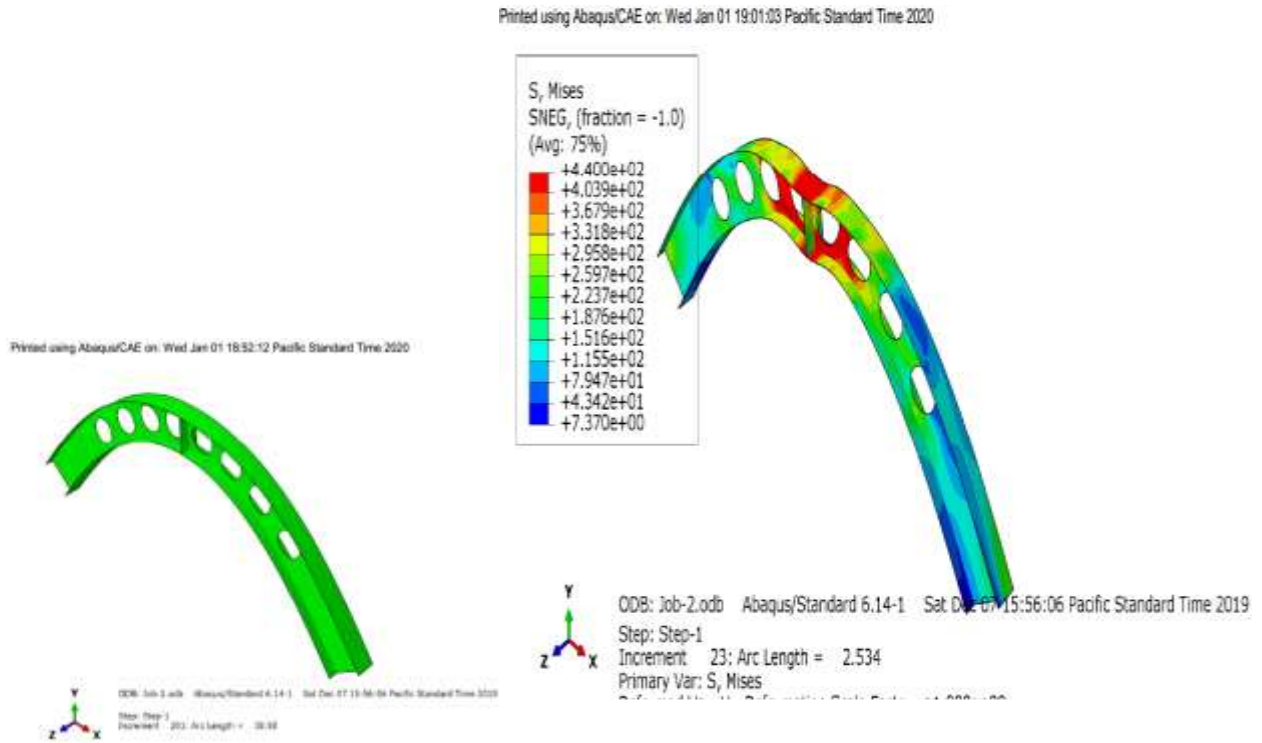


PDC-1, un-deformed and deformed shape under mid span concentrated load

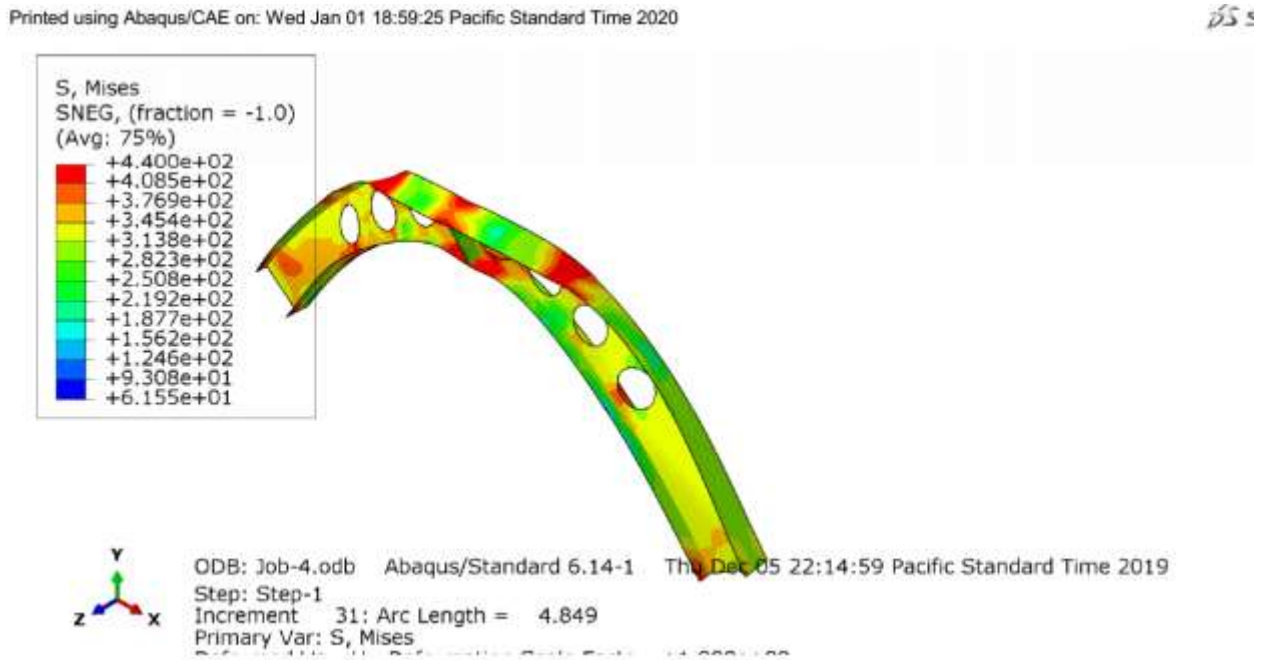
Printed using Abaqus/CAE on: Wed Jan 01 18:35:05 Pacific Standard Time 2020



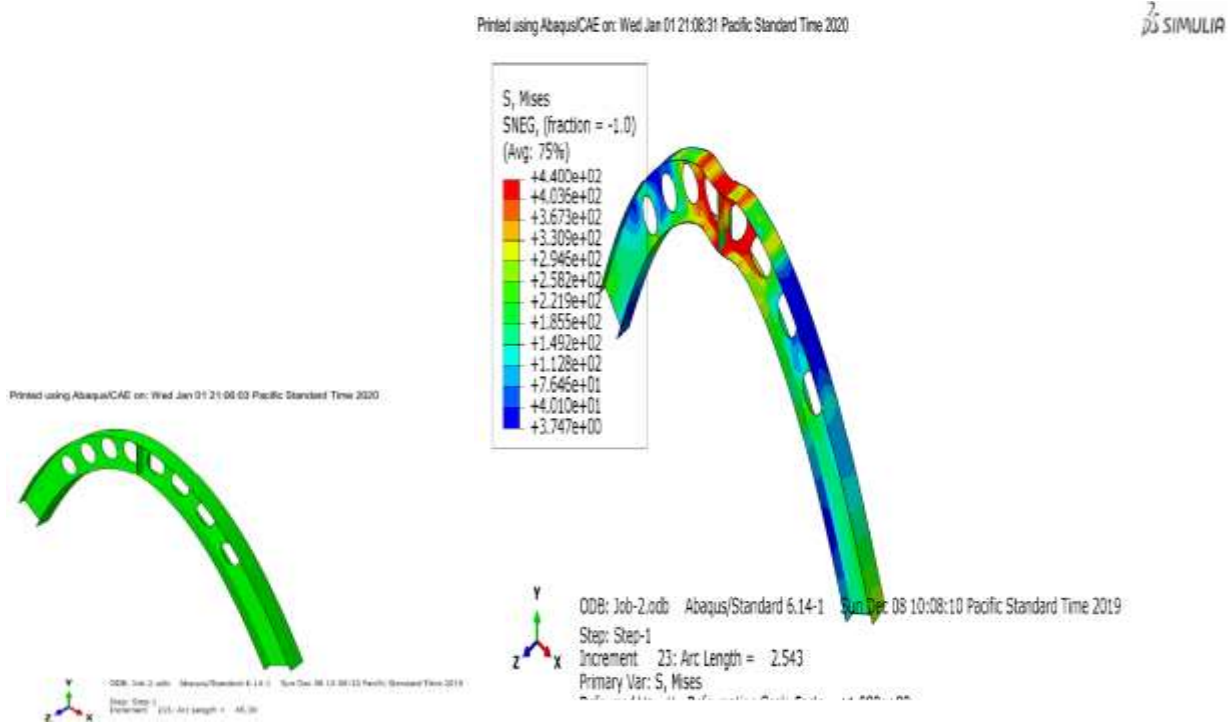
PDC-1, deformed shape uniform radially distributed vertical load



PDC-2, un-deformed and deformed shape under mid-span concentrated load



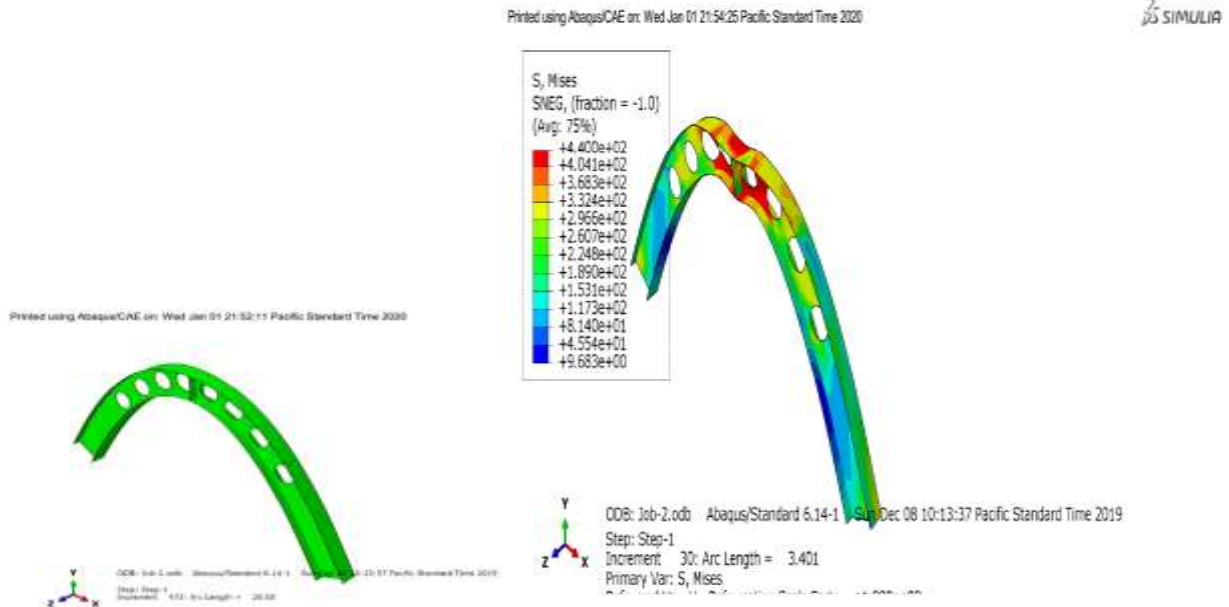
PDC-2, deformed shape under uniform radially distributed load



PDC-3, un-deformed and deformed shape under mid span concentrated load.

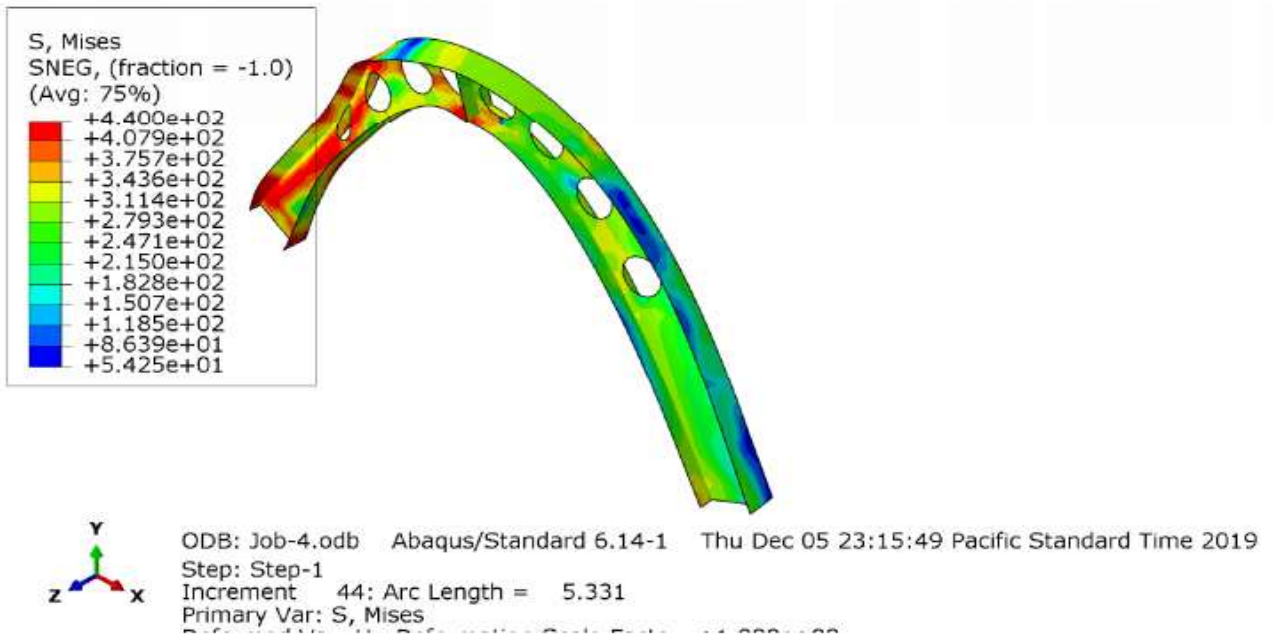


PDC-3, deformed shape under uniform radially distributed vertical load



PDC-4, un-deformed and deformed shape under mid-span concentrated load

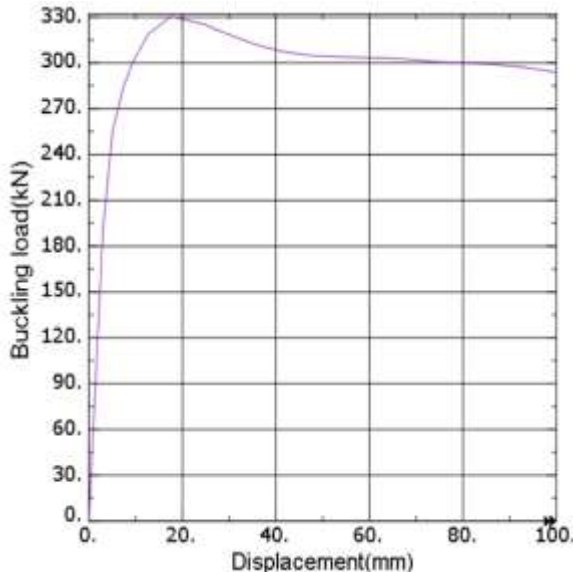
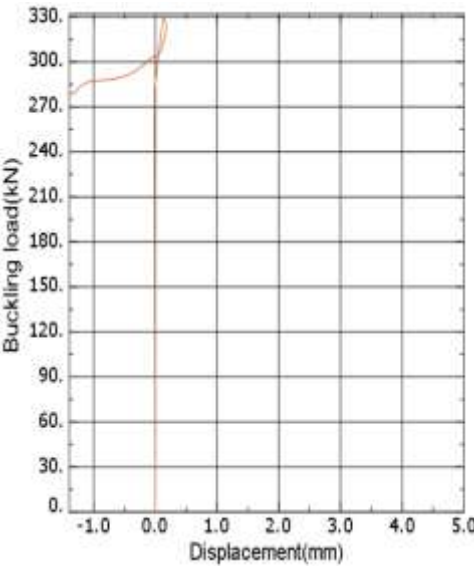
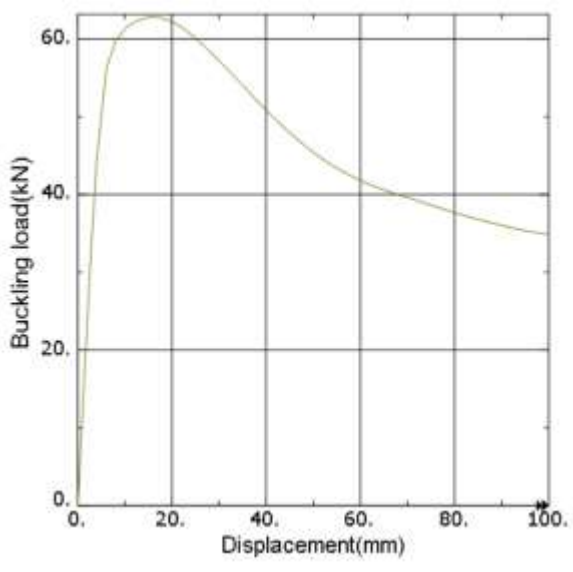
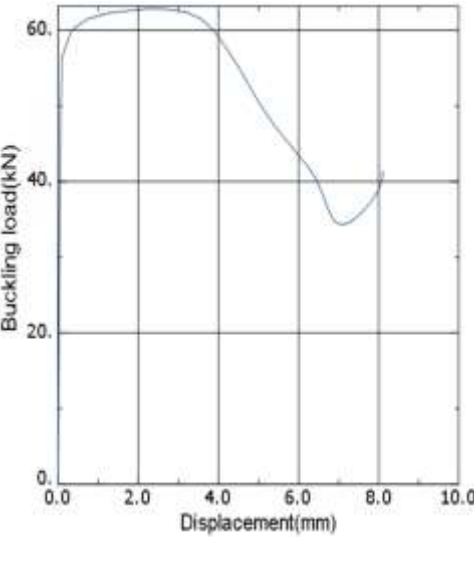
Printed using Abaqus/CAE on: Wed Jan 01 22:05:43 Pacific Standard Time 2020

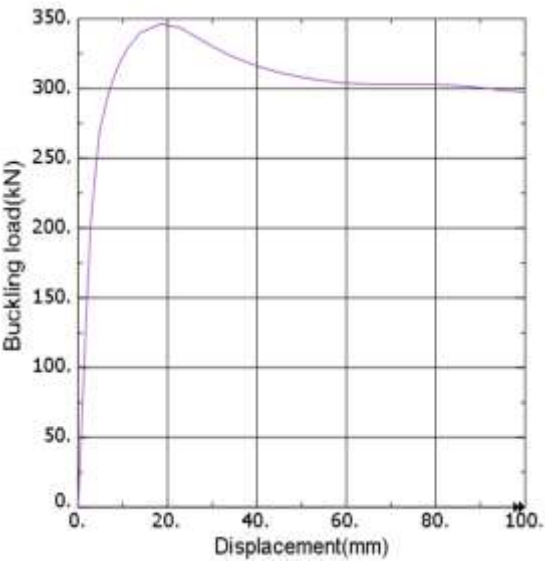
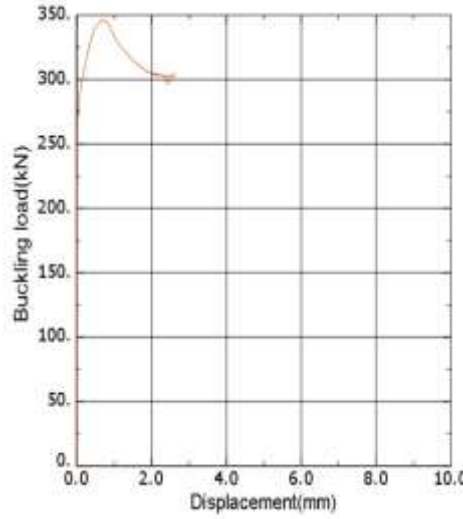
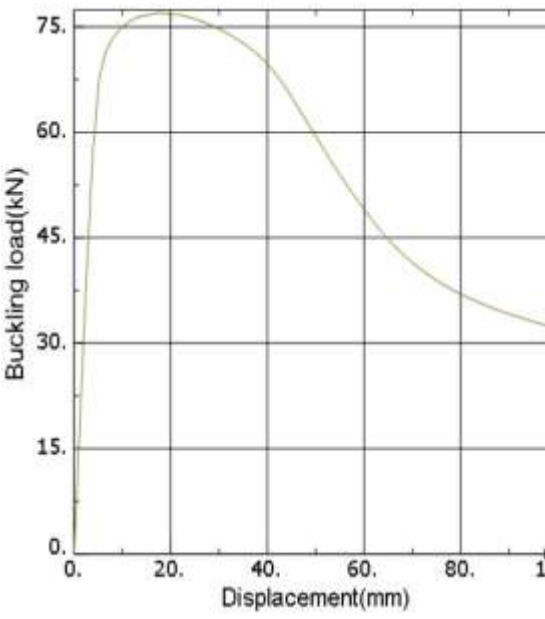
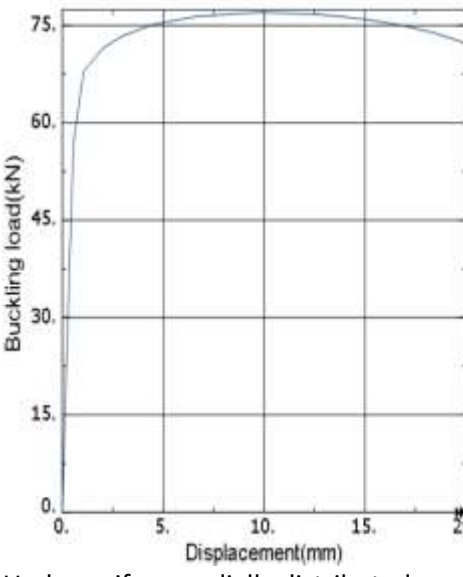


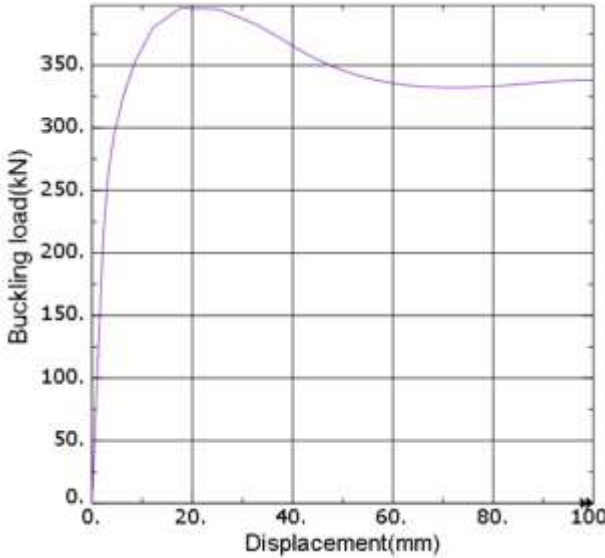
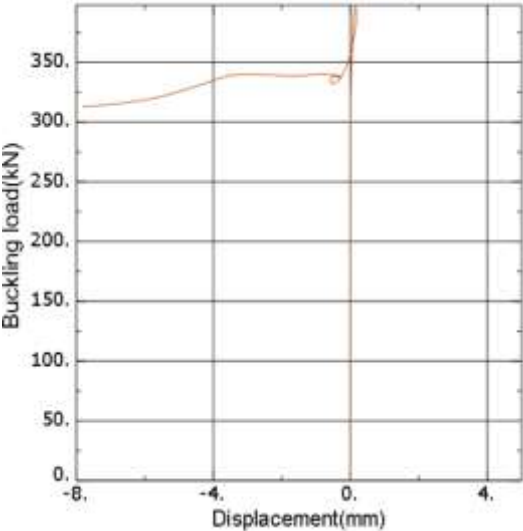
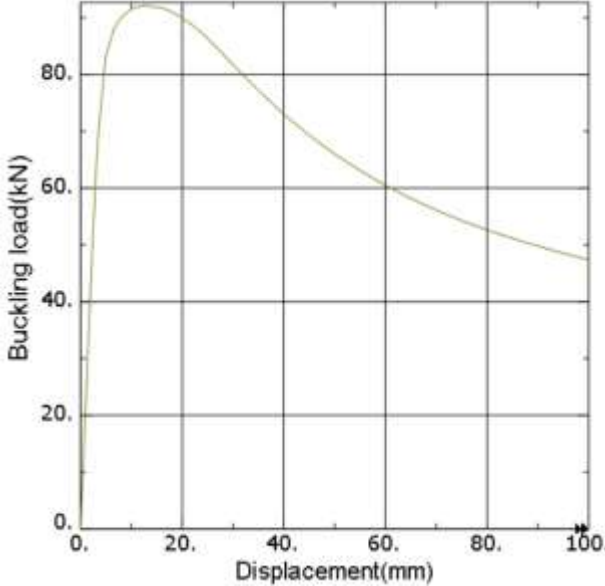
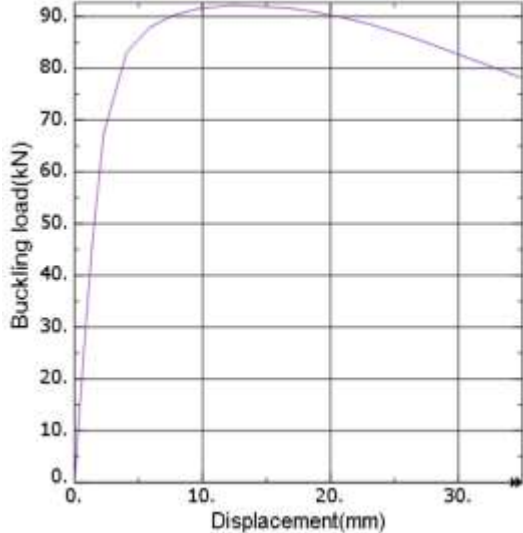
PDC-4, deformed shape under uniform radially distributed vertical load.

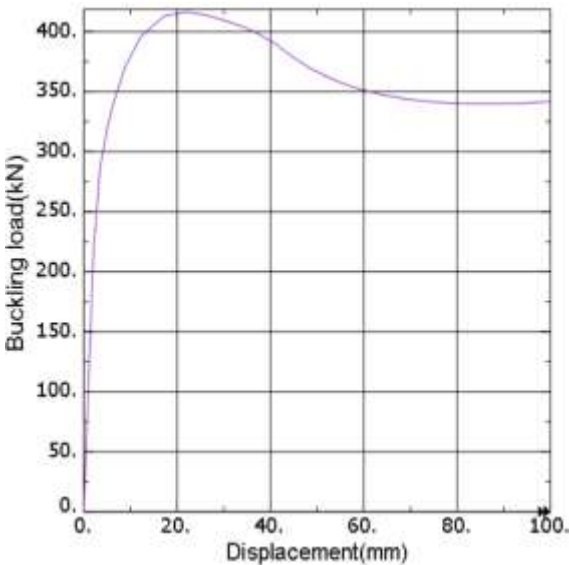
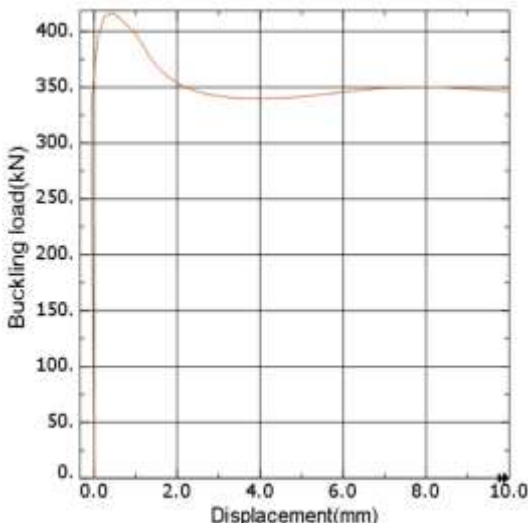
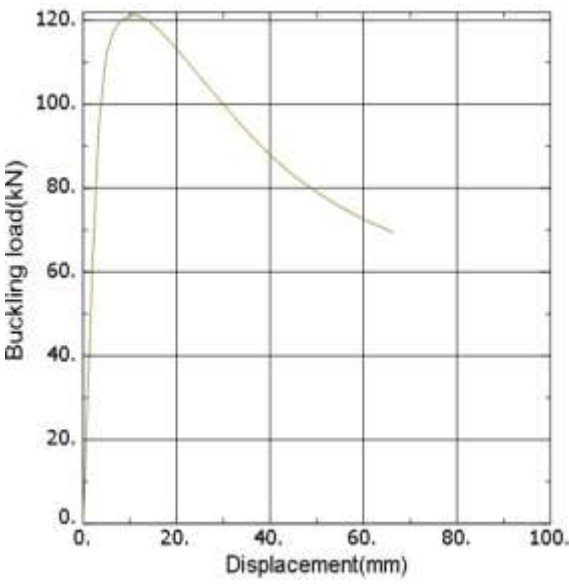
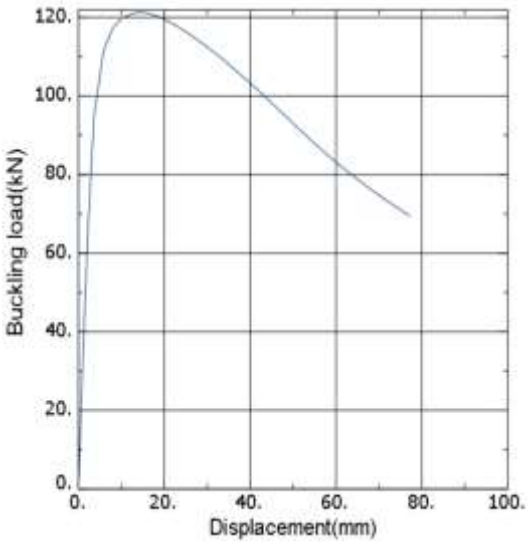
APPENDIX –C

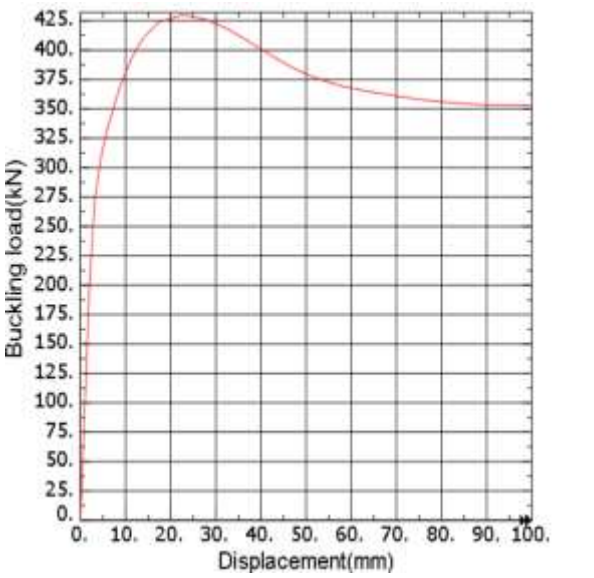
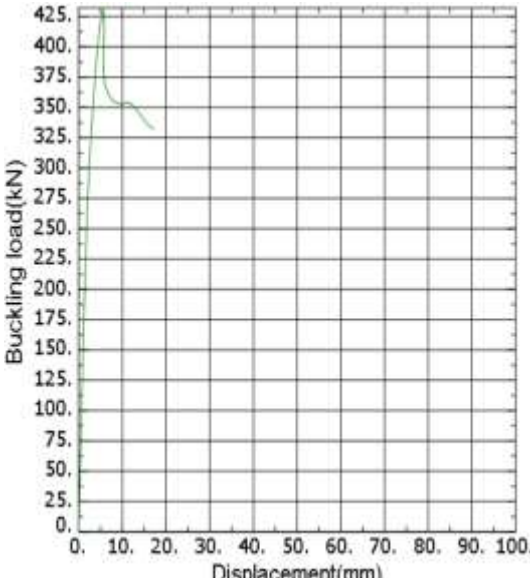
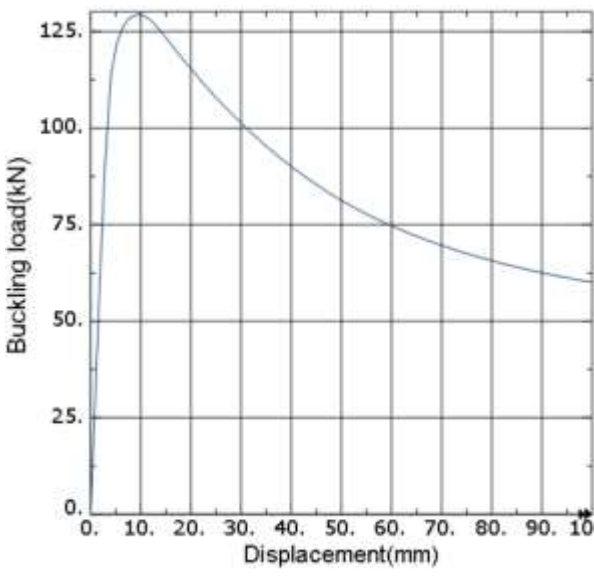
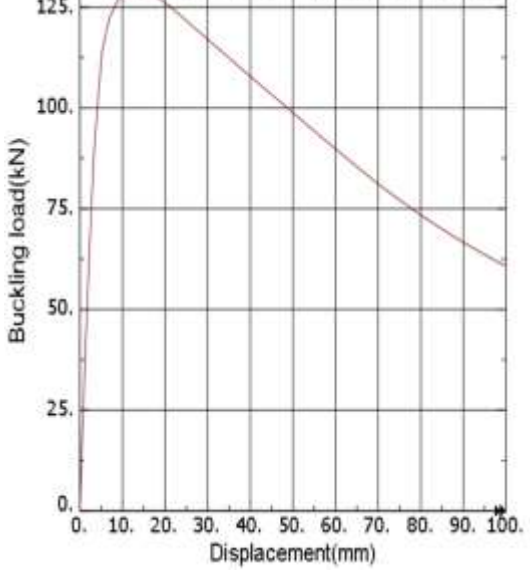
Circular shape buckling load to in plane and buckling load to out of plane contour result from Abaqus result under mid span point load and uniform vertical load.

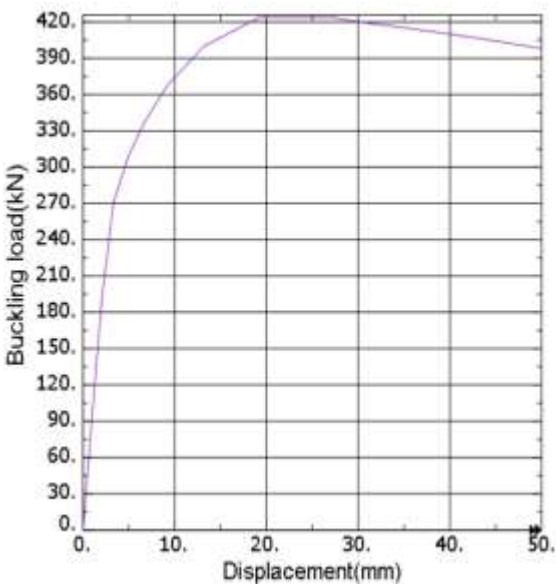
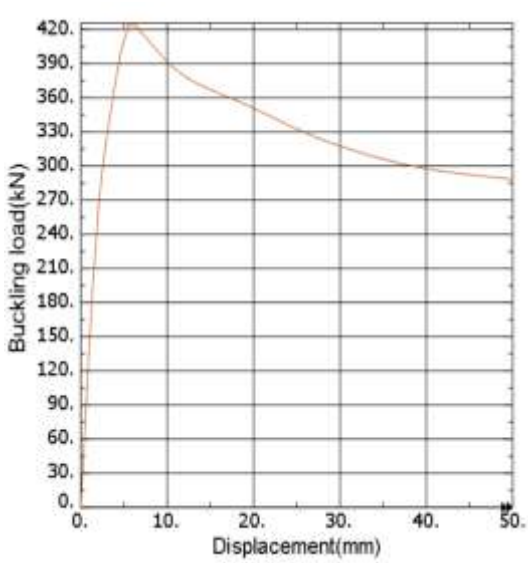
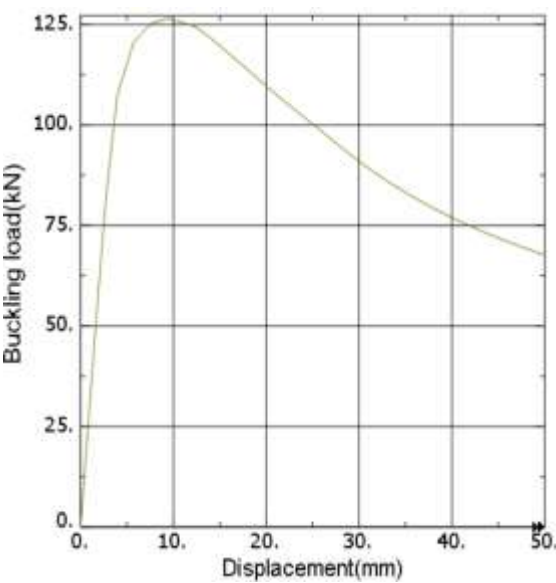
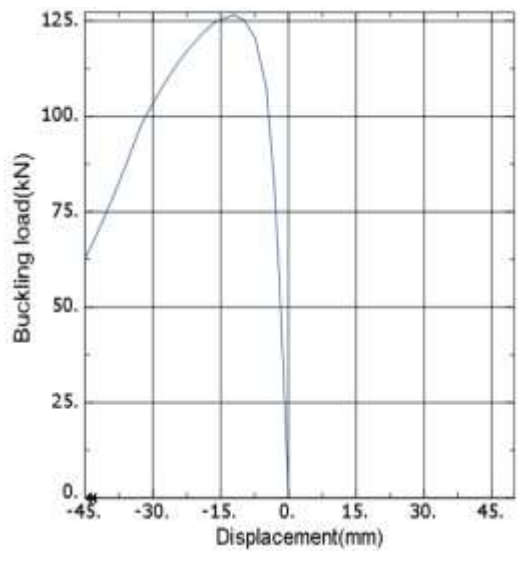
SPECI MEN	Buckling load to in plane displacement	Buckling load to out plane displacement
SCC-1	 <p>Under mid span concentrated load.</p>	 <p>Under mid span concentrated load.</p>
SCC-1	 <p>Under uniform radially distributed vertical load</p>	 <p>Under uniform radially distributed vertical load</p>

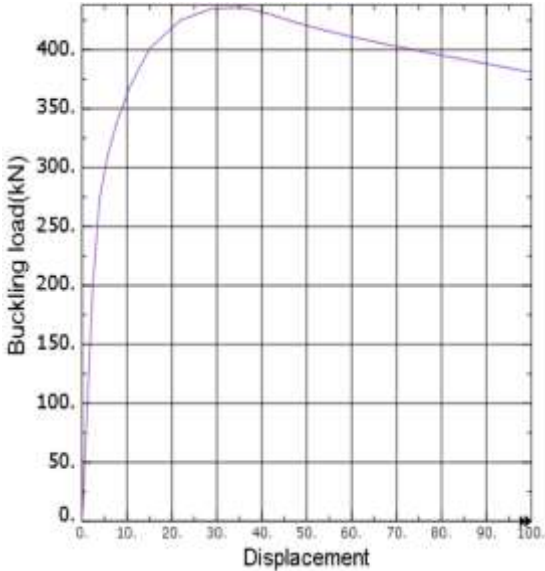
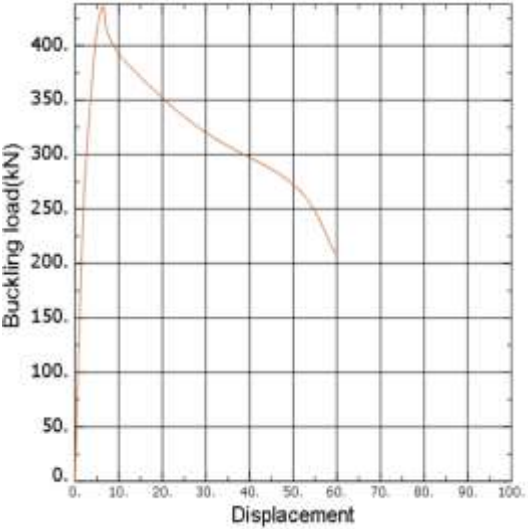
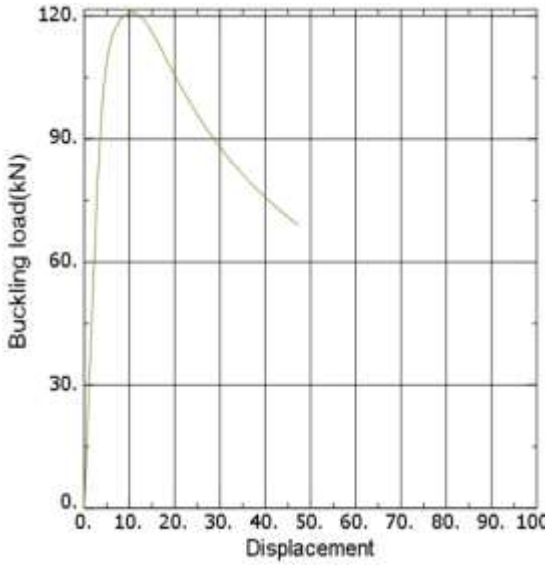
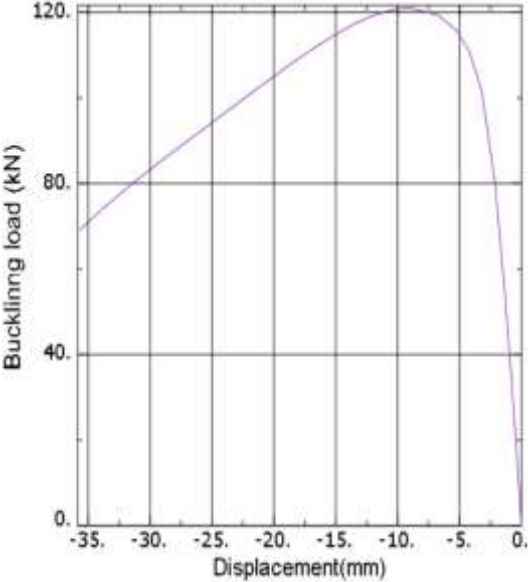
SPECIMEN	Buckling load to in plane	Buckling load to out plane
SCC-2	 <p>Under mid span concentrated load.</p>	 <p>Under mid span concentrated load.</p>
SCC-2	 <p>Under uniform radially distributed vertical load</p>	 <p>Under uniform radially distributed vertical load</p>

SPECIMEN	Buckling load to in plane	Buckling load to out of plane
<p>SCC-3</p>	 <p>Under mid span concentrated load.</p>	 <p>Under mid span concentrated load.</p>
<p>SCC-3</p>	 <p>Under uniform radially distributed vertical load</p>	 <p>Under uniform radially distributed vertical load</p>

SPECIMEN	Buckling load to in plane	Buckling load to out of plane
DCC-1	 <p>Under mid span concentrated load.</p>	 <p>Under mid span concentrated load.</p>
DCC-1	 <p>Under uniform radially distributed vertical load</p>	 <p>Under uniform radially distributed vertical load</p>

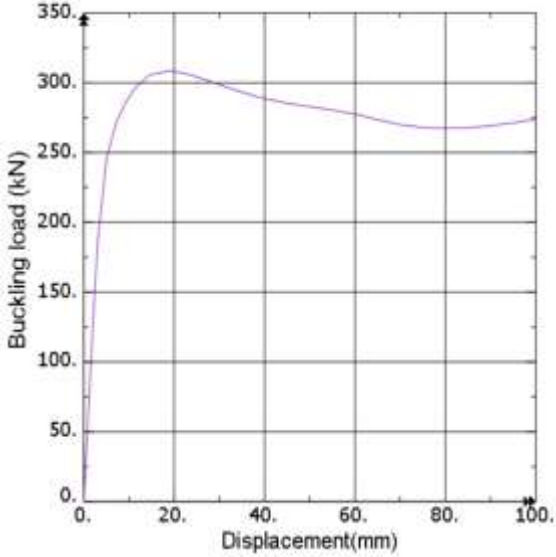
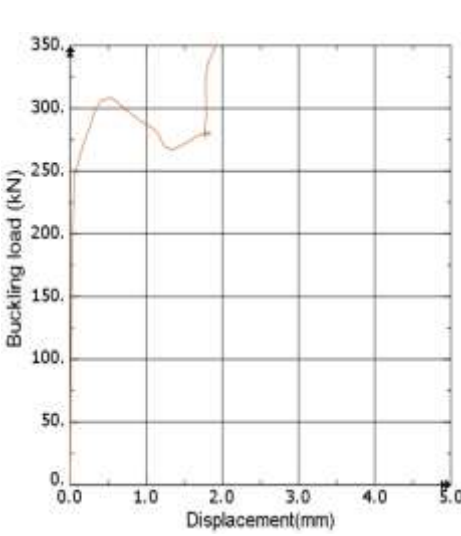
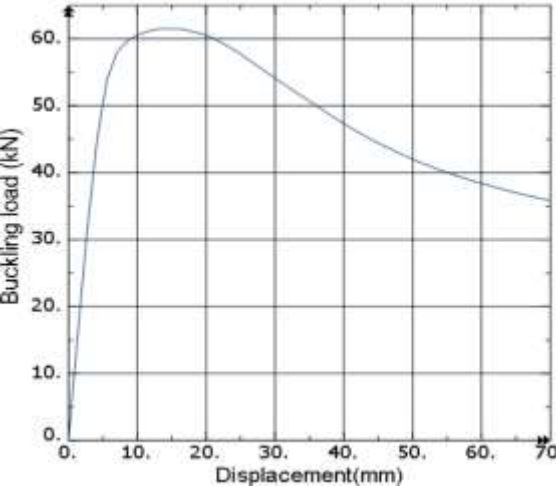
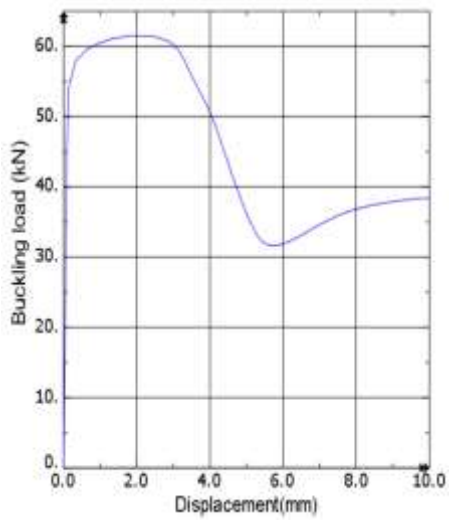
<p>DCC-2</p>	 <p>Under mid span concentrated load.</p>	 <p>Under mid span concentrated load.</p>
<p>DCC-2</p>	 <p>Under uniform radially distributed vertical load</p>	 <p>Under uniform radially distributed vertical load</p>

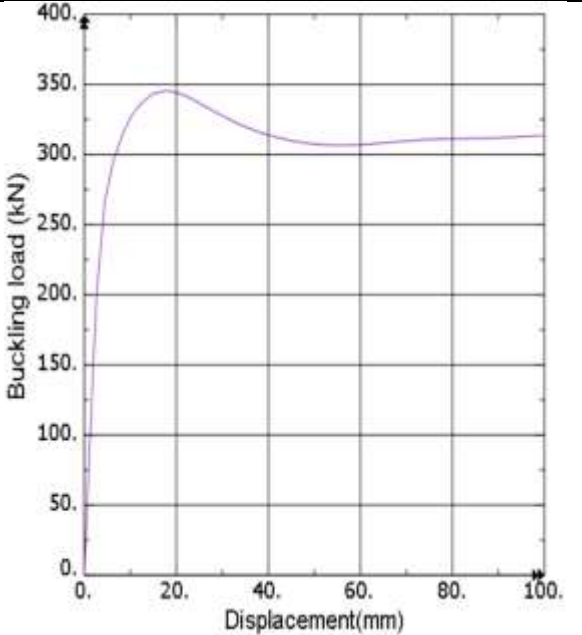
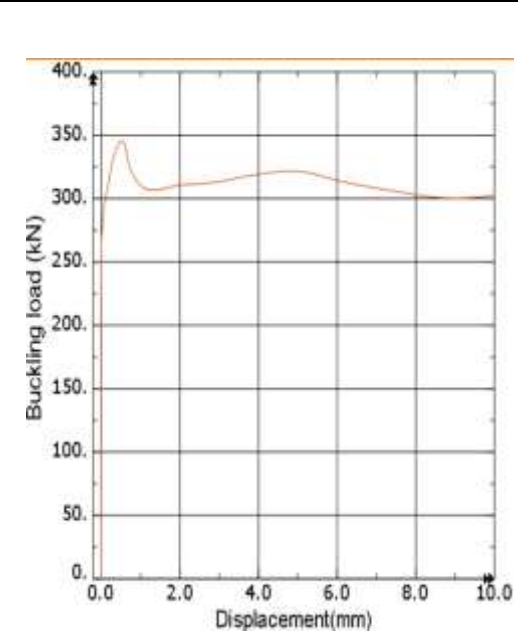
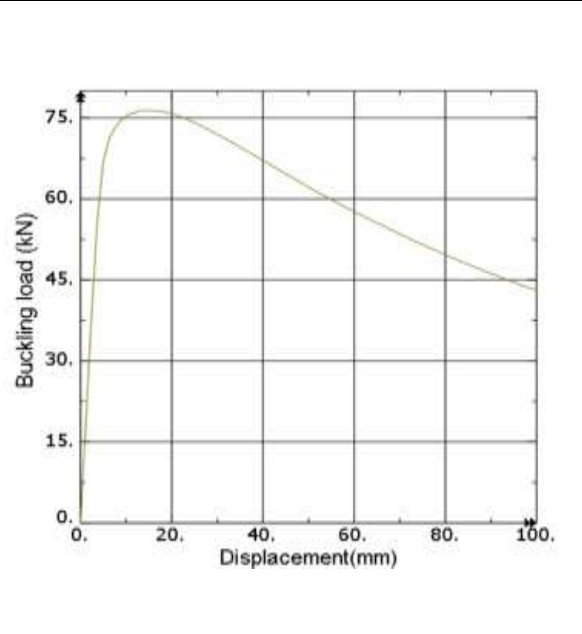
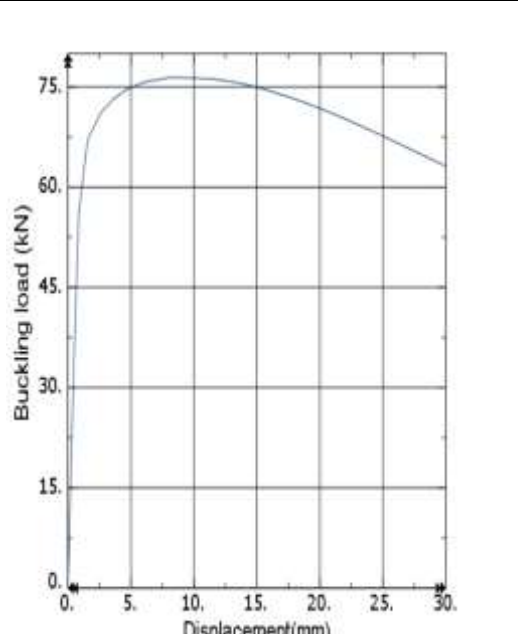
<p>DCC-3</p>	 <p>Under mid span concentrated load.</p>	 <p>Under mid span concentrated load.</p>
<p>DCC-3</p>	 <p>Under uniform radially distributed vertical load</p>	 <p>Under uniform radially distributed vertical load</p>

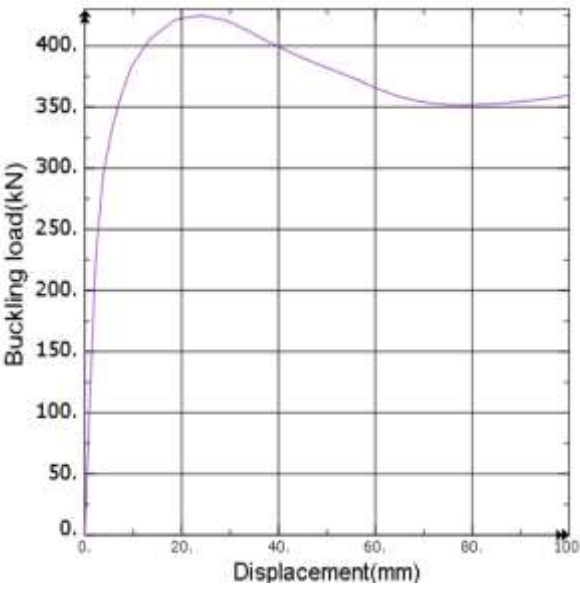
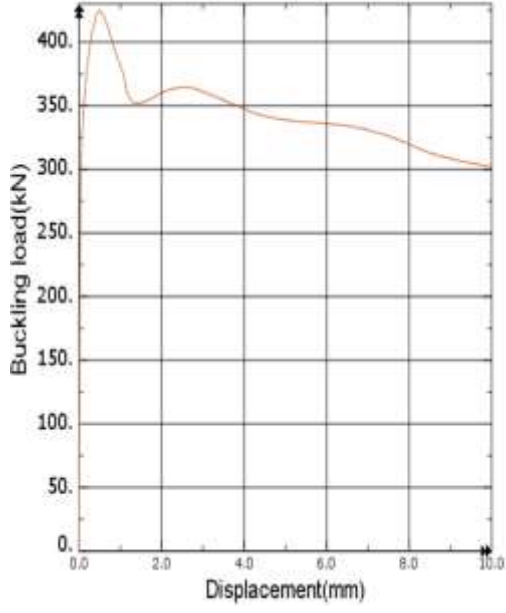
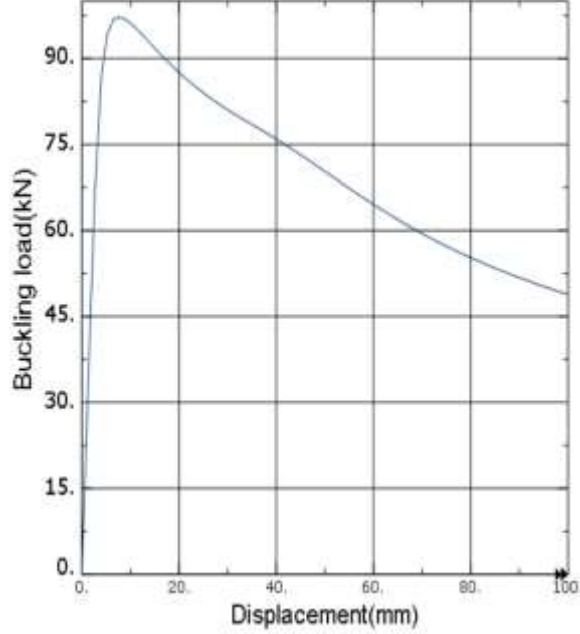
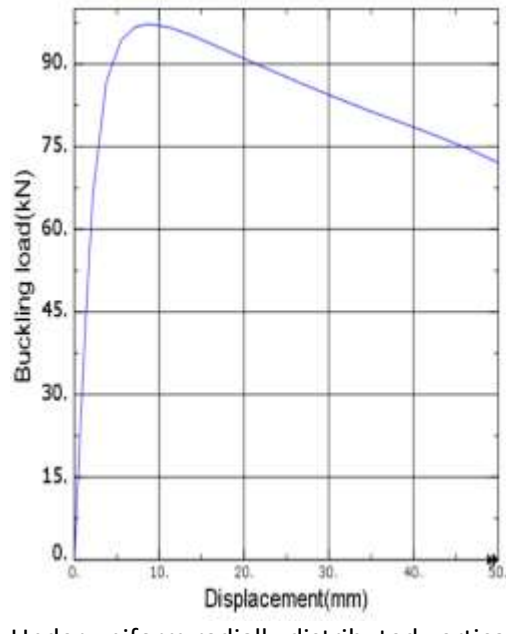
<p>DCC-4</p>	 <p>Under mid span concentrated load.</p>	 <p>Under mid span concentrated load.</p>
<p>DCC-4</p>	 <p>Under uniform radially distributed vertical load</p>	 <p>Under uniform radially distributed vertical load</p>

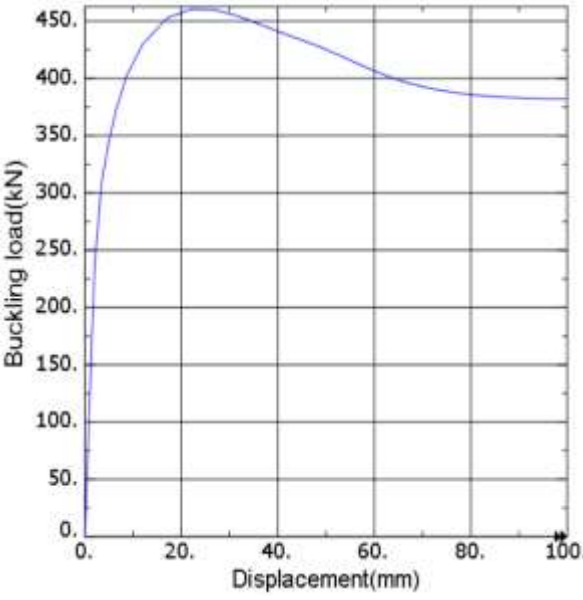
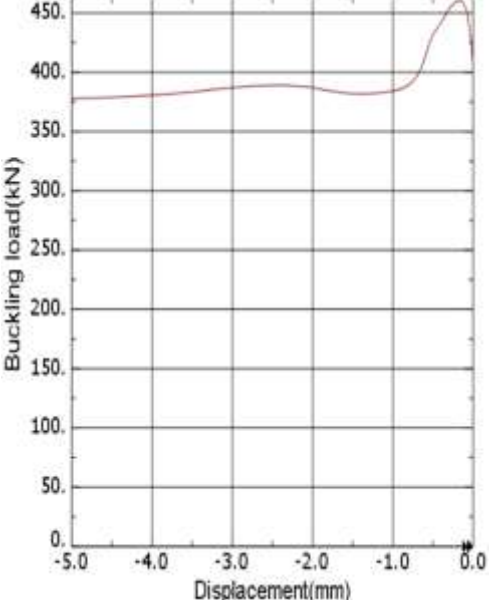
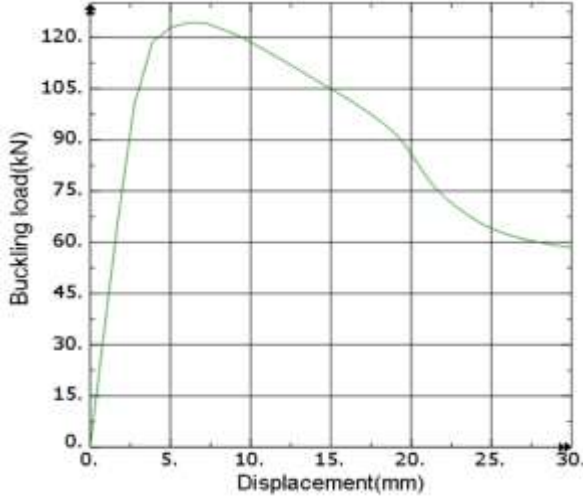
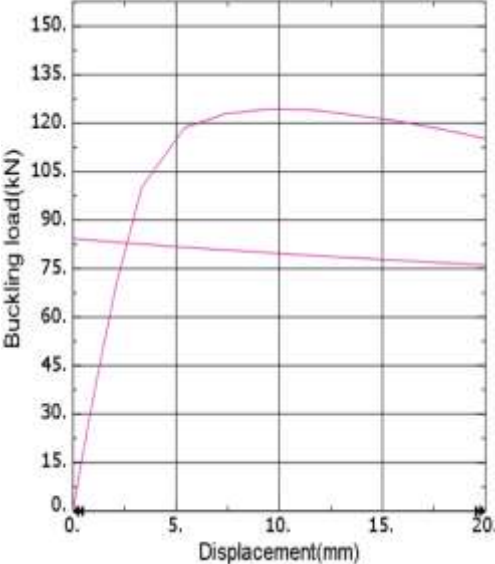
APPENDIX -D

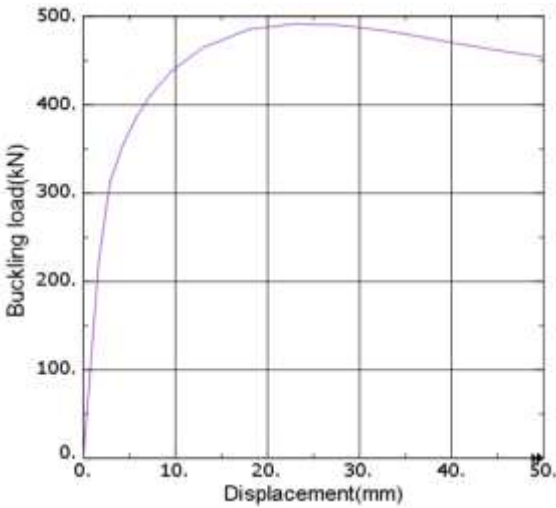
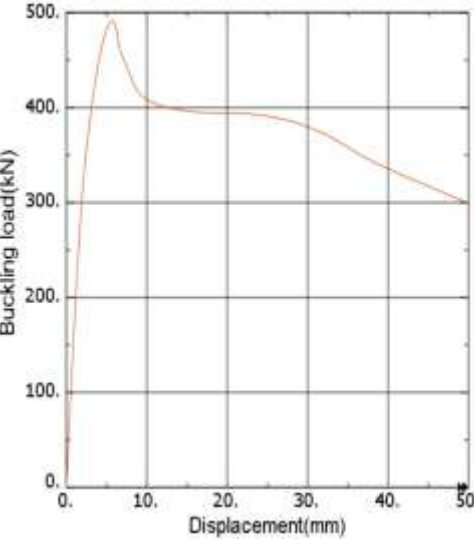
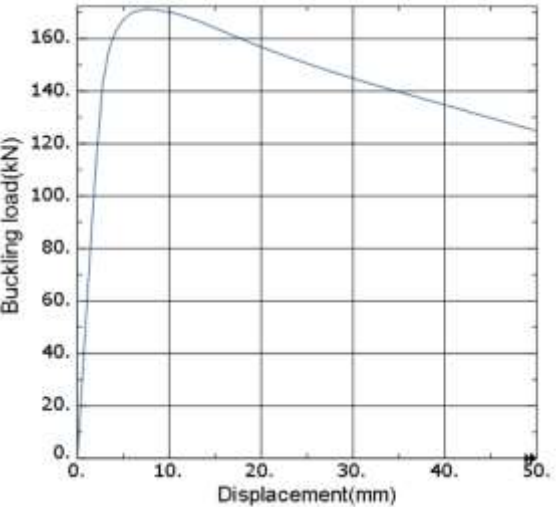
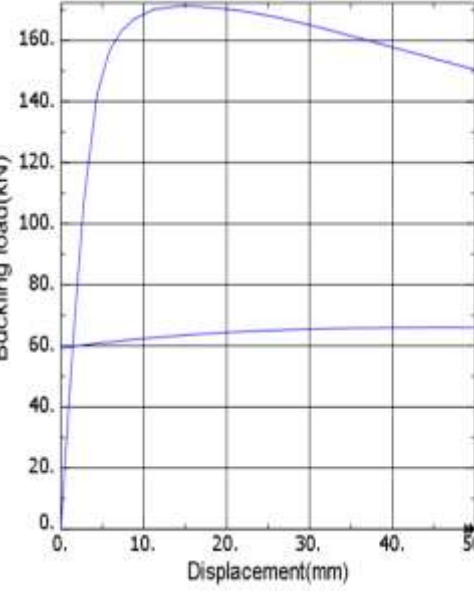
Parabolic arched cellar buckling load to in plane displacement and buckling load to out of plane displacement Abaqus analysis result.

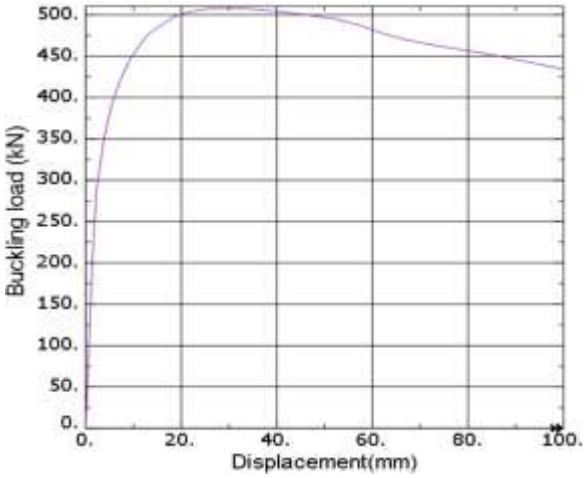
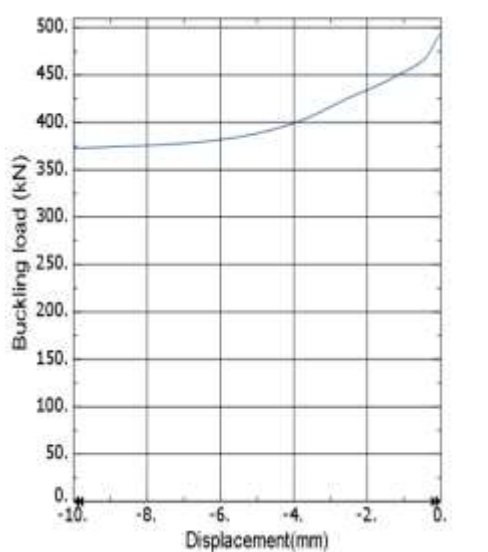
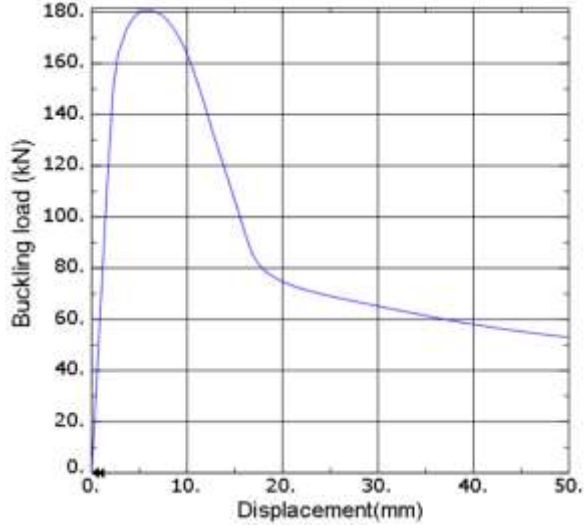
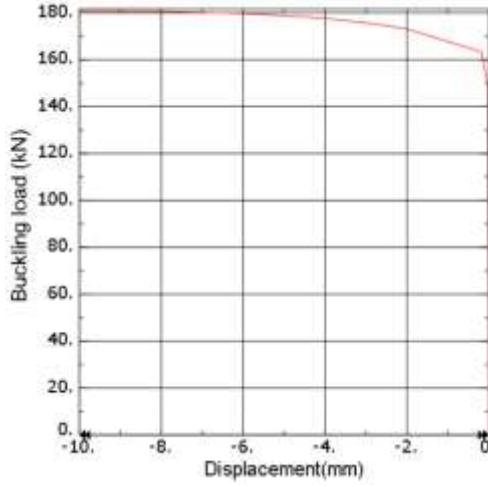
model	Buckling load to in plane displacement	Buckling load to out of plane displacement
PSC-1	 <p>Under mid span concentrated load.</p>	 <p>Under mid span concentrated load.</p>
PSC-1	 <p>Under uniform radially distributed vertical load</p>	 <p>Under uniform radially distributed vertical load</p>

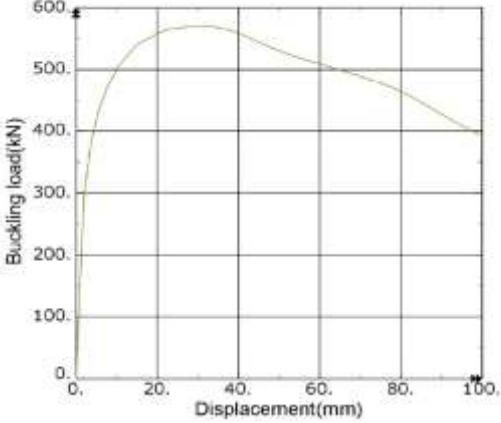
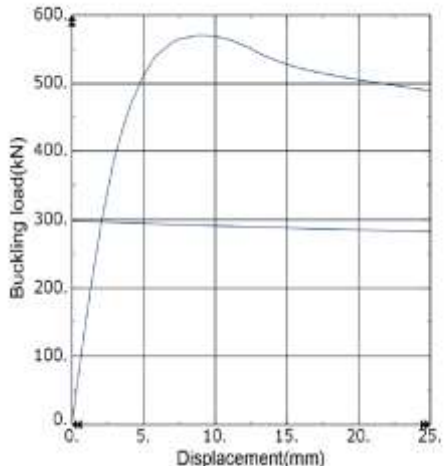
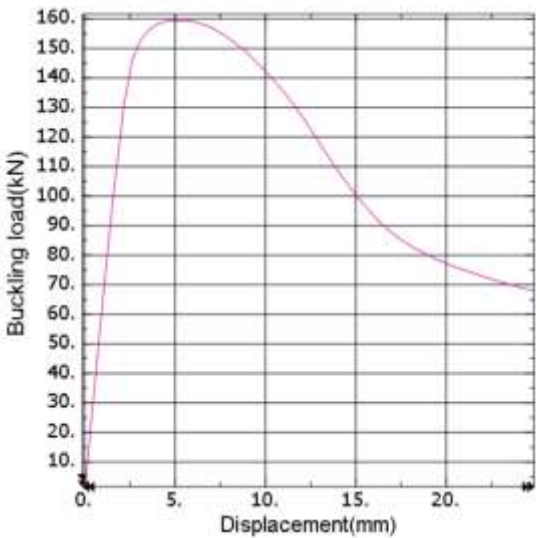
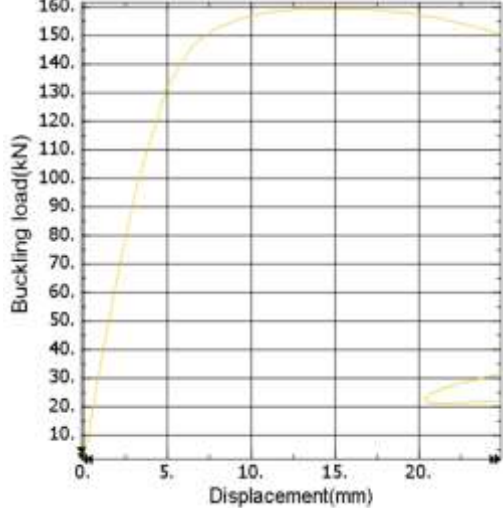
mode I	Buckling load to in plane displacement	Buckling load to out of plane displacement
PSC-2	 <p data-bbox="289 1058 711 1092">Under mid span concentrated load.</p>	 <p data-bbox="889 1016 1312 1050">Under mid span concentrated load.</p>
PSC-2	 <p data-bbox="289 1801 850 1835">Under uniform radially distributed vertical load</p>	 <p data-bbox="889 1780 1393 1835">Under uniform radially distributed vertical load</p>

		Buckling load to in-plane displacement	
PSC-3	 <p>Under mid span concentrated load.</p>	 <p>Under mid span concentrated load.</p>	
	 <p>Under uniform radially distributed vertical load</p>	 <p>Under uniform radially distributed vertical load</p>	

model	Buckling load to in plane displacement	Buckling load to out of plane displacement
PDC-1	 <p>Under mid span concentrated load.</p>	 <p>Under mid span concentrated load.</p>
PDC-1	 <p>Under uniform radially distributed vertical load</p>	 <p>Under uniform radially distributed vertical load</p>

model	Buckling load to in plane displacement	Buckling load to out of plane displacement
PDC-2	 <p>Under mid span concentrated load.</p>	 <p>Under mid span concentrated load.</p>
PDC-2	 <p>Under uniform radially distributed vertical load</p>	 <p>Under uniform radially distributed vertical load</p>

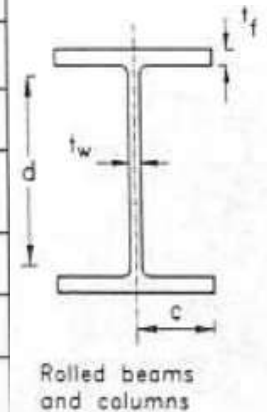
model	Buckling load to in plane displacement	Buckling load to out of plane displacement
PDC-3	 <p>Under mid span concentrated load.</p>	 <p>Under mid span concentrated load.</p>
PDC-3	 <p>Under uniform radially distributed vertical load</p>	 <p>Under uniform radially distributed vertical load</p>

model	Buckling load to in plane displacement	Buckling load to out of plane displacement
PDC-4	<p>Printed using Abaqus/CAE on: Wed Jan 01 21:46:39 Pacific Standard Time 2020</p>  <p>Under mid span concentrated load.</p>	<p>Printed using Abaqus/CAE on: Wed Jan 01 21:50:57 Pacific Standard Time 2020</p>  <p>Under mid span concentrated load.</p>
PDC-4	 <p>Under uniform radially distributed vertical load</p>	 <p>Under uniform radially distributed vertical load</p>

APPENDIX -E

Cross-section properties according to EBCS, 1995.

Type of element	Type of section	Class of Section		
		(1) Plastic	(2) Compact	(3) Semi-compact
Outstand element of compression flange	Built-up by welding	$\frac{c}{t_f} \leq 7.5\epsilon$ (10)	$\frac{c}{t_f} \leq 8.5\epsilon$	$\frac{c}{t_f} \leq 13\epsilon$
	Rolled section	$\frac{c}{t_f} \leq 8.5\epsilon$	$\frac{c}{t_f} \leq 9.5\epsilon$	$\frac{c}{t_f} \leq 15\epsilon$
Internal element of compression flange	Built-up by welding	$\frac{c}{t_f} \leq 23\epsilon$	$\frac{c}{t_f} \leq 25\epsilon$	$\frac{c}{t_f} \leq 28\epsilon$
	Rolled Section	$\frac{c}{t_f} \leq 26\epsilon$	$\frac{c}{t_f} \leq 32\epsilon$	$\frac{c}{t_f} \leq 39\epsilon$
Web, with neutral axis at mid-depth	All sections	$\frac{d}{t_w} \leq 79\epsilon$	$\frac{d}{t_w} \leq 98\epsilon$	$\frac{d}{t_w} \leq 120\epsilon$
Web, generally	All sections	$\frac{d}{t_w} \leq \frac{79\epsilon}{0.4+0.6\alpha}$	$\frac{d}{t_w} \leq \frac{98\epsilon}{\alpha}$	see Section 4.3.2.2(4)
Web, where whole section is subject to compression	Built-up by welding	$\frac{d}{t_w} \leq 28\epsilon$	$\frac{d}{t_w} \leq 28\epsilon$	$\frac{d}{t_w} \leq 28\epsilon$
	Rolled section	$\frac{d}{t_w} \leq 39\epsilon$	$\frac{d}{t_w} \leq 39\epsilon$	$\frac{d}{t_w} \leq 39\epsilon$



$$t_f = 8\text{mm} \quad b_f = 120\text{mm}$$

$$t_w = 12\text{mm} \quad H = 250\text{mm}$$

$$d = H - 2t_f = 250 - 2(12) = 226\text{mm}$$

$$C = \frac{b_f}{2} = \frac{120\text{mm}}{2} = 60\text{mm} \quad f_{y(\text{web})} = 315\text{MPa} \quad f_{y(\text{flange})} = 285\text{MPa} \quad \epsilon = \sqrt{\frac{275}{f_y}} \quad \epsilon_{\text{web}} = \sqrt{\frac{275}{315}} = 0.9343 \quad , \quad \epsilon_{\text{flange}} = \sqrt{\frac{275}{285}} = 0.9822$$

Outstand element of compression flange (rolled section), for class 1 section

$$\frac{c}{t_f} \leq 8.5\epsilon_{\text{flange}} = \frac{60}{12} \leq 8.5(0.9822) = 5 < 8.348 \dots \dots \text{ok}$$

Web with neutral axis at mid depth (all section), for class 1 section

$$\frac{d}{t_w} \leq 79\epsilon_{\text{web}} = \frac{226}{8} \leq 79(0.9343) = 28.25 < 73.76 \dots \dots \text{ok}$$

According to EBCS, 1995 the section used for these investigation is classified in to class 1

